Title
Transport in Internal Waves with a Background Flow: Lessons Learned from Robotic Larval Mimics

Permalink
https://escholarship.org/uc/item/0bx6n5s6

Author
Carriere-Garwood, Jessica

Publication Date
2019

Peer reviewed|Thesis/dissertation

UNIVERSITY OF CALIFORNIA SAN DIEGO

**Transport in Internal Waves with a Background Flow:
Lessons Learned from Robotic Larval Mimics**

A dissertation submitted in partial satisfaction of the
requirements for the degree
Doctor of Philosophy

in

Oceanography

by

Jessica Carrière-Garwood

Committee in charge:

    Peter J. S. Franks, Chair
    Andrew J. Lucas, Co-Chair
    Matthew H. Alford
    Andrew D. Barton
    Jules S. Jaffe
    Jonathan B. Shurin

2019

The dissertation of Jessica Carrière-Garwood is approved, and it is acceptable in quality and form for publication on microfilm and electronically:

_____

_____

_____

_____

_____
Co-Chair

_____
Chair

University of California San Diego

2019

DEDICATION

To Henri, and all the little ones conceived by friends during this work;

May they be strong as they fix the world and the oceans we wrecked.

It goes, boys.

Lynn Hill

TABLE OF CONTENTS

LIST OF ABBREVIATIONS

ADCP: accoustic Doppler current profiler

KDV: Korteweg-de Vries

M-AUE: mini-Autonomous Underwater Explorer

LIST OF SYMBOLS

c_0: linear wave propagation speed [m s^{-1}]

c_p: wave propagation speed [m s^{-1}]

Δx_T: total horizontal displacement [m]

Δx_W: wave-induced horizontal displacement [m]

H: water column height [m]

k: horizontal wavenumber [rad m^{-1}]

η: wave-induced isopycnal displacement [m]

λ: wavelength [m]

ϕ: wave vertical structure function

Q_ρ: environmental property that varies with density

Q_z: environmental property that varies with depth

ρ: density [kg m^{-3}]

t: time [s]

T: wave period [s]

τ: residence time in the wave [s]

u_B: ambient cross-shore velocities [m s^{-1}]

$\tilde{u}_B(z)$: wave-deformed ambient cross-shore velocity profile [m s^{-1}]

u_W: wave cross-shore velocities [m s^{-1}]

w_B: ambient vertical velocities [m s^{-1}]

$\tilde{w}_B(z)$: wave-deformed ambient vertical velocity profile [m s^{-1}]

w_W: wave vertical velocities [m s^{-1}]

ω: wave frequency [rad s^{-1}]

x: horizontal axis or horizontal position [m] (positive towards shore)

z: vertical axis or vertical position [m] (positive up)

LIST OF FIGURES

ACKNOWLEDGEMENTS

First and foremost, I must acknowledge Peter Franks who invited me to join SIO with the promise of absolute freedom in terms of research direction. What a gift! Peter made himself available and showed deep commitment to the success of his students, while allowing me to grow into my own research project. I am also grateful to Drew Lucas who, at key points in my degree, helped me gain perspective on my data and who showed me how to pull off a major field campaign – a true expertise of his. I must also thank Jules Jaffe who not only trusted me to bring back his mini-Autonomous Underwater Explorers, but who also asked about my well-being throughout this rollercoaster that is a PhD. I greatly enjoyed the casual stories, as well as the intellectual conversations following seminars. Working at the intersection of these three scientists' expertise has been a research dream.

I am also indebted to my other committee members. To Matthew Alford for his enthusiasm, his mentoring at sea, and a number of discussions that allowed me to realize that by deforming the ocean, internal waves could move faster waters past depth-keepers. He may not have realized it at the time, but our January 10, 2018 email conversation is now the basis of my entire PhD. His response: *Yes "pulled down isopycnals" would be very important for depth-keepers!* To Andrew Barton who helped me see how internal waves may be important not only to plankton transport, but also to their overall experience of environmental properties. A full chapter stemmed from a conversation we had prior to my qualifying exam. The project I developed weekly in his class also evolved into the inclusion of weak swimmers in two manuscripts. To Jonathan Shurin who challenged me to present my work in terms of hypotheses and questions, even if I initially had no idea of what the larval mimics would face in the ocean.

I must also acknowledge my Honours' and Master's advisor, Paul Hill, for introducing me to the field of oceanography, and more specifically for sharing his passion of particle transport. Throughout his mentorship, Paul made sure that I was given all the advice

and opportunities I would need to start a professorial career on the right foot. I hope he will recognize his influence in this work. The many scientists and students at Dalhousie University, Bedford Institute of Oceanography, and Saint Mary's are also to thank for providing an inclusive, generous, and supportive environment in which to conduct research. They made me discover the beauty of oceanography and prepared me well.

If not for the mentorship of Ruth Musgrave, my dissertation would have been entirely different. Ruth is clearly committed to seeing our field progress; she generously shares her perspective and resources with many. Whenever I discussed my research with her, she was always many steps ahead, pointing me in the right direction, while being patient as I took the time to fully understand concepts on my own. I must also thank Paul Roberts, Devin Ratelle, and Ben Laxton for always encouraging me, for sharing engineering and programming knowledge, and for making sure data would be collected without hiccups. Thank you to superwoman Laura deGelleke who suggested annual adventure trips and volunteered her time in our field campaign; to Perry Naughton who joined climbing trips, helped in the field, and worked extremely hard so that I could have reliable underwater tracks; as well as to Arnaud LeBoyer, Jean-Michel Leconte, Jennifer MacKinnon, Jerry Molnar, Andy Mullen, Jonathan Nash, Eric Orenstein, Emily Shroyer, Brian Stock, and Amy Waterhouse for additional help with data collection and processing.

When I was contemplating where to pursue a PhD, I was impressed by the energy and achievements SIO students displayed; it seemed quite the privilege to have the opportunity to spend many years with individuals who would undoubtedly become stellar colleagues. The students did not disappoint! I want to express my gratitude and admiration to Effie Fine and Olavo Badaró Marques for making up a great working group, which quickly morphed into a group of friends meeting for coffee and donuts; to Lilly McCormick, Matt Costa, Ben Whitmore, Abby Cannon, Regina Guazzo, AJ Schlenger, Belli Valencia, and Josh Jones for being such a positive and dynamic cohort; to Stephanie Sommer for being a

wonderful officemate open to discussing both serious topics and funny incidents; to past and present members of the Franks Lab – Darcy Taniguchi, Fanny Chenillat, Alain deVerneil, Christian Briseño-Avena (and James), Stephanie Snyder, Eiren Jacobson, Bryce Inman, Ashlyn Giddings, Angie Szesciorka, Eric Orenstein, Kasia Zaba, Pichaya Lertvilai, and, proudly, a student I co-mentored in summer 2018, Shailja Gangrade – as well as to past and present members of MOD, who always welcomed me when I crashed their parties.

To the crew at the OCC, and to all the friends with whom I climbed, backpacked, and camped: Daniela Faggiani Dias, Courtney Schatzman, Emily Wei, Lauren Manck, Hanah Mirahmadi, Daniel Trugman, Greg Wagner, Spencer Jones, Travis Wong, Joanne Shin, Natasha/Cody/Evie Gallo, Emma Harrison, Stephanie Mumma, Greg & Doug, and many more, with a special mention to my cycling friend Navid Constantinou, to Kaitlin & Andrew the friends we met in LA, as well as to my supportive roommates Yeara & Albert. Thank you for keeping me sane and helping me enjoy the best this region has to offer!

Being a community-oriented person, I have also interacted with numerous individuals at SIO and being able to greet them on my way to any building has always made me feel at home. They are too numerous to name, but they include the staff in the SIO Graduate Student Office, in the Scientific Diving Program, at Caroline's, the Diversity Advisory Committee, Scripps IT, Scripps Administration, fellow students, engineers, scientists, and faculty, as well as the many e-mail lists and their stimulating exchanges. It has been a pleasure to be a part of such a vibrant community.

Finally, when I first visited SIO, many graduate students warned me of the toll a PhD could take on partners; I responded that I had no grounds for concerns given I only had eyes for data. Fortunately, I have now met someone who shares a love of both data and outdoor adventures, and who is happy to take turns leading in climbing and in life so that we can both reach our goals together. To many more years of science and adventure, Jesse Cusack. Thank you for your patience, as you lived through a second PhD.

Now, the formalities:

Chapter 2, in full, has been submitted for publication of the material as it may appear in *Limnology and Oceanography*, 2019, Garwood, J.C., Lucas, A.J., Naughton, P., Alford, M.H., Roberts, P.L.D., Jaffe, J.S., deGelleke, L., and Franks, P.J.S. The dissertation author was the primary investigator and author of this paper.

Chapter 3, in full, is currently being prepared for submission for publication of the material. Garwood, J.C., Lucas, A.J., Naughton, P., Roberts, P.L.D., Jaffe, J.S., deGelleke, L., and Franks, P.J.S. The dissertation author was the primary investigator and author of this material.

Chapter 4, in full, is currently being prepared for submission for publication of the material. Garwood, J.C., Musgrave, R.C., Lucas, A.J., and Franks, P.J.S. The dissertation author was the primary investigator and author of this material.

2011	Combined Honours in Marine Biology and Oceanography, *First Class Honours*, Dalhousie University, Halifax
2014	Master of Science in Oceanography, *Governor General's Gold Medal*, Dalhousie University, Halifax
2019	Doctor of Philosophy in Oceanography, University of California, San Diego
2014 - 2019	Instructor, Outback Climbing Center

PUBLICATIONS

Garwood, J.C., Lucas, A.J, Naughton, P., Roberts, P.L.D., Jaffe, J.S., deGelleke, L., and Franks, P.J.S. Larval cross-shore transport estimated from internal waves with a mean flow: the effects of larval vertical position and depth regulation. *In preparation for Limnology and Oceanography.*

Garwood, J.C., Lucas, A.J., Naughton, P., Alford, M.H., Roberts, P.L.D., Jaffe, J.S., deGelleke, L., and Franks, P.J.S. A novel cross-shore transport mechanism revealed by subsurface, robotic larval mimics: internal wave deformation of the background velocity field. *Under review for Limnology and Oceanography.*

Franks, P.J.S., **Garwood, J.C.**, Ouimet, M., Cortes, J., Musgrave, R., and Lucas, A.J. Stokes drift of plankton in linear internal waves: Cross-shore transport of neutrally buoyant and depth-keeping organisms. *Under review for Limnology and Oceanography.*

Garwood, J.C., Hill, P.S., MacIntyre, H.L., and Law, B.A. (2015). Grain sizes retained by diatom biofilms during erosion on tidal flats linked to bed sediment texture. *Continental Shelf Research*, 104:37-44.

J. Carrière-Garwood. (2014). *Seasonal Variation and Biological Effects on Mudflat Erodibility in the Minas Basin, Bay of Fundy.* Master's thesis, Dalhousie University, Halifax.

Garwood, J.C., Hill, P.S., and Law, B.A. (2013). Biofilms and size sorting of fine sediment during erosion in intertidal sands. *Estuaries and Coasts*, 36:1024-1036.

ABSTRACT OF THE DISSERTATION

**Transport in Internal Waves with a Background Flow:
Lessons Learned from Robotic Larval Mimics**

by

Jessica Carrière-Garwood

Doctor of Philosophy in Oceanography

University of California San Diego, 2019

Peter J. S. Franks, Chair
Andrew J. Lucas, Co-Chair

Many coastal, benthic species, such as mussels and lobsters, have larval stages that rely on physical mechanisms for their cross-shore transport to suitable adult habitats. One of these physical mechanisms include internal waves. Because they transport mass, only highly nonlinear internal waves were traditionally assumed to induce significant cross-shore transport. However, the work presented in this dissertation shows that by deforming ambient velocities, even weakly nonlinear internal waves may enhance cross-shore transport of depth-keeping organisms. This mechanism was first observed *in situ* using novel,

subsurface, trackable larval mimics, the mini-Autonomous Underwater Explorers. Results from the larval mimics were then related to mooring observations, using virtual swimming organisms and established theoretical wave models. Following this model validation, the total cross-shore transport of both passive and depth-keeping organisms was estimated for > 500 observed, shallow-water, weakly nonlinear internal waves during a 14-day deployment. Results show that in these waves, depth-keeping promoted onshore transport throughout the water column, compared to passive organisms. Moreover, the largest transport estimates for depth-keepers were on the same order of magnitude as average transport estimates for passive organisms in highly nonlinear internal waves. This dissertation also highlights the importance of considering larval horizontal displacement throughout an internal wave, and not only in bulk, to properly assess the environmental conditions planktonic organisms experience.

Chapter 1

Introduction

1.1   Larvae, internal waves, and ocean currents

When it comes to reproduction, many marine organisms espouse a dispersal strategy similar to that of the dandelion. In the same way a dandelion's seeds are dispersed by the wind, ocean currents carry larvae of fish, corals, and other bottom-dwelling animals as they develop. The ocean conditions these larvae encounter will determine their development time, health, and survival. Ultimately, larvae will prosper into adulthood if they remain uneaten and alive throughout their odyssey, and encounter a suitable adult habitat at just the right time. To better protect the marine species that inhabit our coastal oceans, we must therefore understand how populations are linked to each other, which pathways larvae take to reach their adult habitats, and how changing ocean conditions will affect not only the environmental conditions larvae may encounter, but also the physical processes that transport them.

Unlike dandelion seeds, however, marine larvae can exhibit swimming behavior, and although all are too weak to supersede horizontal ocean currents, some can move up or down. Other larvae may also regulate their depths through density adjustments. If the

ocean moved uniformly from the surface to the bottom, being able to move up or down would not influence a larva's final destination. However, a stratified ocean will exhibit "layers" that can travel in different directions and at different speed; thus, a larva's preferred depth will influence its travels. These ocean layers are caused by variations in density; surfaces of constant density are called "isopycnals".

Similar to gusts of wind that entrain dandelion seeds, waves that propagate within the ocean's interior, i.e., internal waves, can accelerate larvae and enhance their transport. However, internal waves do not act in isolation: their velocities combine with the slower-varying background ocean velocities, such as those associated with internal tides and winds. Horizontal velocities in high-frequency internal waves often exceed 10 cm s^{-1}, whereas vertical velocities are on the order of 1-10 cm s^{-1}. Only the strongest larvae, such as late-stage crab and lobster larvae, may reach swimming speeds of 10 cm s^{-1}; larval swimming speeds on the order of 0.01-1 cm s^{-1} are far more common. Thus, most larvae cannot control their horizontal position in internal waves, and only some may control their vertical position. Throughout this dissertation, the term "passive" will be used for larvae that are completely vulnerable to ocean and wave velocities in both the vertical and horizontal, while the term "depth-keeping" will be used for larvae that drift horizontally, but resist all vertical velocities.

Due to the small range in density variation in the ocean compared to the density difference between seawater and air, internal waves can be much larger than their surface counterparts. Indeed, internal waves with amplitudes on the order of 1-10 m are not uncommon in the coastal ocean, and some can even have amplitudes exceeding 100 m in the open ocean. Thus, as internal waves propagate, they deform the layered structure of the ocean upward and downward significantly. Passive larvae will experience the same vertical deformation and remain within the same water parcels, however depth-keeping larvae will not. Indeed, a range of isopycnals will move past depth-keeping larvae. Because background

velocities are constant along isopycnals, depth-keeping larvae will also experience a range of background velocities throughout a wave; their total horizontal transport will, therefore, be different than that of passive larvae within the same wave. Moreover, many environmental properties such as ocean temperature, nutrient concentrations, and oxygen levels remain constant along isopycnals, while light levels are predominantly set by depth. Thus, the environmental conditions experienced by depth-keeping larvae over a wave period will also differ from those experienced by passive larvae.

Most field studies of internal-wave-induced transport rely on velocity measurements taken at fixed locations, and do not account for the fact that larvae move with internal waves. Moreover, actual transport measurements are difficult to obtain, as larvae cannot easily be followed. Analytical and numerical models, on their part, may follow virtual larvae in a wave, but do not always incorporate larval swimming behavior, and/or realistic background currents. As such, the work presented in this dissertation sought to provide the first direct *in situ* measurements of cross-shore transport in coastal internal waves relevant to larvae that swim vertically. To obtain these measurements, swarms of novel underwater larval mimics were deployed in the shallow, stratified coastal waters of Southern California. To emulate some larvae's tendency to maintain a fixed depth, the larval mimics were programmed to counteract the waves' vertical displacements, while they drifted horizontally, i.e., the mimics were depth-keeping. To put these deployments into a broader context, the larval mimics' measurements were also supplemented with data-based numerical simulations, which included > 500 waves with their background currents, as well as both passive and depth-keeping virtual larvae.

Due to the unprecedented spatial and temporal resolution of the larval mimics' 3-D underwater tracks, the *in situ* measurements of wave-induced cross-shore transport could be compared to estimates derived from measurements collected at a nearby mooring for a given internal wave, and not only in bulk. A detailed investigation of a single internal

wave event revealed a new cross-shore transport mechanism specific to larvae that swim vertically in internal waves with a depth-varying background current.

To test whether depth-keeping generally promoted onshore transport in realistic ocean conditions, wave-induced transport estimates were generated for both passive and depth-keeping virtual larvae released in the flow field associated with > 500 internal waves observed at a mooring over two weeks. Overall, depth-keeping was found to enhance onshore transport in the upper water column, and to reduce offshore dispersal at depth. Traditionally, only the largest and steepest internal waves were assumed to induce significant horizontal transport. However, the realistic wave conditions replicated in this study show that even small waves can induce significant transport when considering the three-way interaction between internal waves, background currents, and larval swimming behavior.

Finally, although many studies have considered the effects of internal wave vertical motions on the total solar radiation experienced by passive plankton, none appears to have included the effects of horizontal displacements within the wave. Moreover, the effects of wave-induced isopycnal displacements on the environmental conditions experienced by depth-keeping plankton has largely been ignored. As such, an entire chapter of this dissertation is dedicated to demonstrating that both internal-wave induced horizontal motions and swimming behavior must be considered to accurately estimate the environmental conditions experienced by any planktonic organism, including larvae.

1.2 Objectives

Overall, this dissertation aims to investigate how larval swimming behavior, internal waves, and background ocean currents interact to modify the environmental conditions experienced by larvae, as well as how this three-way interaction modulates larval cross-shore transport in shallow, stratified coastal waters. More specifically, the research presented

4

seeks to answer the following questions:

1. What background flow properties and larval swimming behavior promote onshore vs. offshore transport in shallow water, weakly nonlinear internal waves?

2. Given the measured weakly nonlinear internal wave flow field at Mission Beach, California, what magnitude of cross-shore transport can be expected for depth-keeping and passive larvae throughout the water column?

3. Do the overall conditions observed at Mission Beach, California promote onshore transport of depth-keeping larvae, compared to passive organisms?

4. How do the vertical and horizontal motions of passive and depth-keeping plankton within internal waves affect the environmental conditions they experience?

5. How can mooring measurements be adapted to account for both the vertical and horizontal motions of passive and depth-keeping plankton in internal waves?

1.3   Organization of the dissertation

The second chapter of this dissertation, *A novel cross-shore transport mechanism revealed by subsurface, robotic larval mimics: internal wave deformation of the background velocity field*, describes in detail a mechanism by which depth-keeping larvae may experience sudden changes in transport direction and magnitude due to the internal wave deformation of background ocean currents. This mechanism was first observed during the field work associated with this dissertation. Simple wave models paired with mooring observations were used to investigate how internal waves, background ocean currents, and swimming behavior interacted to enhance onshore transport of the larval mimics.

The third chapter, *Larval cross-shore transport estimated from internal waves with a mean flow: the effects of larval vertical position and depth regulation*, builds from the

three-way interaction between larvae, internal waves, and background ocean currents presented in the previous chapter. A numerical framework that combines internal wave theory with *in situ* mooring measurements and larval swimming behavior is developed and used to derive cross-shore transport estimates over a two-week sampling period off Mission Beach, California. Depth-keeping in the weakly nonlinear internal waves observed is found to promote onshore transport and/or retention at all depths, with some cross-shore transport estimates near the surface matching those for passive larvae in much stronger, highly nonlinear waves. Traditionally, only the largest and steepest internal waves have been assumed to induce important cross-shore transport; accounting for larval swimming behavior brings nuance to this statement.

This dissertation's final chapter, *Life in Internal Waves*, places the novel contributions of this dissertation within the context of known interactions between marine organisms and internal wave vertical motions. Oceanographic measurements obtained at fixed locations are often used to estimate the vertical motions of planktonic organisms and the environmental properties they experience, yet horizontal motions are rarely considered. Field experiments and numerical simulations carried out throughout this dissertation have shown that horizontal motions in internal wave must be considered to derive accurate larval transport estimates. This chapter demonstrates that the relative horizontal motions of planktonic organisms within an internal wave field must also be considered to fully capture the environmental conditions they experience. To promote more accurate assessments and modeling of coastal plankton populations in the future, simple data-based and modeling approaches are also presented.

Chapter 2

A novel cross-shore transport mechanism revealed by subsurface, robotic larval mimics: internal wave deformation of the background velocity field

2.1 Abstract

Coastal physical processes are essential for the cross-shore transport of meroplanktonic larvae to their benthic adult habitats. To investigate these processes, we released a swarm of novel, trackable, subsurface vehicles, the Mini-Autonomous Underwater Explorers (M-AUEs), which we programmed to mimic larval depth-keeping behavior. The M-AUE swarm measured a sudden net onshore transport of 30-70 m over 15-20 min, which we investigated in detail. Here we describe a novel transport mechanism of depth-keeping

7

plankton revealed by these observations. *In situ* measurements and models showed that, as a weakly nonlinear internal wave propagated through the swarm, it deformed surface-intensified, along-isopycnal background velocities downward, accelerating depth-keeping organisms onshore. These higher velocities increased both the depth-keepers' residence time in the wave and total cross-shore displacement, leading to wave-induced transports twice those of fully Lagrangian organisms and four times those associated with the unperturbed background currents. Our analyses also show that integrating velocity time series from virtual larvae or mimics moving with the flow yields both larger and more accurate transport estimates than integrating velocity time series obtained at a point (Eulerian). The increased cross-shore transport of organisms capable of vertical swimming in this wave/background-current system is mathematically analogous to the increase in onshore transport associated with horizontal swimming in highly nonlinear internal waves. However, the mechanism described here requires much weaker swimming speeds (mm s^{-1} vs. cm s^{-1}) to achieve significant onshore transports, and meroplanktonic larvae only need to orient themselves vertically, not horizontally.

2.2   Introduction

Meroplanktonic larvae of coastal benthic organisms such as barnacles, mussels, and oysters must either remain in or be transported back to the nearshore environment for recruitment to adult populations. Simple hydrodynamic models that assume larvae to be completely passive and vulnerable to ocean currents tend to overestimate dispersal distances, both in the cross-shore and alongshore directions, when compared to estimates inferred from *in situ* larval abundance (Largier, 2003; Shanks, 2009). Accounting for simple behaviors such as vertical swimming can reconcile some of these estimates (Shanks and Brink, 2005). By regulating their depths, for instance, organisms can exploit vertical

variations in cross-shore velocities (Peterson et al., 1979; Morgan et al., 2009), or limit offshore transport (Shanks and Brink, 2005). Such physical-biological interactions have been suggested to occur in internal gravity waves (Shanks and Wright, 1987; Pineda, 1999), but less attention has been focused on the implications of internal waves interacting with depth-varying ambient velocities for the transport of depth-keeping organisms.

As they propagate through a stratified ocean, internal waves deform isopycnal surfaces. Because background currents flow mainly along isopycnals, internal waves similarly deform the ambient velocity field, and more precisely its streamlines (Stastna and Lamb, 2002; Klymak et al., 2006). Using measurements collected by a swarm of novel, subsurface larval mimics, the Mini-Autonomous Underwater Explorers (M-AUEs) (Jaffe et al., 2017), combined with simple models, we will show that this deformation has a significant impact on the transport of depth-keeping vs. passive larvae, particularly when the background horizontal currents are vertically sheared. To avoid any ambiguity associated with the term Lagrangian, we use the terms "passive" to refer to fully Lagrangian organisms, i.e., advected by both horizontal and vertical velocities, and "depth-keeping" for organisms that are advected by horizontal velocities, but which resist vertical velocities.

Shanks (1983) demonstrated the potential of internal waves to transport plankton by deploying drifters in visible surface slicks – the surface expression of internal waves. Although the surface drifters occasionally showed no net horizontal displacement, at other times they were displaced as much as 1-2 km onshore in a few hours. Since then, a number of field studies have shown plankton and larvae to be concentrated above internal wave troughs (e.g., Shanks and Wright, 1987; Pineda, 1999; Lennert-Cody and Franks, 2002; Omand et al., 2011), and theoretical arguments have shown the potential for internal waves to both accumulate (Franks, 1997; Lennert-Cody and Franks, 1999) and transport (Lamb, 1997; Helfrich and Pineda, 2003; Scotti and Pineda, 2007) organisms with vertical swimming behaviors. Planktonic larvae have been shown to respond to a number of environmental

cues that could orient them vertically – a necessary condition for these physical-biological interactions to exist. Scallop larvae, for instance, exhibit negative geotaxis and swim faster with increased pressure (Cragg, 1980), while other invertebrate larvae aggregate in surface or bottom waters based on water temperature and stratification (Daigle and Metaxas, 2011). Gastropod and oyster larvae sink or actively dive when encountering turbulence (Fuchs et al., 2004; Fuchs et al., 2013), a behavior that has been suggested to increase shoreward transport in the surf zone (Fujimura et al., 2014; Morgan et al., 2017).

The timing and strength of internal waves, including the internal tide, can be highly variable due to interactions with ambient stratification and velocities (e.g., Nash et al., 2012). Nonetheless, internal waves with frequency on the order of local buoyancy are common in stratified, shallow coastal waters, where waves are refracted by the sloping bathymetry and propagate largely in the onshore direction (incidence angles $< 25°$) (Richards et al., 2013; Colosi et al., 2018; Sinnett et al., 2018).

Many studies that focus on internal wave transport have considered water parcels; such studies apply to passive organisms, but not to swimming organisms (e.g., Wunsch, 1971; van den Bremer et al., 2019; but note the exceptions of Dewar, 1980 and Franks et al., unpubl.). Using linear wave theory in the absence of background velocities, Franks et al. (unpubl.) showed that both the direction and magnitude of transport experienced by passive and swimming organisms in internal waves depended on the organisms' depths and vertical swimming velocities. Sinusoidal, linear internal waves alone, however, are not expected to induce significant net transport: positive velocities are matched in magnitude by negative velocities, and integrate to zero at a fixed depth. In these waves, any net transport can thus be attributed to Stokes drift (Thorpe, 1968; Dewar, 1980). Unlike linear internal waves, the wave velocities associated with highly nonlinear internal waves of depression are both larger in magnitude as well as persistently in the direction of the wave's propagation at the surface, i.e., onshore for onshore-propagating waves, and negative/offshore at depth

(Apel et al., 1985). The associated surface transports are thus expected to be greater than transports due to linear internal waves, particularly since the large isopycnal depressions drive strong surface velocities (e.g., Lamb, 1997). For instance, surface transport distances calculated for nonlinear internal wave packets on the New Jersey shelf averaged to 1-2 km, but reached as much as 10 km for a particularly large-amplitude wave event (Shroyer et al., 2010). On other continental shelves, nonlinear internal waves have been found to account for sustained horizontal transports of 0.2-0.5 m^2 s^{-1} integrated over the surface layer (Inall et al., 2001; Zhang et al., 2015).

High densities of larvae of benthic organisms can be found within $\sim$5 km of the coast (e.g., Shanks and Brink, 2005; Morgan et al., 2009), suggesting that the internal-wave-induced transport estimates reported above could be sufficient to return surface larvae to the nearshore habitat and maintain recruitment in some populations. Translating internal-wave-induced transport estimates to studies of larval displacement directly, however, is challenging because 1) estimates often focus only on wave-induced transport, not total transport, 2) the methodologies are based on passive water parcels, not swimming organisms, and 3) estimates are typically Eulerian and not along an organism's path.

To assess the total transport associated with an impinging internal wave, both the background currents and planktonic swimming must be taken into account, as they modify the residence time of organisms in a wave (Shanks, 1995; Lamb, 1997; Pineda, 1999). Internal waves and background currents, however, do not act independently: during their passage, internal waves deform the vertical structure of ambient currents (Stastna and Lamb, 2002; Klymak et al., 2006), while background currents modify the shape of internal waves and affect their propagation speeds.

Here we focus on describing a novel cross-shore transport mechanism specific to depth-keeping organisms. This mechanism was revealed by the 3-D, underwater positions collected *in situ* by our larval mimics as they encountered a weakly nonlinear internal wave.

11

Using data analyses and simple wave models, we show that the sudden increase in the mimic's cross-shore transport can be explained by the deformation of surface-intensified, onshore-flowing waters downward to the depths of the mimics. We also demonstrate that the internal wave deformation of vertically sheared background flows will influence the transport of depth-keeping organisms, but not that of non-motile organisms. Thus, where internal waves deform an onshore-flowing surface layer downward, depth-keeping has the potential to increase onshore transport of larvae, and to aid their recruitment to suitable nearshore habitats.

2.3 Materials and Methods

2.3.1 Field site

Experiments were conducted in June 2016 using small boats within 3 km of Mission Beach, California (Fig. 2.1). The coastline at Mission Beach roughly aligns in the north-south direction, and the shelf bathymetry is smooth and shore-parallel. The uniform alongshore bathymetry facilitates comparisons with simple 2-D internal wave models. These characteristics, and the proximity to Scripps Institution of Oceanography, have led to the use of the region as an internal wave laboratory for more than 50 years (Armstrong and LaFond, 1966).

Deployments targeted water depths < 30 m where trains of onshore propagating internal waves have been previously observed (Lerczak, 2000; Lucas et al., 2011a). Given the local quasi-two-layer stratification, high-frequency internal wave trains have properties that agree well with linear theory, with phase speeds on the order of 10-20 cm s^{-1} (Lerczak, 2000). The present study took place in similar conditions to previous experiments in the region.
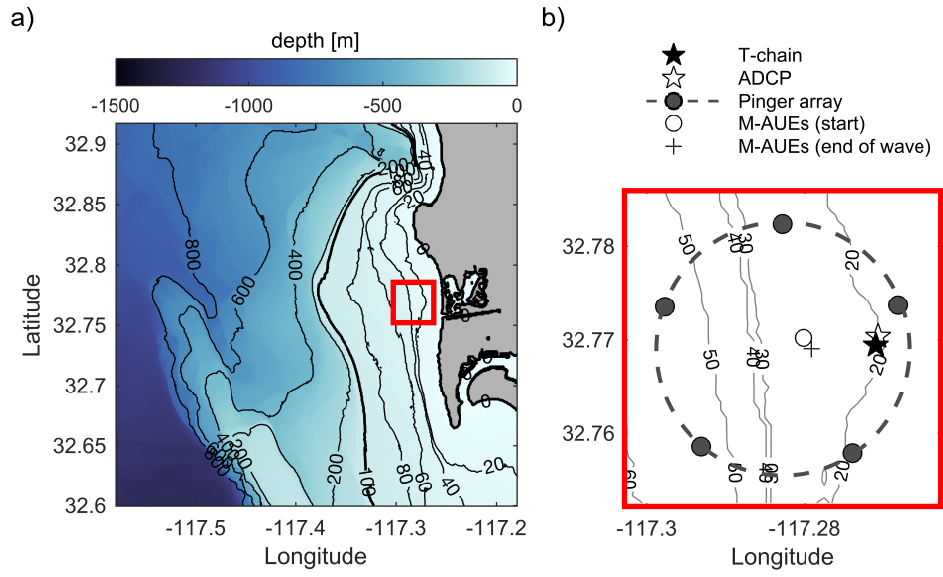
Figure 2.1: Map of field site. (a) Bathymetric contours at every 20 meters (0-100 m depth) and at every 200 meters (> 100 m depth). Red box shows location of inset (b). (b) Bathymetric contours at every 10 meters are shown, as well as locations of the T-chain, ADCP, pingers, and mean M-AUE start and end positions for the wave event described in this study.

2.3.2 Larval mimics

The Mini-Autonomous Underwater Explorers (M-AUEs) are novel subsurface vehicles designed to mimic larvae and other plankton (Fig. 2.2A): they are small (1.5 liters) and can be prescribed vertical swimming behaviors (Jaffe et al., 2017). Because the vehicles' 3-D underwater positions can be determined on spatial scales of meters and temporal scales of tens of seconds, the M-AUEs are ideal to study biological implications of high-frequency physical processes. To control their vertical positions, the M-AUEs use small piston adjustments to regulate their buoyancy relative to a target pressure/depth (Jaffe et al., 2017). The vehicles are equipped with pressure and temperature sensors to characterize their physical environment, an internal clock, and a hydrophone to record acoustic ranging pings emitted by an array of surface buoys.

In the present instance, the M-AUEs were programmed to maintain an approximately constant depth to simulate the tendency of some larvae to swim against vertical velocities,

13
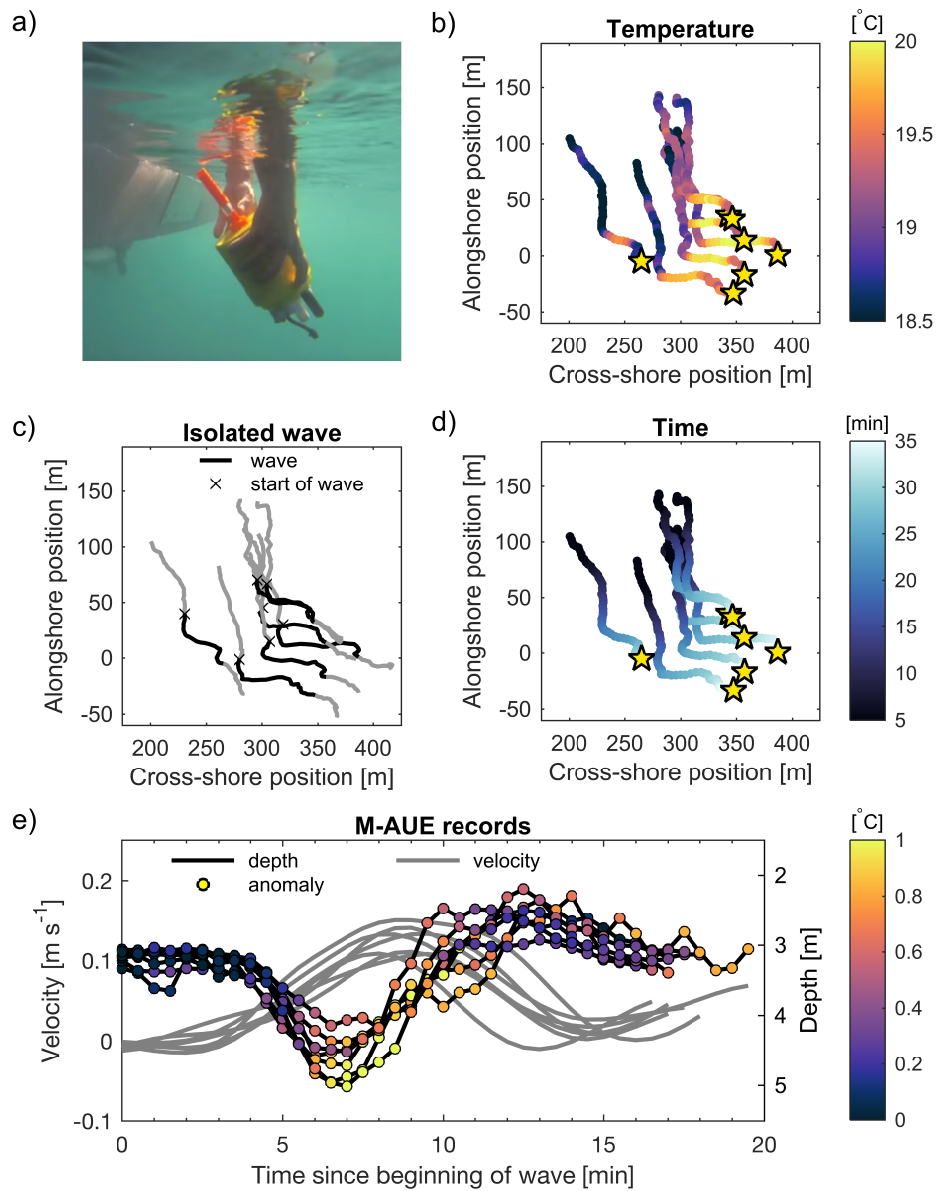
Figure 2.2: M-AUE deployment on the afternoon of June 27, 2017. (a) Underwater picture of one M-AUE being deployed from a small boat. (b) M-AUE tracks, with color showing the temperature [°C] recorded by each vehicle. Stars show the location of the M-AUEs at the end of the wave of interest. (c) M-AUE tracks showing the wave event isolated for this study in black. Black 'Xs' show the start of the wave. (d) Same as (b), but color shows time since the start of the deployment [min]. (e) Vertical displacement [m] (right axis), temperature anomaly [°C] relative to temperature recorded at the start of the wave, and smoothed cross-shore velocities [m s^{-1}] (left axis) experienced by the M-AUEs during the wave event highlighted. Time is shown from when the wave first reached each M-AUE, shown by the black 'Xs' in (c).

14

i.e., maintain depth, as inferred from cross-shore concentration surveys (Shanks and Brink, 2005), and confirmed by tracking individual plankters both *in situ* (Genin, 2005) and in a laboratory flume (DiBacco et al., 2011). Seven plankton mimics were deployed for approximately 2 hours near the surface (3-m target depth), where internal-wave-induced horizontal currents were expected to be large. To ensure the M-AUEs were above the pycnocline, the target depth was selected immediately prior to deployment based on real-time water column data transmitted via cellular network every 20 minutes from a moored, profiling Wirewalker (Rainville and Pinkel, 2001; Lucas et al., 2011a; Pinkel et al., 2011). We focus here on the analysis of one particularly well-resolved wave event on the afternoon of June 27, 2016.

2.3.3 Pinger array

The underwater positions of the M-AUEs were estimated using time-of-flight measurements of acoustic pings from a moored pinger array (Jaffe et al., 2017). Five acoustic pingers were mounted just below the water surface on separate moorings, each with continuous GPS navigation (Fig. 2.1). The pentagonal pinger array spanned isobaths from 10 to 50 m, and was about 3 km in diameter. Each pinger emitted a GPS-time-scheduled ping every 12 s, and pings between adjacent pingers were separated by 2 s; there was a pause of 4 s between each 5-ping sequence (Jaffe et al., 2017). The horizontal positions of the M-AUEs deployed inside the pinger array were then calculated post-deployment by trilateration, using the time delays between ping emission and its recorded arrival time at the M-AUE (Jaffe et al., 2017). Under optimal conditions the horizontal position of each mimic could be obtained every 12 seconds. However, the noise from the M-AUE piston motor occasionally obscured the recorded ping, reducing the temporal resolution of the M-AUE navigation. Keeping only the sequences for which all 5 pings were properly recorded resulted in successful localizations every 12 seconds more than 50% of the time.

Overall, vehicles were located on average every 19-25 seconds, so their positions were interpolated to a common time vector with 30-second time intervals. Vehicle velocities were derived from the tracks, and smoothed with a LOESS filter (Cleveland and Grosse, 1991) and a 12.5-minute window. The precision of the position estimates varied from one vehicle to the other and depended on sea state, but using an error of +/- 5 m horizontally encompasses > 95% of the residuals in estimated distance from each pinger, based on a test deployment that presented more localization issues (not shown). Residuals were calculated by subtracting the distances between each pinger and vehicle, estimated by trilateration, from the distances calculated using the time delays. The 2-hour duration of the M-AUE swarm deployment was set by the time it took the M-AUEs to drift out of the 3-km wide pinger array, as estimated from initial test deployments.

2.3.4 Moorings

To characterize the physical and hydrographic environment, an acoustic Doppler current profiler (ADCP) and thermistor chain (T-chain) were deployed within the pinger array in 20 m of water (Fig. 2.1). The bottom-mounted, upward-looking five-beam Teledyne RD Instruments Sentinel V ADCP sampled at 2 Hz with vertical bin sizes of 0.25 m. Adjacent to the ADCP was a taut mooring T-chain with 15 RBRsolo temperature sensors secured every meter along a line; at the top and bottom positions were Sea-Bird Scientific SBE-56 temperature sensors, while the middle position held an RBRduo temperature /pressure recorder. The ADCP and T-chain were deployed on the same isobath and were separated by 25 m in the cross-shore, and 105 m in the alongshore direction. The T-chain was configured to be taut relative to the bottom, and thus in the same frame of reference as the ADCP. Because the M-AUEs referenced their depth relative to the surface, which varies relative to the bottom as a function of the surface waves and tide, both the ADCP velocity records and the T-chain measurements were converted from distance above the bottom to

depth below the surface. The velocity data were then linearly interpolated to a fixed-depth grid, with a vertical resolution of 0.25 m, and filtered in both the forward and backward direction, with a moving average window of 60 s in time, and 3 bins in depth. This filtering method was selected to avoid phase distortion of the signal. Temperature data for each T-chain logger were filtered using a 10-s moving average filter, and decimated to a common 10-s time vector before also being linearly interpolated to the same fixed-depth grid as the velocity data. Isotherm depth was estimated using linear interpolation between sensors. Because there was a small horizontal offset, the temperature and velocity time series of the moorings were aligned based on their respective internal wave arrival time.

Minute-averaged wind data were obtained from the Scripps Pier weather station, located 25 km to the north of the site, as measured with a RM Young 05106 anemometer and recorded using a Scripps DL4 Hydroclimate data logger.

2.3.5   Wave model

The Kortewe-de Vries (KdV) equation is one of the models commonly used to study shallow-water, weakly nonlinear internal waves (reviewed in Apel, 2002) . The better-known solitary wave solution to the KdV equation describes weakly nonlinear, nonsinusoidal internal waves. Cnoidal functions, cn, can be used to extend the KdV solutions to oscillatory waves with a broader range in nonlinearity (Apel, 2002):

$$\eta\left(x, z, t\right) = \eta_c + \eta_{max}\phi\left(z\right)\operatorname{cn}^2\left(\gamma\left(x - ct\right); m\right) + d \tag{2.1}$$

where η_c is the crest elevation [m], η_{max} is the maximum isopycnal displacement [m], $\phi\left(z\right)$ is the wave's vertical structure function, c is the wave propagation speed [m s^{-1}], t is time [s], m is the modulus of the Jacobi function cn, d is the mean value of η over a period, and

$$\gamma = \frac{\alpha \eta_{max}}{12 m \beta}. \tag{2.2}$$

In this case, x [m] is positive in the direction of wave propagation, and z [m] is positive up. Both the crest elevation and the wave propagation speed can be related to the complete elliptical integrals of the first and second kind, $K(m)$ and $E(m)$ respectively:

$$\eta_c = \frac{\eta_{max}}{m} \left(1 - m - \frac{E(m)}{K(m)} \right), \tag{2.3}$$

$$c = c_0 + d\alpha + \frac{\alpha \eta_{max}}{3} \left(\frac{2-m}{m} - 3 \frac{E(m)}{mK(m)} \right). \tag{2.4}$$

Given this solution, the wavelength $\lambda = 2K(m)/\gamma$, with period $T = \gamma/c$.

As presented by Shroyer et al. (2009) and Grimshaw et al. (2004), the nonlinear and dispersive coefficients, α and β respectively, can be calculated from the linear wave propagation speed, c_0, and a background velocity profile, u_B, using

$$\alpha = \frac{3 \int_{-H}^{0} (c_0 - u_B)^2 \left(\frac{\partial \phi(z)}{\partial z} \right)^3 dz}{2 \int_{-H}^{0} (c_0 - u_B) \left(\frac{\partial \phi(z)}{\partial z} \right)^2 dz} \tag{2.5}$$

$$\beta = \frac{\int_{-H}^{0} (c_0 - u_B)^2 \phi(z)^2 dz}{2 \int_{-H}^{0} (c_0 - u_B) \left(\frac{\partial \phi(z)}{\partial z} \right)^2 dz}. \tag{2.6}$$

Here, $\phi(z)$ and c_0 were calculated from our observed background stratification and velocities using Smyth et al.'s (2010) Taylor-Goldstein equation solver, following the method of Shroyer et al. (2011). Because the profiling Wirewalker showed that temperature dominated the vertical and temporal variability of density (not shown), we calculated the background stratification from temperature using a salinity of 33.5. The ADCP did not cover the top 3 m of the water column, so we varied the extrapolation of cross-shore velocities to the

surface until the KdV flow field best matched the distribution and magnitude of cross-shore velocities measured at 3-m. We set d to zero, and used the computed values for c_0, α, and β, as well as our observed η_{max} and T to estimate m numerically.

Wave-induced velocities are commonly defined as velocity anomalies relative to the unperturbed background velocity profile (e.g., Stastna and Lamb, 2002), i.e., they include contributions from the propagating wave and the deformation of background velocities. We separate the wave- and background-velocity contributions to total velocities by using a tilde to denote the velocities associated with the deformed background profile $(\tilde{u}_B, \tilde{w}_B)$ and reserve u_B for the un-deformed background profile ahead of the wave (Fig. 2.3). We calculate the wave velocities (u_W, w_W) by subtracting background velocities interpolated along isopycnals from total velocities (u_T, w_T) (Shroyer et al., 2010):

$$u_W = u_T - \tilde{u}_B \tag{2.7}$$

and

$$w_W = w_T - \tilde{w}_B \tag{2.8}$$

where $\tilde{u}_B(z) = u_B(z - \eta)$, and $\tilde{w}_B = 0$ due to negligible background vertical velocities.

2.3.6   Modeled organisms

To assess the effects of vertical swimming on horizontal transport, we introduced virtual organisms into the theoretical wave flow field. These organisms covered a range of swimming strategies, going from 1) Passive/Lagrangian, i.e., they were advected by the wave and background horizontal and vertical velocities, to 2) Depth-keeping, i.e., they exactly countered external vertical velocities, but were advected by horizontal velocities (see Scotti and Pineda, 2007 for comments on depth-keeping vs. directed swimming).
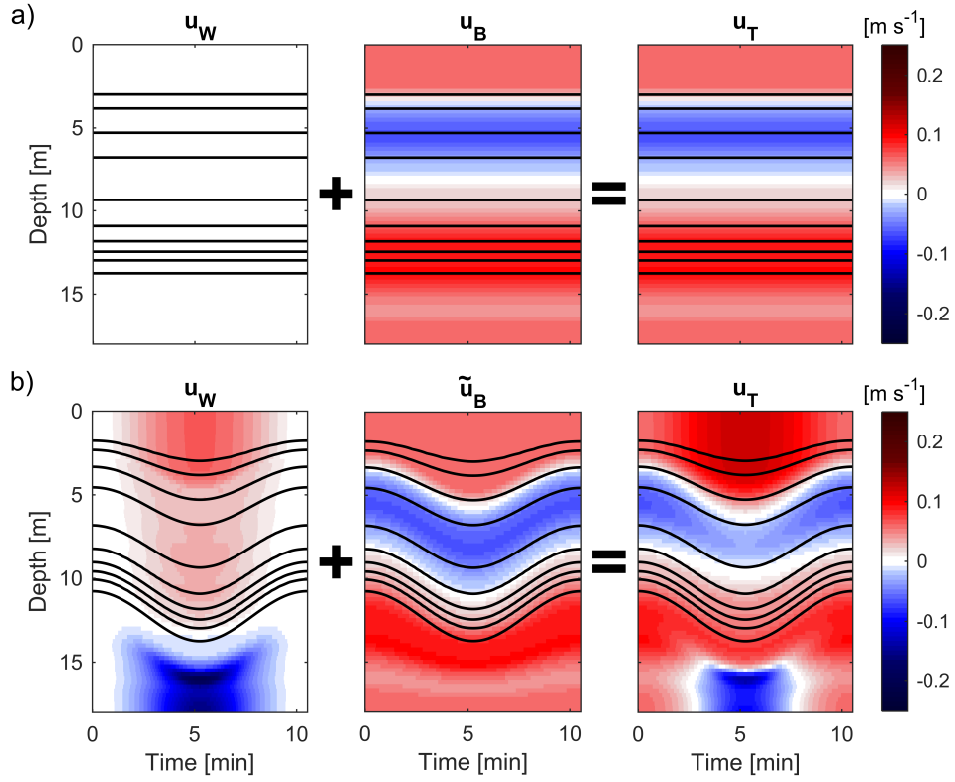
Figure 2.3: Wave and background contributions to total cross-shore velocities, u_T [m s^{-1}]. a) Unperturbed background, u_B. b) Wave event, with u_W showing the wave velocities and $\tilde{u}_B$ the deformed background velocities. Black lines show isopycnals and red is positive onshore.

2.4   Results

2.4.1   M-AUE transport

The M-AUE records revealed a 15- to 20-minute time period with elevated temperatures that coincided with the M-AUEs' downward displacements and increased horizontal velocities onshore (Fig. 2.2). These data are consistent with an internal wave of depression propagating through the swarm, as the downward isotherm displacement will draw warm near-surface water past the depth-keeping M-AUEs. However, the M-AUEs were not perfectly depth-keeping, as can be seen by the ~ 1 m vertical excursions in Fig. 2.2E. Noting that the M-AUEs exhibited a time lag in their response to vertical displacement by the wave (Fig. 2.2E), and assuming that the wave's downward and upward vertical velocities were equal (as would be the case with a sinusoidal wave), the M-AUEs' maximum swimming speeds were estimated by subtracting their upward and downward velocities. Overall, the M-AUEs' vertical swimming velocities were < 0.15 cm s^{-1}.

As the wave trough passed, the 7 M-AUEs were advected onshore, with net cross-shore displacements ranging from 30-70 m (mean of 50 m). None of the M-AUEs returned to their initial horizontal locations after the wave's passage (Fig. 2.2B, D), as would be expected in a linear internal wave without background currents. Because the Stokes drift in linear internal waves tends to be small compared to transport by strongly nonlinear waves (Lamb, 1997), a reasonable hypothesis would be that a nonlinear internal wave moved the M-AUEs onshore. However, the maximum isotherm displacement during wave passage was small compared to the water depth ($\sim$10-15%), consistent with a linear or weakly nonlinear wave. These observations suggested that some other mechanism contributed to the observed cross-shore transports.

Table 2.1: Total cross-shore transport experienced by depth-keepers at 3-m depth, over a wave period. Values are positive onshore.

Source of estimate	Δx [m]	τ [min]
M-AUEs (n = 7)	30-70, mean of 50	15-20
KdV simulation		
Full simulation, $u_W + \tilde{u}_B$	95	17
Using wave velocities alone, u_W	25	12
Using background velocities alone*, u_B	25	17*
ADCP		
Integrated	55	10.5
Propagated with $c = 0.3$ m s^{-1}	90	15

Time of integration determined by residence time in the full wave.

2.4.2 Background velocities

A spectral analysis of our ADCP time series of cross-shore velocities showed that variance was elevated in both the near-f and M2 tidal frequency (Fig. 2.4). A band-pass filter centered between 1/14.5 and 1/11 cycles per hour was used to isolate the M2 velocities (Lerczak, 2000). Over the 14-day period, depth-independent (barotropic) cross-shore tidal velocities reached a maximum of 0.03 m s^{-1}, while the amplitude of the mode-1 baroclinic (internal) tide reached a maximum of 0.08 m s^{-1} (Fig. 2.5E). Although the barotropic tidal velocity was onshore during the M-AUE deployment, baroclinic velocities in the upper half of the water column were negative (offshore), and background cross-shore velocities at 3-m depth were only 0.02 m s^{-1} (Fig. 2.5C). Ambient velocities alone can, therefore, only account for roughly half of the ∼50-m mean M-AUE cross-shore transport (Table 2.1). The observed background velocity profile was within the variability of hourly-averaged currents measured throughout the 14-day deployment (Figs. 2.5C, 2.6).
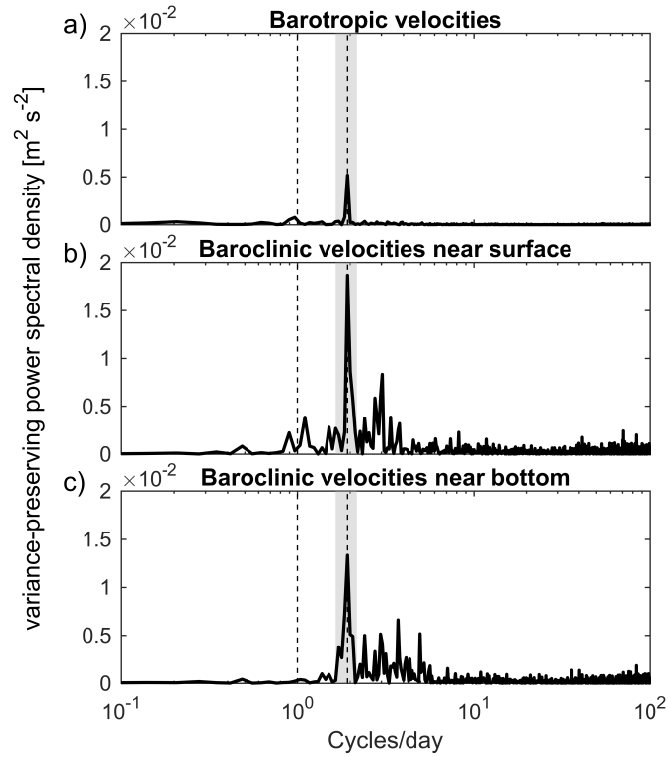
Figure 2.4: Variance-preserving power spectral density [m^2 s^{-2}] of total cross-shore (a) barotropic velocities, (b) baroclinic velocities near the surface (z = -4 m), and (c) baroclinic velocities near the bottom (z = -18 m). The dashed lines show the diurnal and M2 frequencies, with the frequency band used to isolate the M2 tide (Fig. 2.5E) in grey.

23
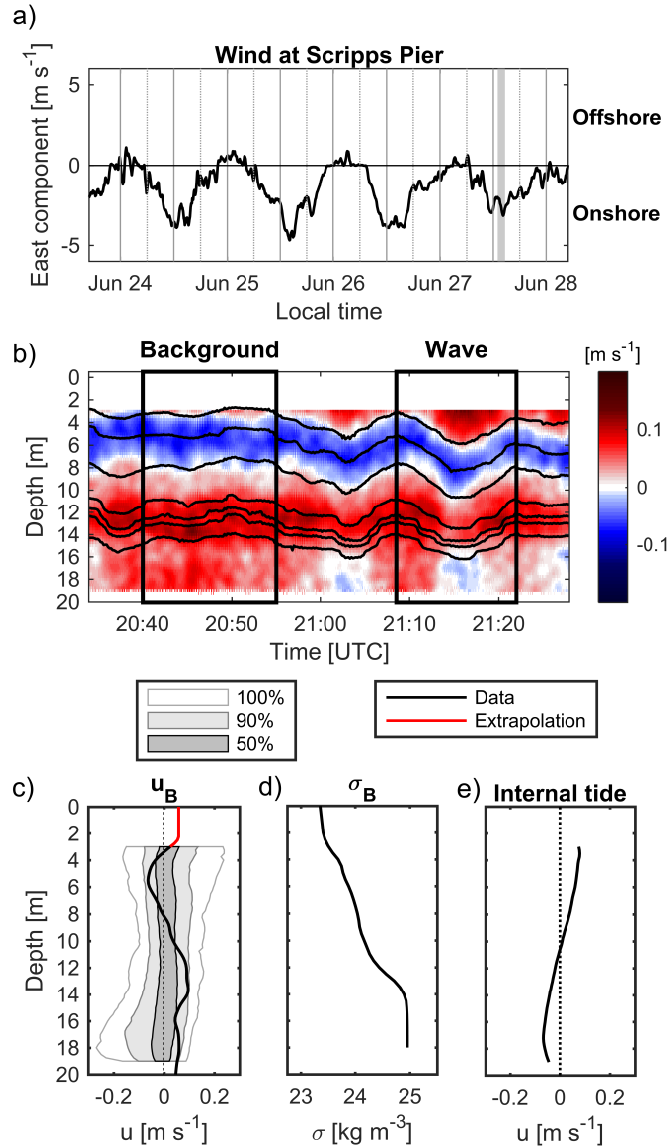
Figure 2.5: Wave and background flow properties. (a) Thirty-minute moving average of east component of the wind [m s^{-1}] measured at the Scripps Pier. Negative values indicate wind blowing from the west (i.e., onshore). The M-AUE deployment time is shown by the grey box. (b) ADCP time series. The black rectangles show the wave of interest (right box), as well as the time period over which the mean background velocity and stratification profiles were calculated (left box). (c) Mean cross-shore background velocities [m s^{-1}], calculated every 0.25 meters (black line), and extrapolation of background velocities to the surface, as described for the KdV 2 model (red line) (Fig. 2.7). The shaded areas show the envelopes containing 100%, 90% and 50% of the low-pass filtered velocity data (< 1 cycle per hour) shown in Fig. 2.6. The dotted line shows no cross-shore velocity. (d) Background stratification [kg m^{-3}]. (e) Maximum cross-shore velocity amplitude of the M2 baroclinic tide. This vertical structure explains 85% of the M2 baroclinic variance. The dotted line shows no cross-shore velocity.

24
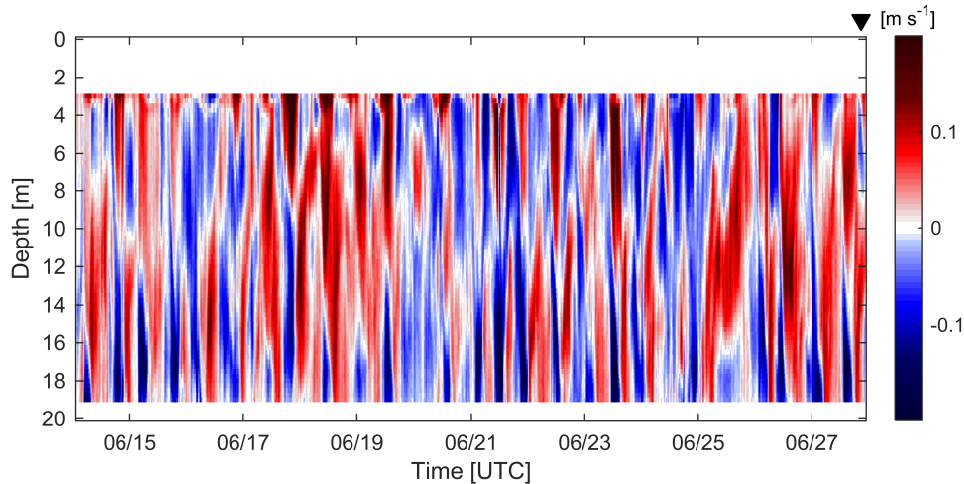
Figure 2.6: Low-pass filtered (< 1 cycle per hour) cross-shore velocities [m s^{-1}] measured at the ADCP during the full 14-day deployment. The black triangle shows the time of the M-AUE deployment. Positive velocities are onshore.

2.4.3 Wave event

Nearly 50 minutes after propagating through the M-AUE swarm, the internal wave event was recorded at both the ADCP and T-chain (Fig. 2.5B, **Wave**). Based on these arrival times and the 10.5-min wave period, T, measured at the ADCP, the wave's cross-shore propagation speed, c_p, and its cross-shore wavelength, λ, were estimated to be 0.3 m s^{-1} and 190 m, respectively. At the T-chain, the wave had a maximum isotherm displacement of $\sim$3 m. Although an internal wave appears to have preceded the wave of interest (Fig. 2.5B), we focus on the second wave because of its stronger and more complete signal in the M-AUE record.

Prior to the wave's arrival, background cross-shore velocities were negative/offshore between $\sim$3- and 8-m depth, and positive/onshore below (Fig. 2.5B, **Background**). Background cross-shore velocities above 3-m depth appeared to be positive/onshore, possibly due to the afternoon sea breeze blowing onshore (Fig. 2.5A). As it propagated past the ADCP and T-chain, the internal wave appears to have vertically deformed this along-isopycnal, onshore background flow downwards, potentially drawing positive/onshore

25

velocities downward to depths of 6 m (Fig. 2.5B, **Wave**). The total transport experienced by the M-AUEs was, therefore, a combination of both the waves' velocities and the deformed background velocities.

2.4.4   KdV model

To address the lack of ADCP coverage in the top 3 m, various extrapolations of cross-shore background velocities toward the surface were tested to find the best match of the KdV model to observations. A constant extrapolation of background velocities measured at 3-m depth to the surface produced a wave of elevation from the KdV model (Fig. 2.7, **KdV 1**), while observations indicate that a wave of depression propagated through the M-AUEs. Experiments showed that positive, surface-intensified velocities above 3 m were necessary to reverse the polarity predicted by the model from a wave of elevation to a wave of depression such as was observed (e.g., Fig. 2.7, **KdV 2**). Testing a range of cases, it became clear that an extrapolation of the vertical shear to 2.5 m, with velocities then held constant to the surface (Fig. 2.5C), best reproduced the distribution and magnitude of cross-shore velocities measured at the ADCP (Fig. 2.8). The observed wave period was best reproduced when $m = 0.13$; however, the calculated η_c had to be set to zero for isopycnals to return to their unperturbed depths at the internal wave crests, as observed (Fig. 2.5B). It is unclear whether isopycnals did indeed return to their unperturbed depths, or if this impression was a result of the background being calculated at a time when isopycnals were raised, despite appearing flat. Nevertheless, the flow field associated with the modeled wave of depression in Fig. 2.7 (**KdV 2**) was an excellent match to observations, and subsequent references to a theoretical/KdV flow field will imply this specific solution. The 0.23 m s^{-1} wave propagation speed associated with the KdV solution selected was 25% less than the field estimate based on the wave arrival times at the M-AUEs and mooring; however, it is not uncommon for theory to underestimate wave
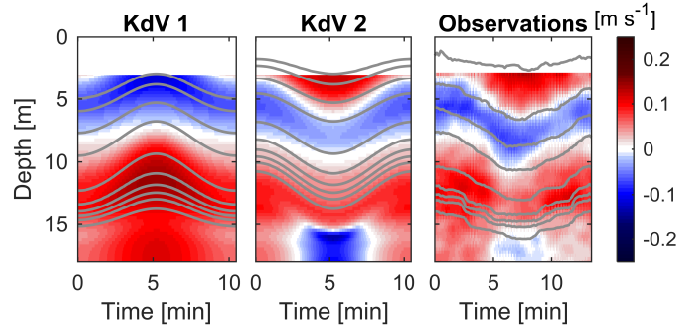
Figure 2.7: Observation and model comparisons. The background velocity profile in **KdV 1** has the velocity measured at 3-m depth held constant to the surface, while in **KdV 2** the background vertical shear measured at 3 m is extrapolated to 2.5-m depth, with velocity then held constant to the surface. Red colors are positive onshore and in the direction of the wave propagation. The grey lines show isopycnals every 0.15 kg m^{-3}.
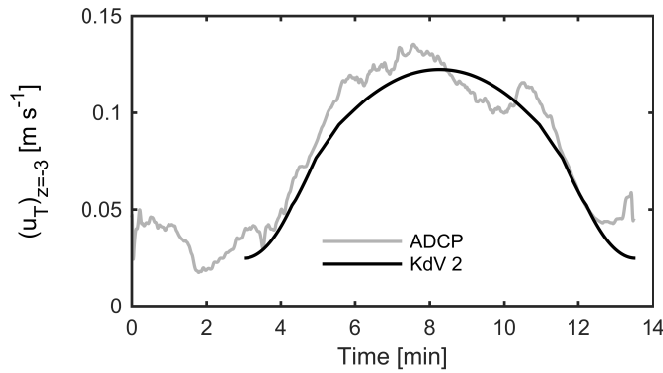
Figure 2.8: Total cross-shore velocity [m s^{-1}] at 3-m depth. The grey line shows 30-s smoothed ADCP measurements, while the black line shows the scaled KdV 2 velocities (Fig. 2.7).

propagation speeds (Lien et al., 2012). The calculated value of m was small, supporting the hypothesis that the observed wave was only weakly nonlinear.

2.4.5   Transport of modeled organisms

To estimate total cross-shore transport of organisms in the wave, virtual organisms with swimming behaviors ranging from completely passive to depth-keeping were seeded at 3-m depth in the theoretical flow fields generated from the KdV equation (Fig. 2.7, **KdV 2**).

27
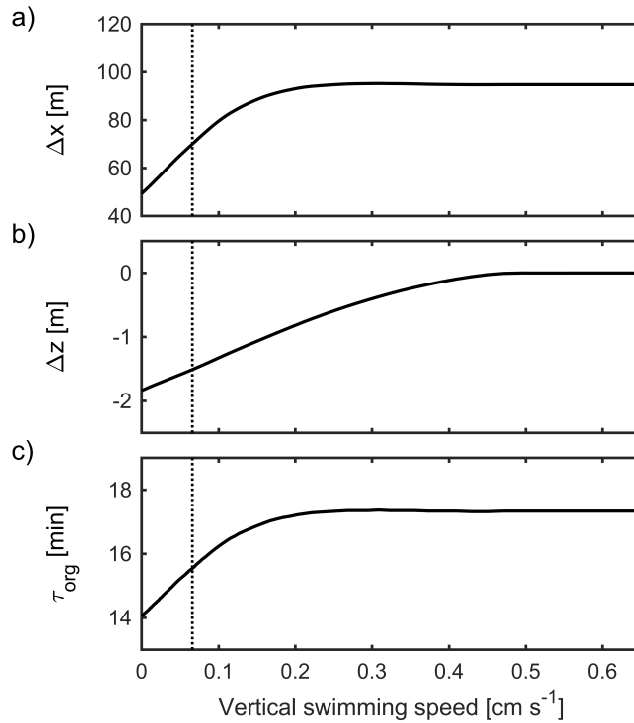
Figure 2.9: (a) Total cross-shore transport [m], (b) maximum vertical displacement [m], and (c) residence time of organisms in the KdV 2 theoretical flow field (Fig. 2.7), as a function of swimming speed [cm s^{-1}]. The dotted line shows the predicted vertical swimming speed associated with the maximum cross-shore transport experienced by the M-AUEs (70 m).

The total cross-shore transport distance experienced by modeled depth-keeping organisms was ∼95 m, with a residence time in the wave, τ, of ∼17 min (Fig. 2.9). Propagating virtual depth-keepers in the velocities captured by the ADCP during the wave event yielded a transport estimate of ∼90 m with residence time of ∼15 min, showing good agreement with the theoretical estimate.

Horizontal transport of passive organisms in the same wave flow field and depth was estimated to be ∼50 m, with a residence time of ∼14 min, while transport and residence time estimates for weak swimmers fell somewhere between those associated with passive and depth-keeping organisms (Fig. 2.9). In comparison, the total cross-shore transport of the M-AUEs ranged from ∼30-70 m (mean 50 m), with residence times from 15-20 min.
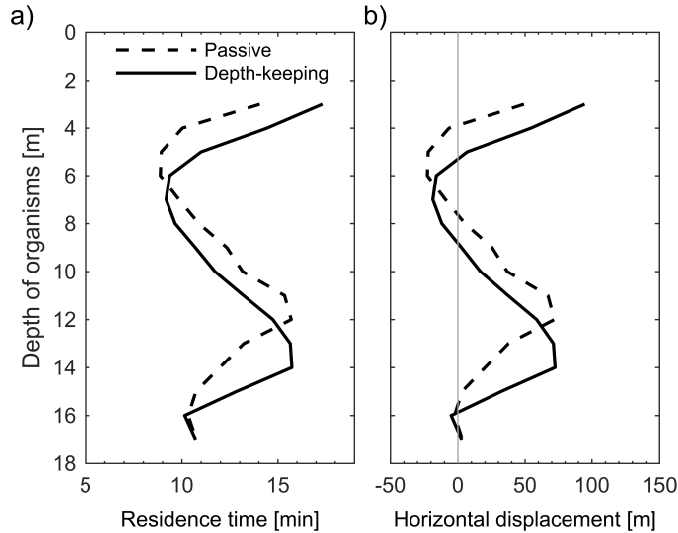
Figure 2.10: (a) Residence time [min] and (b) total cross-shore displacement [m] experienced by passive/Lagrangian (dashed) and depth-keeping organisms (solid) in the KdV 2 theoretical flow field (Fig. 2.7). Depth is based on vertical position at the crest of the waves. The thin grey line in (b) shows no net transport.

Seeding passive and depth-keeping organisms throughout the water column of the KdV flow field yielded residence time estimates ranging from 9 to 17 min, with cross-shore transport ranging from roughly -25 to 95 m onshore (Fig. 2.10).

2.5   Discussion

A drifting swarm of M-AUE larval mimics programmed to maintain 3-m depth was observed to suddenly move onshore, with net horizontal displacements of 30-70 m over 15-20 minutes. The anomalously warm waters recorded by the M-AUEs were consistent with them being transported in the trough of an internal wave. However, the amplitude of the internal wave indicated that it was not a highly nonlinear wave. Data analysis and modeling support the hypothesis that the M-AUEs were advected onshore in a combination of wave-generated currents, and wave-deformed background currents: a weakly nonlinear internal wave brought surface-intensified onshore currents down to the depths of the M-

AUEs, boosting them onshore. This mechanism not only led to enhanced onshore velocities of the M-AUEs, it also extended the time the M-AUEs spent in the wave, further enhancing their onshore transport.

2.5.1 Mechanisms of transport

As the wave of depression propagated through the M-AUEs and past the moorings, the downward deflection of the isotherms also drew the surface-intensified, along-isopycnal background horizontal velocities downward (Fig. 2.11). Above 6 m, background cross-shore velocities at any given depth were increased by this downward deformation of the fast-moving near-surface currents (Fig. 2.5B, Wave). The M-AUEs and any organisms that could maintain depth in the wave's trough thus experienced total cross-shore velocities that were a combination of the wave's velocities at that depth, and the higher background velocities, $\tilde{u}_B$, drawn downward by the wave from shallower depths. Passive organisms, on the other hand, would have felt only the wave velocities embedded in a steady background velocity. Thus, in this vertically sheared, wave-perturbed flow field, any depth-keeping behavior would have exposed organisms to non-steady, onshore, background velocities and resulted in increased cross-shore transport (Fig. 2.11).

The largest transports experienced by the M-AUEs were within the range expected for plankton with vertical swimming speeds of $\sim$0.05-0.1 cm s^{-1} (Fig. 2.9A). Swimming speeds on the order of 0.1-1 cm s^{-1} are well within the abilities of many larvae (Mileikovsky, 1973; Chia et al., 1984; Weidberg et al., 2014), and zooplankton such as the Antarctic krill (Murphy et al., 2013). With vertical swimming speeds < 0.15 cm s^{-1}, the M-AUEs are thus representative of fairly weak swimmers; stronger swimmers would have experienced even larger cross-shore transports in the observed wave. Although the maximum vertical velocities associated with the wave were $\sim$1-2 cm s^{-1}, our results show that swimming speeds of $\sim$0.25 cm s^{-1} would have been sufficient to experience the same onshore transport
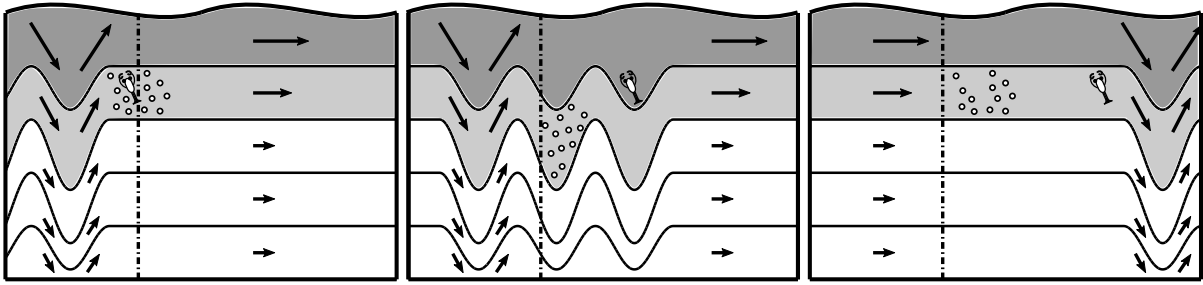
Figure 2.11: Schematic of plankton transport induced by internal-wave deformation of a surface-intensified, vertically sheared background current (black arrows and shading). As the internal wave train propagates to the right, it deforms along-isopycnal background velocities. Passive phytoplankton (circles) are moved up and down by the waves and experience constant background velocities, while depth-keeping zooplankton (lobster larva) are exposed to higher background velocities. Overall, depth-keeping plankton experience greater onshore transport than passive plankton due to both increased velocities and residence time in the waves. The black dash-dot line shows the organisms' initial horizontal position.

as the strongest depth-keepers (Fig. 2.9A).

The total cross-shore transport of any organism over a wave period, Δx_{org}, can be calculated by summing the wave's cross-shore velocities and any additional contribution to cross-shore velocities experienced over time (Lamb, 1997). In our case, we assumed no horizontal swimming, so additional contributions are limited to the background current:

$$\Delta x_{org} = \int_{t1}^{t2} \left[u_W(x_{org}, z_{org}, t) + \tilde{u}_B(x_{org}, z_{org}, t) \right] dt \tag{2.9}$$

where x_{org} and z_{org} represent the horizontal and vertical position of the organism, respectively, and $t1$ and $t2$ are times immediately as the organism enters and exits the wave, respectively. Importantly, because of the wave's deformation of the vertically sheared background current, the $\tilde{u}_B$ experienced by even weakly depth-keeping organisms will vary significantly over the wave's cycle.

An important result arising from equation (2.9) is that the total transport of planktonic organisms cannot be estimated by summing the total transport due to the wave

31

and to background currents independently (e.g., Table 2.1). Rather, equation (2.9) shows that because the background current influences the position of an organism with respect to the wave, both wave and background velocities must be integrated simultaneously along the organism's path over time. Obtaining subsurface, time-varying, 3-dimensional trajectories in the ocean at spatial and temporal scales relevant to high-frequency internal waves is technologically challenging. Using mooring (i.e., Eulerian) velocities to predict transport, however, must be done with caution. Equation (2.9) gives the velocities as experienced by the organisms; substituting a time series of measured mooring velocities for u_W and $\tilde{u}_B$ will not account for how organisms experience the flow, i.e., their residence time in various parts of the wave.

The important difference between Eulerian and Lagrangian frames of reference can be illustrated using time series from the virtual depth-keeping organisms seeded in the KdV theoretical flow field (Fig. 2.12). Though the results are specific to this simulation, the principles apply to any wave field. Integrating the total velocities as sampled by a virtual mooring at 3-m depth over a wave period (Fig. 2.12C, solid line) predicts an onshore transport of $\sim$40 m, in contrast to the $\sim$95 m transport obtained for depth-keeping organisms seeded at the same depth in the same flow. Comparing the velocity time series obtained from the mooring (Fig. 2.12C, solid line) and the velocity time series of an advected organism (Fig. 2.12B, solid line) shows the difference between the two measurements: organisms traveling with the wave spent more time in the wave's trough where the directions of the wave and background velocities aligned.

Stokes drift is derived from the difference between predictions of travel paths and Eulerian measurements over a wave period. It is important to note, however, that the duration of a "wave period" experienced by an organism is distinct from the wave period itself, and also depends on background currents. For instance, in our simulation, background currents increased the residence time of depth-keepers in the wave to $\sim$17 min (Fig. 2.3B,
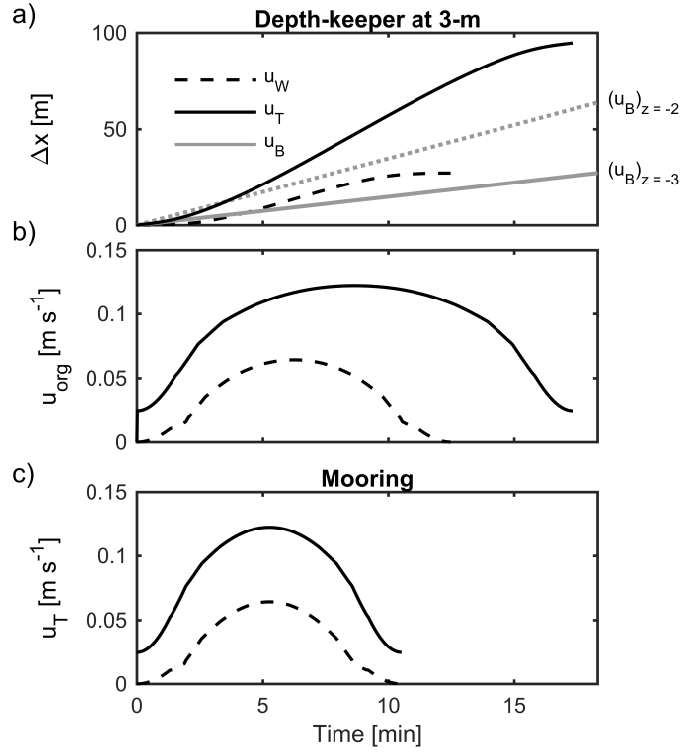
Figure 2.12: Cross-shore transport and velocity of depth-keepers and at a simulated mooring over a wave period, using the KdV 2 theoretical flow field (Fig. 2.7). (a) Cross-shore displacement of 3-m depth-keepers associated with wave velocities alone (black dashed line), and with total velocities over a wave period (black solid line). Grey lines show the displacement associated with the unperturbed background current alone, at 2-m (dotted) and 3-m (solid) depth. (b) Cross-shore velocity of 3-m depth-keepers when propagated using wave velocities alone (dashed line) and using total velocities (solid line), over a wave period. Positive velocities are onshore and negative velocities are offshore. (c) Cross-shore velocity at 3-m depth, as sampled by a mooring. Wave velocities are in dashed, and total velocities are in solid.

solid line, Table 2.1), compared with a ∼12-min residence time associated with the wave velocities alone (Fig. 2.3B, dashed line, Table 2.1). This phenomenon arises from Doppler shifting of the wave in a moving reference frame (the background current). We note that the comparisons between results derived from the full flow field vs. the wave velocities alone are for illustrative purposes and neglect the fact that without background currents, the wave shape would be different.

In general, any background current will affect the transport of both depth-keeping and passive plankton by modulating the total velocities these organisms experience. These background-influenced velocities will in turn influence the time the organisms spend in the wave. When wave propagation speed estimates can be obtained, numerically propagating virtual organisms in a wave-perturbed flow measured by an ADCP will yield better larval transport estimates than simply integrating ADCP velocities (Table 2.1). Including horizontal swimming of 1-5 cm s^{-1} in realistic numerical simulations of the central California upwelling system has been shown to increase larval supply to the nearshore (Drake et al., 2018); although neglected here, horizontal swimming in the direction of wave propagation could also enhance an organism's residence time in the wave and thus total transport (Shanks, 1995). However, we have shown that a wave-deformed, vertically sheared background current obviates the need to invoke any directed horizontal swimming by the plankton.

2.5.2 Vertical structure of velocities

Overall, transport estimates are sensitive to the magnitude, direction, and vertical structure of the background current, the period and direction of the wave, as well as plankton horizontal and vertical swimming behavior (Lamb 1997; Franks et al., unpubl.). For waves of depression, enhanced onshore transport will occur when the background currents above swimming organisms are in the onshore direction, as they were with the

M-AUEs in this study. This can be seen from the virtual organisms seeded throughout the water column in our theoretical flow field (Fig. 2.10). Because the vertical structures of both ambient and wave cross-shore velocities were not uniform, the total transport experienced by both depth-keeping and passive organisms was strongly dependent on their release depth (Fig. 2.10). The background current yielded greatest horizontal transport for depth-keeping organisms at some depths, and for passive organisms at other depths. In comparison, wave velocities alone would generate a weaker, more homogeneous horizontal transport throughout the model water column for both depth-keeping and passive organisms (Franks et al., unpubl.).

An earlier study slightly north of our field site documented cross-shore variation in concentrations of barnacle nauplii and cyprids: the concentrations of the nauplii increased with distance from shore, while the concentrations of the cyprids, which are stronger swimmers, were higher closer to shore (Hagerty et al., 2018). This pattern was consistent with other studies (Tapia and Pineda, 2007; Weidberg et al., 2014) and was more pronounced in spring-summer when stratification would support internal waves. Our observations suggest a possible mechanism driving these differing distributions: passive nauplii may experience weak onshore/offshore transport due to internal waves, while near surface depth-keeping cyprids are brought onshore by the combination of internal waves and deformed, surface-intensified background currents. Likewise, the variability in transport of surface drifters reported by Shanks (1983), which was attributed to linear versus nonlinear internal waves (Shanks, 1995; Pineda, 1999), may also have arisen from a wave-current interaction similar to that described here.

The vertical structure of background velocities will be determined by a variety of dynamics on timescales longer than the high-frequency internal waves, including the sea breeze, the internal tide, and other lower-frequency flows. In regions where the sea breeze drives a strong onshore surface flow, such as the coast of California (Hendrickson and

MacMahan, 2009), the phasing of the sea breeze, the internal tide, and high-frequency internal wave activity will vary from day to day, leading to variations in larval transport (Hill, 1998). Tapia and Pineda (2007), for instance, reported higher cyprid settlement after a day of sustained onshore winds. Alternately, where ambient velocities are predominantly driven by the internal tide, nonlinear wave trains may be phase-locked with preferentially onshore surface currents, as observed in the South China Sea (Alford et al., 2010). Prior studies at our site found cross-shore velocities on the shelf to be predominantly driven by a near-inertial response to the diurnal sea breeze and semidiurnal baroclinic tidal motions (Lerczak, 2000; Lucas et al., 2011b). Spectral analysis of our ADCP time series confirmed elevated cross-shore variability at both the near-f and M2 tidal frequencies, but the direct effects of the sea breeze could not be distinguished from higher tidal modes due to a lack of velocity data in the top 3 m.

Although this study focused on the transport implications of internal waves deforming ambient velocities specific to depth-keeping plankton, it is worth noting that the vertical structure of background velocities will also affect the shape and period of the internal waves planktonic organisms will experience (Fig. 2.7), and thus their transport.

2.6   Conclusions

A deployment of 7 subsurface vehicles, the M-AUEs, programmed to mimic planktonic depth-keeping behavior showed a pronounced onshore transport during the passage of an internal wave. *in situ* data and results from simple models showed that depth-keeping organisms can experience increased cross-shore transport through an internal wave-mediated deformation of a vertically sheared background current. By displacing isopycnals and high-velocity surface waters downward, internal wave troughs can increase both the residence time and total transport of organisms capable of even weak depth-keeping behavior.

A KdV model, parameterized with mooring data, reproduced transport of the M-AUEs remarkably well: both model and observations showed that onshore transport on the order of 100 m could take place over 15-20 minutes, as internal waves displaced faster background cross-shore surface velocities downward to the M-AUE depths. The increased cross-shore transport associated with the time-varying background velocities experienced by organisms capable of vertical swimming is mathematically analogous to the increase in onshore transport associated with horizontal swimming in strongly nonlinear internal waves (Shanks, 1995; Lamb, 1997): "residence time" in the wave is increased relative to a case without swimming or vertically sheared ambient velocities. However, to experience a similar enhancement in transport, exploiting the deformation of a strongly sheared background flow requires much weaker swimming speeds than swimming horizontally, and is thus energetically less costly to organisms.

Predictions of larval transport will be improved by quasi-Lagrangian measurements of high-frequency physical processes and better understanding of plankton swimming behaviors (Metaxas and Saunders, 2009). Given the predictability of the diurnal sea breeze in many areas – including the coast of Southern California (Dorman, 1982; Lerczak et al., 2003) – it is conceivable that populations of some organisms have adapted to exploit the interacting wind and internal wave velocity field to enhance onshore transport. Other mechanisms could be responsible for driving a vertically sheared background current in other areas; larvae located near riverine input, for instance, could maintain depth at optimum salinity concentrations and benefit from internal waves propagating offshore for dispersal (Nash and Moum, 2005). Ultimately, the direction of the transport boosts will be set by the shallower ambient currents advected by internal waves to the depth-keeping organisms.

2.7   Acknowledgements

Chapter 2, in full, has been submitted for publication of the material as it may appear in *Limnology and Oceanography*, 2019, Garwood, J.C., Lucas, A.J., Naughton, P., Alford, M.H., Roberts, P.L.D., Jaffe, J.S., deGelleke, L., and Franks, P.J.S. The dissertation author was the primary investigator and author of this paper.

Chapter 3

Larval cross-shore transport estimated from internal waves with a mean flow: the effects of larval vertical position and depth regulation

3.1 Abstract

Cross-shore velocities in the coastal ocean typically vary with depth. The direction and magnitude of transport experienced by meroplanktonic larvae will therefore be influenced by their vertical position. To quantify how swimming behavior and vertical position in internal waves influence larval cross-shore transport in the shallow ($\sim$20 m), stratified coastal waters off Southern California, we deployed swarms of novel, subsurface larval mimics, the mini-Autonomous Underwater Explorers (M-AUEs). The M-AUEs were programmed to maintain a specified depth, and were deployed near a mooring. Transport of the M-AUEs was usually onshore, with average velocities up to 14 cm s^{-1}. To put

the M-AUE deployments into a broader context, we also simulated > 500 individual high-frequency internal waves observed at the mooring over a 14-day deployment. Using the wave's and wave-deformed background currents, virtual passive and depth-keeping larvae were tracked numerically. When released at the same initial depths, depth-keeping larvae throughout the water column were usually found closer to shore than passive larvae, particularly near the top of the water column (3-5-m depth), where $\sim 20\%$ of internal waves enhanced onshore transport of depth-keeping organisms by ≥ 50 m; only 1% of waves gave similar enhancements to passive organisms. Our observations and simulations showed that depth-keeping in high-frequency internal waves resulted in enhanced onshore transport at the top of the water column, and reduced offshore dispersal at the bottom, compared to being passive. Thus, even weak depth-keeping may allow larvae to reach nearshore adult habitats more reliably than drifting passively.

3.2 Introduction

In vertically sheared estuarine and coastal currents, the vertical position and swimming behavior of larvae will influence both their direction and magnitude of cross-shore transport (Sulkin, 1984; Kunze et al., 2013). Nonlinear internal waves of depression are an example of shallow-water, vertically sheared coastal flow: above the pycnocline, wave velocities are in the direction of wave propagation, and opposite at depth (Apel et al., 1985). Larvae that adjust their depths to be above the pycnocline can therefore be transported onshore by shoreward-propagating internal waves (Shanks, 1983; Shanks, 1985; Pineda, 1999). The total transport distances experienced by larvae in a wave will be determined by the larvae's maximum horizontal velocities, along the wave propagation axis (Lamb, 1997). Not only will larger velocities lead to greater larval transport distances in a given time, but also larvae with horizontal velocities that approach the wave propagation speed will spend

more time traveling with a wave (Lamb, 1997).

Background velocities and horizontal swimming are two mechanisms that might enhance larval horizontal velocities in internal waves (Shanks, 1995). Because both wave and background velocities can exhibit vertical structure, the two velocity profiles will combine to yield transport distances that vary with depth. This internal-wave/background-current interaction is complicated by the fact that background currents influence the shapes of the internal waves (Stastna and Lamb, 2002), and internal waves deform along-isopycnal background currents (Klymak et al., 2006). In this context, we define background velocities to be the velocities that fluctuate over time scales longer than a high-frequency internal wave period (i.e., > 1 hour). These background currents could be generated by barotropic and baroclinic tides, wind forcing, and larger-scale geostrophic flows. Because fully Lagrangian/passive organisms follow isopycnals, the background velocity they experience throughout a wave remains relatively constant. However, any subsurface larva that resists the wave's vertical velocities, even weakly, will experience background velocities that vary over a wave period (Garwood et al., chapter 2).

Although only swimmers that at least partially oppose a wave's vertical velocity can regulate their depth in internal waves, passive organisms may still be able to adjust their vertical positions to some extent. For example, even in strongly nonlinear internal waves, weak swimmers such as barnacle nauplii can be found preferentially in surface waters, as opposed to bottom waters (Liévana MacTavish et al., 2016), and various larval species and sizes will occupy distinct parts of the water column (Greer et al., 2014). Here we use "depth selection" to refer to the ability of many organisms to adjust their overall vertical position in the water column. When such organisms neither swim vertically nor regulate their density over the timescale of the internal waves studied, they will be considered passive. "Depth regulation" is reserved for organisms that at least partially counter the vertical velocities of high-frequency internal waves directly; here we focus on an extreme of

depth regulation: perfect depth-keeping.

Field observations have shown that subsurface plankton, including dinoflagellates that swim vertically, can interact with internal waves (Lennert-Cody and Franks, 2002; Omand et al., 2011). Measurements collected by a swarm of novel, subsurface larval mimics, the mini-Autonomous Underwater Explorers (M-AUEs), showed that weak depth-keeping in an background flow field deformed by an internal wave could double larval cross-shore transport compared to passive organisms (Garwood et al., chapter 2). Moreover, vertical swimming speeds an order of magnitude smaller than the wave's maximum vertical velocities (~ 0.25 cm s^{-1} vs. ~ 2 cm s^{-1}, respectively) were sufficient to yield maximum transport distances (Garwood et al., chapter 2). In comparison, horizontal swimming velocities closer to 10 cm s^{-1} would have been necessary to produce a similar increase in transport.

To regulate their depths, larvae must be able to at least partially overcome a wave's vertical velocities (1-10 cm s^{-1} in high-frequency internal waves), and any existing turbulence (Kunze et al., 2013). Large, highly nonlinear internal waves have large vertical velocities and often generate turbulence (Sandstrom et al., 1989), providing a challenging environment for larvae to regulate their depths. Small, linear or weakly nonlinear internal waves, on the other hand, have relatively weak vertical velocities, allowing efficient larval depth regulation. Because weakly nonlinear internal waves are common, even though their individual flow fields may be weak, their cumulative contributions to larval cross-shore transport could be significant. However, few such estimates exist, as it is difficult to acquire *in situ* observations of the underwater transport of individual larvae over high-frequency internal-wave time scales.

To overcome this limitation and to gather direct *in situ* measurements of the internal-wave-induced transport for larvae-inspired vertical swimmers, we deployed swarms of M-AUEs in the shallow, stratified coastal waters of Southern California. To put these direct observations into the larger context of the persistent internal wave and background-

flow conditions, we simulated the transport of passive and depth-keeping larvae in > 500 individual weakly nonlinear internal waves observed at a mooring over a 2-week period. Here we show that depth-keeping in weakly nonlinear internal waves increased onshore transport at the top of the water column, while it limited offshore dispersal at depth, compared to being passive. We also show that depth-keeping in weakly nonlinear internal waves can induce cross-shore transports similar to those previously reported for passive organisms in highly nonlinear internal waves.

3.3   Materials and Methods

The field site and experimental setup were described in detail by Garwood et al. (chapter 2); only the information most pertinent to the current study is repeated here.

3.3.1   M-AUE deployments

To investigate the implications of background current and internal wave interactions on cross-shelf larval transport *in situ*, we deployed a swarm of depth-holding, trackable, subsurface larval mimics, the M-AUEs (Jaffe et al., 2017). The M-AUEs are small vehicles (1.5 L) whose 3-D underwater position can be obtained post-deployment: their vertical position are obtained from their pressure sensors, while their horizontal positions are derived from time-of-flight calculations for acoustic signals emitted by moored, GPS-localized and -synchronized pingers, which are then recorded by the M-AUEs' hydrophones (Jaffe et al., 2017). Because the M-AUEs are relatively small, can be tracked at sub-minute intervals, and localized within 5-m horizontally (Jaffe et al., 2017; Garwood et al., chapter 2), they are ideal to study the effect of submesoscale ocean processes on larvae.

From June 14-27, 2016, swarms of 3-10 M-AUEs were deployed from small boats off Mission Beach, CA up to twice daily; M-AUE mimics were individually programmed to

maintain a specific depth, ranging from 2-16 m, for 2-4 hours. The M-AUE swarms were deployed to span the main pycnocline, estimated from salinity, temperature, and pressure data relayed in real-time by a nearby Wirewalker (Rainville and Pinkel, 2001; Pinkel et al., 2011), moored on the 50-m isobath. The M-AUEs were deployed at various depths between the 25- and 30-m isobaths, with a common start time and surfacing time. At the start time, the M-AUEs reduced the volume of their external casings and sank to their target depths. The target depths were then maintained for the duration of the deployments through small piston adjustments for buoyancy regulation. At a pre-determined time, the process was reversed and the M-AUEs surfaced. They were located via radio and GPS signals, and recovered.

Underwater positions could not reliably be obtained when the M-AUEs' hydrophones were saturated by piston motor noise or heavy boat traffic. Motor noise was problematic when M-AUEs had to correct their positions more regularly, perhaps due to weaker stratification at some depths, and/or frequent/large surface swell. To maximize the number of deployments incorporated in this study, we thus rely only on the M-AUEs' GPS positions immediately prior to their dive, and immediately upon surfacing. These positions matched well with the beginning and end of the tracks for the deployments with full underwater tracking. The M-AUEs' cross-shelf displacements were calculated by differencing the two GPS readings along an axis perpendicular to the coast. In general, the M-AUEs took ∼10 minutes to sink to their target depths and stabilize their control algorithms, while they took 1-2 minutes to surface during the 2-4 hour deployments. Thus, during the bulk of the deployment, the M-AUEs were at their target depths.

3.3.2 Internal waves from time series

To characterize the hydrographic environment, a taut mooring thermistor chain (T-chain) was deployed on the 20-m isobath, next to a bottom-mounted, upward-looking

acoustic Doppler current profiler (ADCP). All instruments sampled at a rate of 2 Hz. Sea-Bird Scientific SBE-56 temperature sensors were placed at the top and bottom of the T-chain, with 15 RBRsolo temperature sensors placed every meter in between, except for an RBRduo pressure/temperature recorder at the middle position. The Teledyne RD Instruments Sentinel V ADCP had vertical bin sizes of 0.25 m. Due to surface contamination, velocity measurements were reliable only up to 3-m below the surface.

To match the frame of reference of the M-AUEs, pressure measurements were used to convert both the ADCP and temperature time series from a frame of reference above the bottom to depth below the surface. Both time series were linearly interpolated to a fixed depth grid with bin spacing of 0.25 m and 0.5 m, respectively, and decimated to a common time vector with one-minute intervals. The time series were filtered using a second-order Butterworth filter, with a frequency threshold of 1 cycle per hour to separate low- and high-frequency signals. Background conditions were calculated from the low-passed time series, while internal waves were isolated from the high-passed temperature time series.

Solitary internal waves of depression, i.e., solitons, and oscillatory internal wave troughs were identified from positive peaks in temperature anomalies (n = 3265). To eliminate instances of multiple waves traveling over each other, only single temperature peaks bounded by minimum temperature anomalies were retained (n = 1361). To limit our analyses to weakly nonlinear internal waves, we excluded waves with maximum vertical displacements, η_{max}, greater than 20% of the water column height. Waves with vertical displacements less than our T-chain vertical resolution, i.e., < 1 m were also excluded. A total of 538 weakly nonlinear internal waves were parameterized from our observations, and used in our simulations.

3.3.3 Wave simulations

Because the ADCP and thermistor chain were not precisely collocated, and the measured velocity field included non-wave induced flows, we used the Korteweg-de Vries (KdV) equation to obtain velocity fields for waves observed at the T-chain, following the method of Garwood et al. (chapter 2). To model the shallow-water, weakly nonlinear internal waves observed at our site, we used the linear limit of the cnoidal solution to the KdV equation (Apel, 2002). In this model, wave shape is described by a cosine function:

$$\eta\left(x, z, t\right) = \eta_c + \eta_{max}\phi\left(z\right)\cos^2\left(\frac{kx - \omega t}{2}\right) \tag{3.1}$$

where η_{max} is the maximum isopycnal displacement [m], η_c is an amplitude adjustment at the crests [m], $\phi(z)$ is the wave's vertical structure function, k is the horizontal wavenumber [rad m^{-1}], ω is the wave frequency [rad s^{-1}], and t is time [s]. In this case, x [m] is positive in the direction of wave propagation, and z [m] is positive up. However, to match the frame of reference of the M-AUEs, all vertical coordinates are plotted as depth.

To ensure the best match to the *in situ* flow field, parameters such as η_{max}, ω, and k were diagnosed from the observations and used to generate the waves. The wave frequency was calculated from the observed period, T, with $\omega = 2\pi/T$, while the wavenumber k was calculated from the wavelength, λ, using $k = 2\pi/\lambda$. The wave propagation speed was necessary to estimate λ. Although it could not easily be observed, the wave propagation speed of high-frequency internal waves at our site was shown to agree well with linear theory (Lerczak, 2000). Thus we used the linear wave propagation speed, c_0, which we calculated from our observed background stratification and velocities (Smyth et al., 2010). within $10 \pm 10\%$ of the KdV wave speeds. This translated to a general overestimate of the wavelengths by $10 \pm 12\%$. The calculations of the KdV internal wave speed were more sensitive to the characterization of background velocities and stratification than the

linear wave speeds. Given the uncertainty in the top 3-m velocity field, we chose the more conservative approach and used the linear wave speed. Finally, water height, H, was set to the minimal tidal height above bottom of 17.5 m, η_c was set to 0, and $\phi(z)$ to $\sin(\pi z/H)$.

For the transport calculations, local (in time) background velocity profiles, u_B, were calculated from one-hour averages of the low-pass filtered cross-shore ADCP velocity data, centered on each wave trough. The velocity profiles were extrapolated to the surface following Garwood et al. (chapter 2). Background temperature profiles were also calculated from the low-pass filtered signal, averaged over an hour centered on each wave trough. Wirewalker profiles showed that temperature dominated the variability in density; background stratification was thus calculated from temperature using the average salinity of 33.5.

3.3.4 Virtual organisms

To calculate the cross-shore larval transport associated with the combined background flows and internal waves observed, both passive and depth-keeping virtual organisms were released every meter in the vertical from 3 to 16-m depth, at the KdV wave crests. Because η_c was set to zero, as suggested by previous observations (Garwood et al., chapter 2), all simulated organisms thus started in a background flow that was unperturbed by the wave. ll simulated organisms thus started in a background flow that was unperturbed by the wave. The organisms' average total cross-shore velocity $\bar{u}_T$ and transport Δx_T were quantified for each wave. Because organisms moved with the flow, their residence time in the wave τ was not the same as the wave period T measured at the mooring; residence times also varied with depth within a single wave. Average velocities and transports were therefore assessed over the time period organisms spent in the wave, i.e., their residence time, and not the intrinsic wave period. The wave component of the average velocities $\bar{u}_W$ and transport Δx_W were calculated from the simulated total velocities and transports

by subtracting the unperturbed, background velocity at an organism's initial depth, as well as the background velocity's associated transport over the organism's residence time, respectively:

$$(\bar{u}_W)_{org} = (\bar{u}_T)_{org} - u_B(z = z_{org, t_0}) \tag{3.2}$$

$$(\Delta x_W)_{org} = (\Delta x_T)_{org} - \tau_{org} u_B(z = z_{org, t_0}). \tag{3.3}$$

where the subscript org indicates that the value is calculated for a given organism and z_{org, t_0} indicates the depth of the organism at the start of the wave t_0, i.e., the organism's initial depth.

The average wave-induced transport, as defined here, thus includes both the transport associated with the wave velocities themselves, and the transport associated with the variable background velocity anomalies experienced by depth-keeping organisms. These anomalies arise from the deformation of the background currents by the wave (Garwood et al., chapter 2).

3.4 Results

3.4.1 M-AUE cross-shore velocities

Over the 2-4 hours they were deployed, the M-AUE larval mimics showed averaged *in situ* total cross-shore velocities ranging from -0.05 m s^{-1} (offshore) to 0.14 m s^{-1} (onshore), with variability both between deployments and in depth (Fig. 3.1B). Generally, M-AUE cross-shore velocities were skewed to be onshore, with maximum velocities recorded by the shallowest M-AUEs, i.e., those programmed to maintain depth 3-m below the surface. Although background velocities measured at the ADCP during each M-AUE deployment
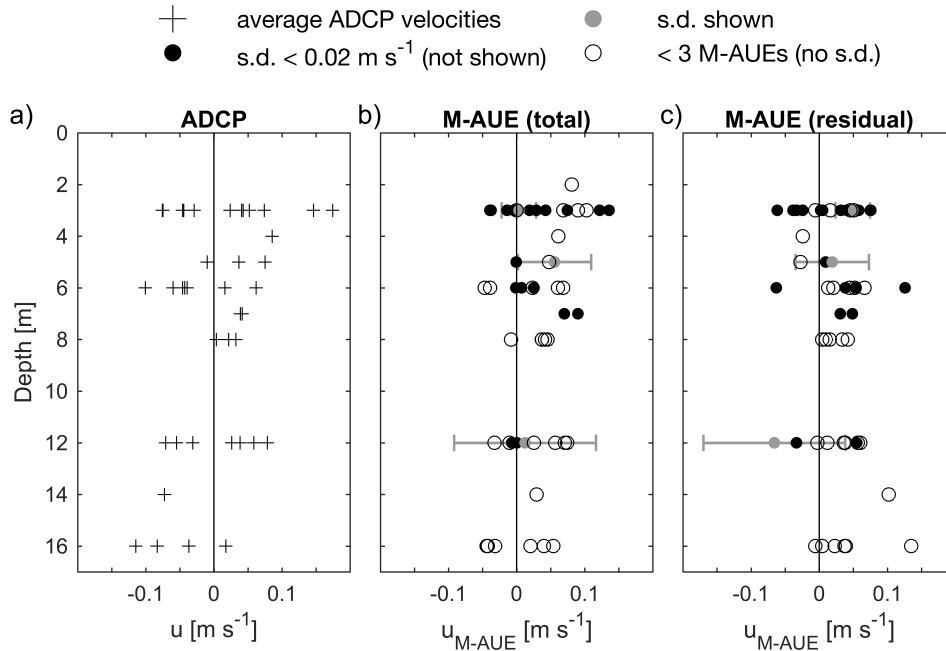
Figure 3.1: Averaged cross-shore velocities measured during 14 *in situ* deployments. Crosses show the average ADCP velocity at each depth where M-AUEs were deployed. Filled dots show data points obtained from at least 3 M-AUEs; black/grey dots have standard deviation less/more than 0.02 m s^{-1}. Black error bars were omitted for clarity. Empty circles show data points obtained from less than 3 M-AUEs. Positive velocities are onshore. (a) Average ADCP cross-shore velocities [m s^{-1}], (b) total M-AUE cross-shore velocities [m s^{-1}], and (c) residual M-AUE cross-shore velocities [m s^{-1}] after the average background velocities at each M-AUEs' depths were subtracted.

were predominantly onshore in surface waters, and offshore at depth (Fig. 3.1A), the median M-AUE velocities in excess of background currents (residual) were ~2-3 cm s^{-1} onshore throughout the water column (Fig. 3.1C).

3.4.2   Total transport and velocities

Overall, 538 weakly nonlinear internal waves were isolated from a 14-day time series of temperature measurements at a moored T-chain. Depth-keeping and passive organisms were seeded every meter vertically in wave flow fields parameterized using the observed properties of each of these waves - including the background currents. Predicted cross-shore
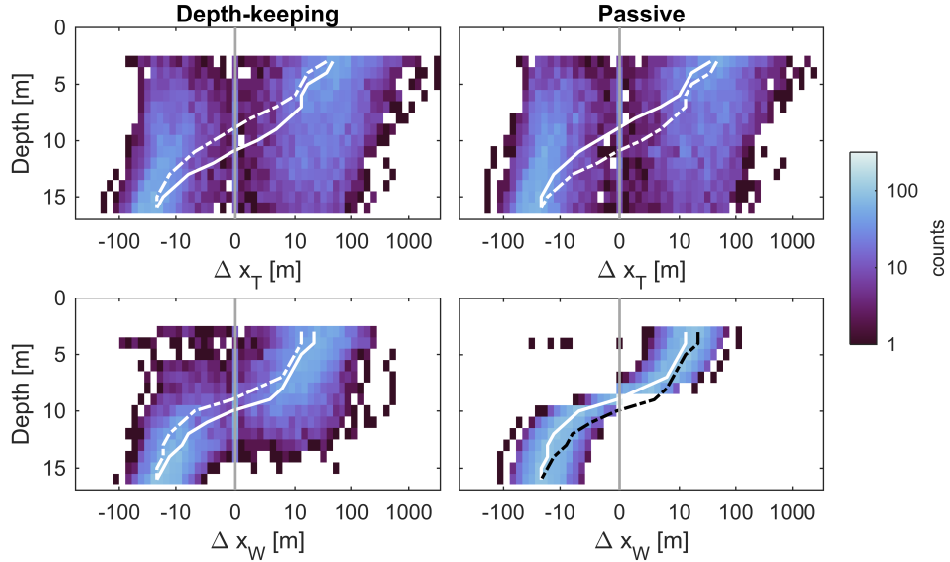
Figure 3.2: (Top) total and (bottom) wave-induced cross-shore displacement [m] for both (left) depth-keeping and (right) passive organisms in the simulated weakly nonlinear internal waves observed (n = 538 waves, 14 depths). The logarithmic colorbar shows the number of counts in each bin. Bins are linear in ±logarithmic space, with values from ±1 m binned as 0; the grey vertical lines shows 0 net transport. The white lines show median values on each plot; the dash-dot lines show the median values for the other swimming strategy.

transports over the organism's residence time τ in individual waves ranged from -200 m (offshore) to more than 3000 m (onshore) (Fig. 3.2, top row). Above mid-water (upper 8 m), depth-keeping organisms were transported onshore in 71% of the waves, while only 64% of waves transported passive organisms onshore. Furthermore, onshore transport of depth-keeping organisms was favored over a broader depth range (upper 11 m), compared to passive organisms (upper 8 m) (Fig. 3.2, top row). The largest onshore transport estimates occurred closer to the surface, and the lowest estimates near the bottom, where transports were often offshore.

Averaged cross-shore velocities calculated over the time period organisms spent in the wave ranged from -0.3 m s^{-1} to 0.25 m s^{-1} (Fig. 3.3, top row), again with larger, positive estimates closer to the surface and lower, negative estimates near the bottom. On average, the velocity of depth-keeping organisms were 1 cm s^{-1} more positive than passive
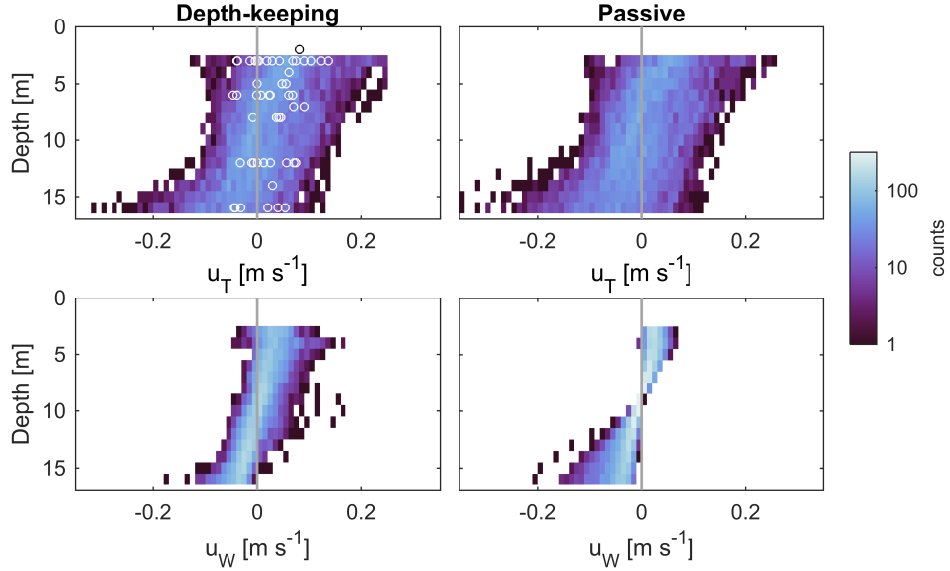
Figure 3.3: (Top) total and (bottom) wave-induced cross-shore velocities $[\text{m s}^{-1}]$ for both (left) depth-keeping and (right) passive organisms in the simulated weakly nonlinear internal waves observed (n = 538 waves, 14 depths). The logarithmic colorbar shows the number of counts in each bin. Bins are 0.01 m s^{-1} in size. Open circles show the M-AUE data, while the grey vertical line shows no velocities.

organisms, implying a faster onshore transport in surface waters, and a slower offshore transport at depth. This difference could reach nearly 4 cm s^{-1} for 10% of the waves. The *in situ* velocities measured by the M-AUEs (Fig. 3.3, open circles) fell well within the range of simulated total velocities, although the M-AUEs appear to have experienced preferentially positive (onshore) velocities.

In most simulations, virtual larvae spent more time in the wave than it took the wave to propagate through the mooring, i.e., $\log_{10} \tau/T > 0$ (Fig. 3.4). The frequency distribution of this ratio was shifted to the right for depth-keeping organisms compared to passive organisms, indicating that depth-keeping organisms spent, on average, more time in the waves (Fig. 3.4).

Compared to passive organisms in these wave-background flow systems, depth-keeping organisms thus experienced more frequent onshore transport in the upper water column, slightly greater onshore velocities, and longer residence times in the waves.

51

3.4.3   Wave-induced transport and velocities

Wave-induced cross-shore transport distances (3.3) were calculated by subtracting the unperturbed background transport from the total transport. Averaged, wave-induced cross-shore velocities ranged from -0.2 to 0.2 m s^{-1} (Fig. 3.3, bottom row). Minimum wave-induced cross-shore transport distances were on the order of -100 m (offshore), while maximum values were closer to 100 and 500 m (onshore) for passive and depth-keeping organisms, respectively (Fig. 3.2, bottom row). In general, both passive and depth-keeping organisms experienced positive, wave-induced onshore transport in the upper water column, and offshore transport below; net onshore transport extended deeper for depth-keeping organisms (10 m) than for passive organisms (8 m) (Fig. 3.2). Estimates for depth-keeping organisms had higher variance than those calculated for passive organisms (Fig. 3.2).

Positive, onshore total transport was often associated with positive, onshore wave-induced transport, and vice-versa, although total and wave-induced transports in opposite directions were also seen (Fig. 3.5). The wave-induced transport represents the wave's *enhancement* to transport, as a large total transport value could be due to a weak wave in a strong background flow (small $\Delta x_W/\Delta x_T$) or a strong wave in a weak background flow (large $\Delta x_W/\Delta x_T$) (Fig. 3.5). Because waves sometimes countered background velocities, wave-induced transports that were higher than total transport were also seen (Fig. 3.5). For example, in cases in which total transport was negative (offshore), positive wave-induced transports reduced the offshore advection of organisms, and thus contributed to nearshore retention.

3.4.4   Depth-keeping vs. passive organisms

Depth-keeping organisms throughout the water column experienced more waves that caused positive (onshore) total and wave-induced transports than passive organisms
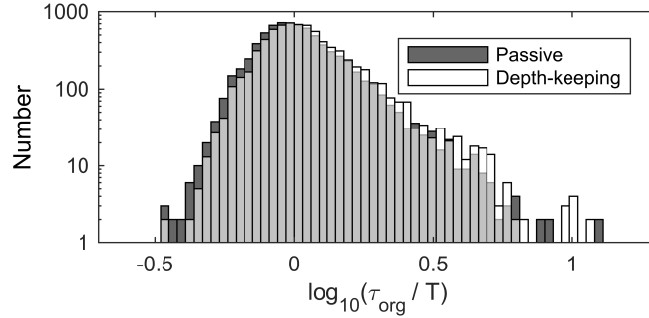
Figure 3.4: Frequency distribution of the ratio of residence time (τ_{org}) and wave period (T), log-transformed, for each virtual organism. Passive and depth-keeping organisms are in dark grey and white, respectively, with regions of overlap in light grey. Note that the frequency distribution for depth-keeping organisms appears shifted to the right compared to passive organisms, indicating that depth-keepers spent, on average, more time in the waves. Wave periods varied from 3-22 minutes.

(Fig. 3.6A (depth-keeping) and B (passive)). For depth-keeping organisms, 39% of the observations showed $\Delta x_T > 0$ and $\Delta x_W > 0$, while this occurred only 30% of the time for passive organisms. Of all the waves simulated, 29% induced transports of depth-keeping organisms with $\Delta x_W \geq 50$ m with $(\Delta x_W / \Delta x_T) \geq 10\%$ for at least one depth of the water column (Fig. 3.6, dashed-dot section). In comparison, only 1% of the waves induced similar transport in passive organisms (Fig. 3.6B, Table 3.1). These large wave-induced onshore transport occurred primarily in the top 5 m of the water column (Table 3.1).

Overall, for the same initial depth in a wave, depth-keeping significantly enhanced onshore transport and/or nearshore retention throughout the water column, compared to drifting passively (Wilcoxon signed rank test, p-value < 0.01 at all depths) (Fig. 3.7A). This was particularly true 3-4 m below the surface, where 10% of the waves transported depth-keeping organisms at least 70 m closer to shore than passive organisms (Fig. 3.7A, yellow line).

The maximum vertical velocities resisted by perfect depth-keeping organisms were generally < 1 cm s^{-1}, although they could reach as high as 4.5 cm s^{-1} (Fig. 3.7B). Because wave vertical velocities decrease towards the surface and bottom boundaries, the swimming
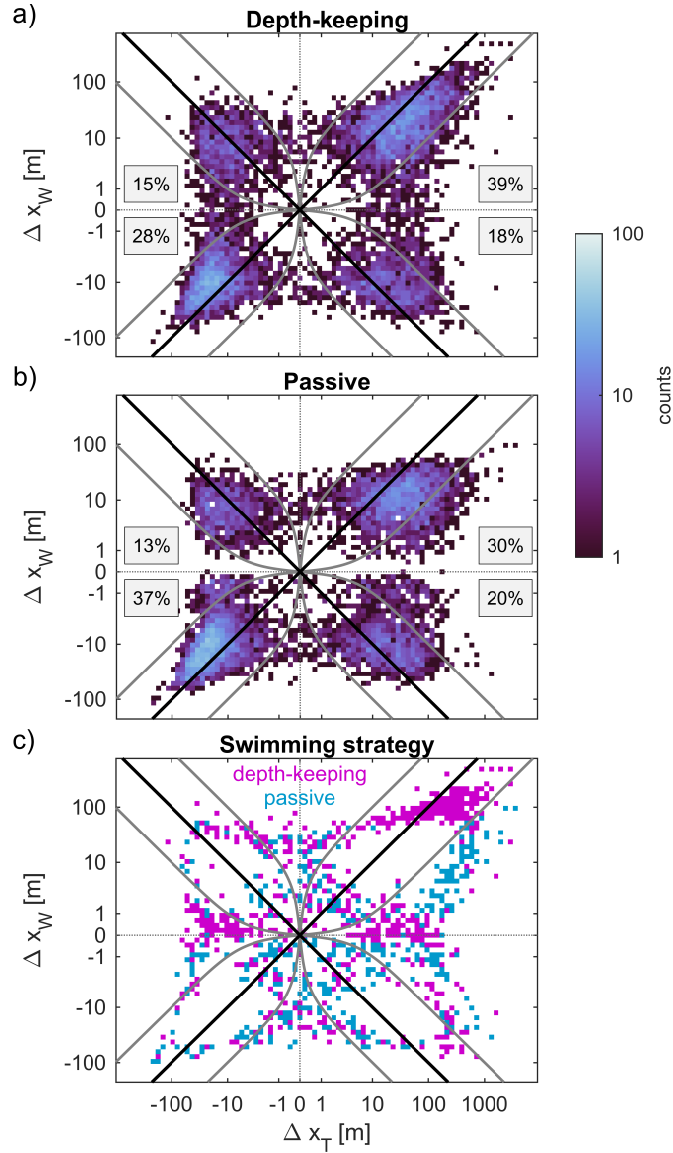
Figure 3.5: Wave-induced and total horizontal displacements [m] for (a) depth-keeping organisms and (b) passive organisms in the simulated weakly nonlinear internal waves observed (n = 538 waves, 14 depths). The logarithmic colorbar shows the number of counts in each bin. (c) Parameter space where only (pink) depth-keeping or (teal) passive organisms were reported. The black line shows where waves were responsible for the total transport calculated. The grey line shows where wave-induced transport is 10% and 1000% that of total transport, i.e., where $\Delta x_W / \Delta x_T = 0.1$ and 10, respectively. Note that waves can contribute more than the total transport when they oppose background velocities, e.g., a wave can transport organisms 100 m onshore, while background currents transport them 90 m offshore, for a total transport of 10 m. This can also lead to wave and total transports of opposite signs. In all plots, displacement bins are linear after an asinh( ) transformation. Positive values are onshore.
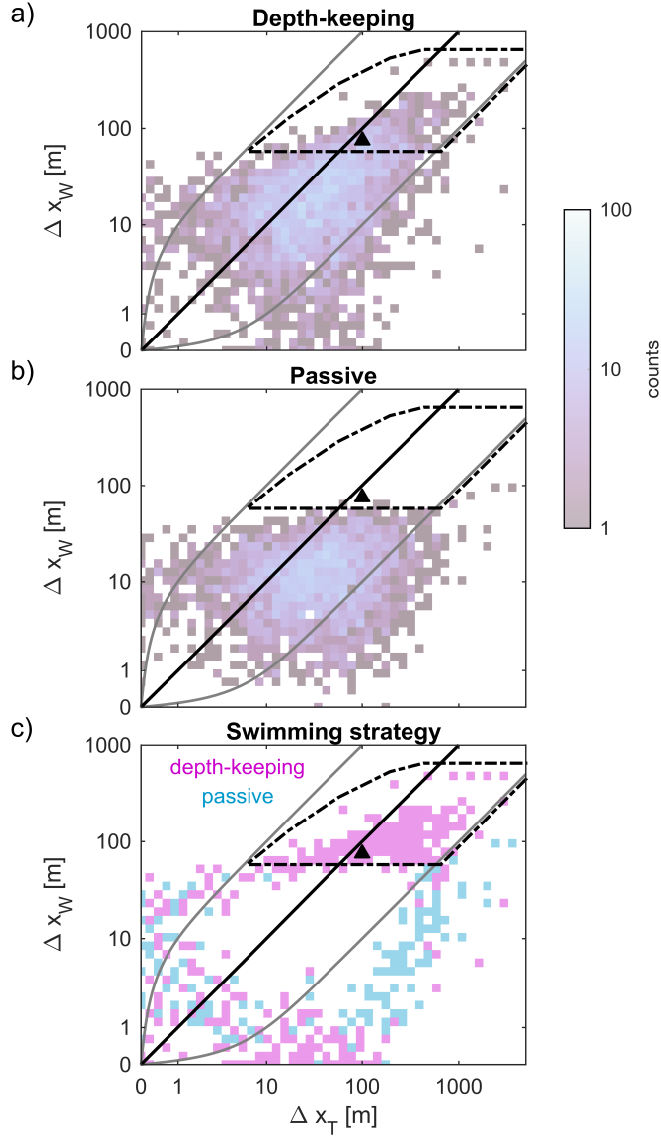
Figure 3.6: Wave-induced displacements [m] as a function of total displacements [m] for (a) depth-keeping and (b) passive organisms. Only waves where both wave and total displacements were positive are shown, i.e., the first quadrats of figure 3.5. The dash-dot area shows waves that were considered to exhibit similar transport to that reported for depth-keeping organisms in Garwood et al. (chapter 2) (black triangle), here defined as $\Delta x_W \geq 50$ m with $(\Delta x_W / \Delta x_T) \geq 10\%$.

Table 3.1: Percentage of waves contributing at least 10% of total transport, i.e., $(\Delta x_W / \Delta x_T) \geq 0.1$, and inducing horizontal displacements (Δx_W) of at least 10, 50, and 100 m above background. Results for depth-keeping and passive organisms at the top (depth = 3-5 m), middle (depth = 6-10 m), and bottom (depth = 11-16 m) of the water column are shown.

Depth-keeping

	$\Delta x_W \geq 10$ m	$\Delta x_W \geq 50$ m	$\Delta x_W \geq 100$ m
Top (3-5 m)	59%	17%	4%
Middle (6-10 m)	26%	3%	1%
Bottom (11-16 m)	3%	0%	0%

Passive

	$\Delta x_W \geq 10$ m	$\Delta x_W \geq 50$ m	$\Delta x_W \geq 100$ m
Top (3-5 m)	48%	1%	0%
Middle (6-10 m)	7%	0%	0%
Bottom (11-16 m)	0%	0%	0%

speed required to perfectly depth-keep also decreased towards the boundaries (Fig. 3.7B).

Ocean conditions that strongly favored onshore transport of depth-keeping organisms, compared to passive organisms at the same initial depth, included cross-shore velocities with a positive vertical shear, i.e., $(\partial u_T / \partial z) > 0$, indicating that cross-shore velocities decreased with depth (e.g., Fig. 3.8A). Above mid-water, these conditions implied that the internal waves moved isopycnals with high background horizontal velocities downward to the depths of depth-keeping organisms, thereby increasing the maximum velocities and residence time in the wave of depth-keeping organisms compared to passive organisms (e.g., Figs. 3.5 and 3.8A). Below mid-water, the positive vertical shear usually implied that slower offshore-flowing waters were brought downward to the depths of depth-keeping organisms thereby slowing their offshore advection, compared to passive organisms. Conversely, onshore transport of passive organisms was favored when there was a negative vertical shear in cross-shore velocities (e.g., Fig. 3.8B).
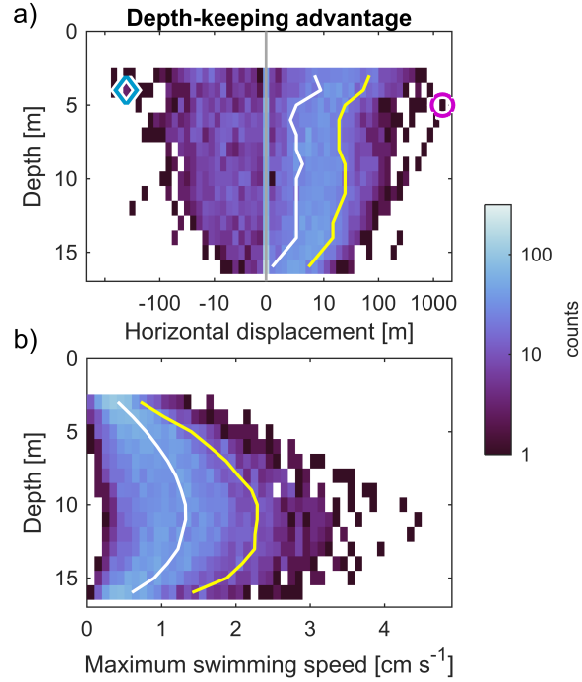
Figure 3.7: (a) Horizontal transport [m] preferentially experienced by depth-keeping organisms, compared to passive organisms with the same initial depth ($\Delta x_{dk} - \Delta x_p$). Bins are linear in ±logarithmic space, with values from ±1 m binned as 0. A paired Wilcoxon signed rank test shows the difference to be greater than zero at all depths at the 1% significance level. The diamond (passive advantage) and circle (depth-keeping advantage) highlight the waves shown in Fig. 3.8. (b) Maximum vertical swimming speed needed for organisms to perfectly maintain depth. Bins are 0.001 m s^{-1} in size. In all plots, the white and yellow lines show the 50$^{\text{th}}$ and 90$^{\text{th}}$ percentiles, respectively, and the logarithmic colorbar represents the counts in each bin.
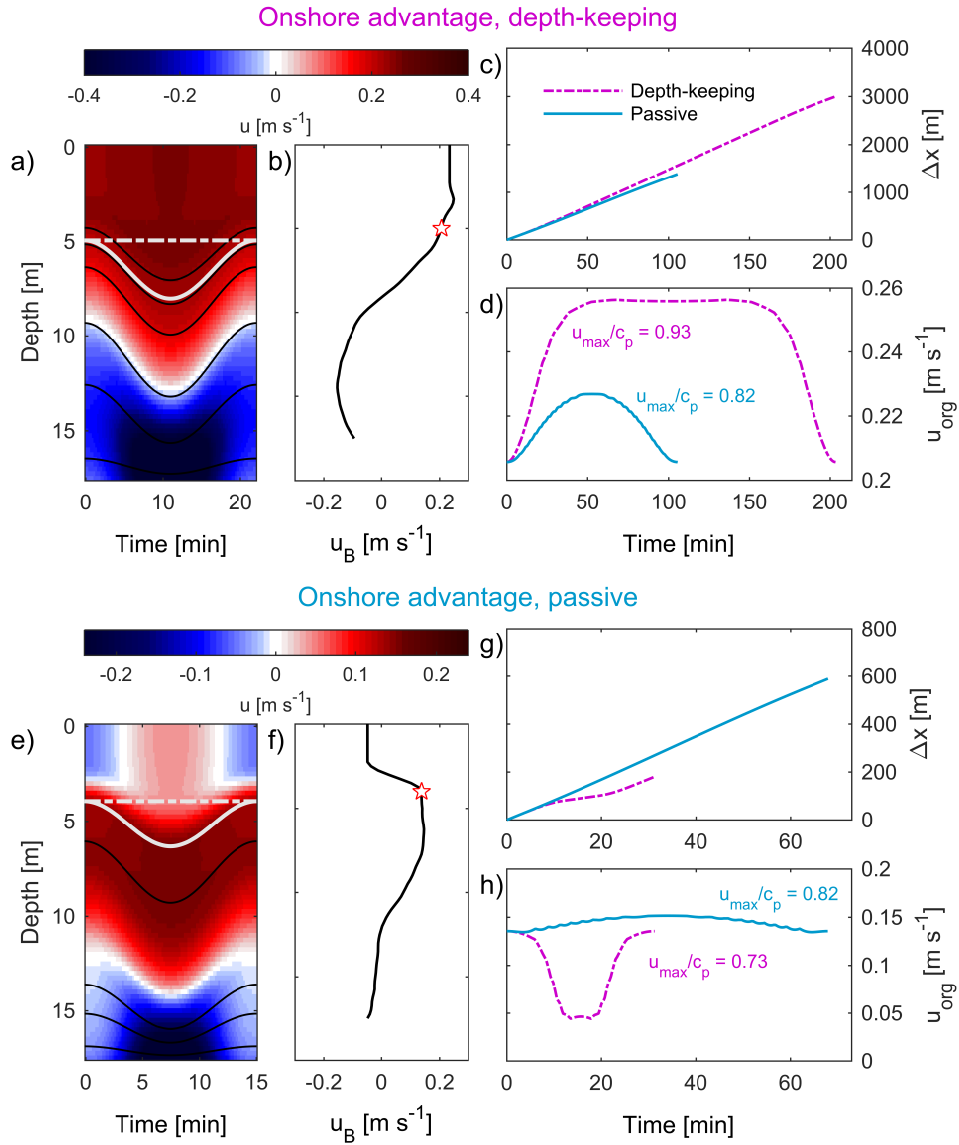
Figure 3.8: Examples of waves promoting the onshore displacement of (top) depth-keeping vs. (bottom) passive organisms. (a)/(e) Total cross-shore velocities [m s^{-1}], as sampled by a mooring in the simulations, with every 0.2°C isotherm shown by the black lines. The grey lines show the depth of (dashed) depth-keeping and (solid) passive organisms throughout the wave. (b)/(f) Low-pass background velocities [m s^{-1}] associated with the waves shown in (a) and (e). The red star indicates the initial depth of the organisms compared. (c)/(g) Total horizontal displacement [m] experienced and (d)/(h) velocities [m s^{-1}] reached by both (pink, dashed) depth-keeping and (teal, solid) passive organisms throughout the wave. The ratio of the organisms' maximum velocity to the wave propagation speed is also shown. Note that the length of each time series corresponds to the organisms' residence times in the waves. In all plots, positive values are onshore.

3.5 Discussion

Our data and analyses have shown that depth-keeping organisms were generally moved closer to shore than passive organisms after the passage of weakly nonlinear internal waves of depression, in the presence of vertically sheared background currents. Above water, this enhanced onshore transport was due to surface-intensified currents being brought down to the depths of depth-keeping organisms by internal waves. This internal-wave-induced deformation of the background currents both increased the cross-shore velocities experienced by depth-keepers, and their residence time in the waves as they propagated. The interaction of even weakly depth-keeping organisms with background flows and weakly nonlinear internal waves may be a significant mechanism for sustained onshore transport or meroplanktonic larvae to their nearshore adult habitats. At depths below mid-water, internal waves of depression often brought slower background currents to depth-keeping organisms, thus reducing their offshore dispersal and promoting their nearshore retention, compared to passive organisms.

Larvae can modulate their cross-shore position by adjusting their depths in flows with different horizontal velocities at different depths - a vertical shear. Such vertical shears in cross-shore velocities can be generated by both internal waves and background currents; these two velocity profiles combine to yield variable transports throughout the water column. However, internal waves and background currents do not act in isolation: background currents influence the shapes of internal waves (Stastna and Lamb, 2002), and internal waves deform along-isopycnal background currents vertically (Klymak et al., 2006). In general, though, the magnitude of background horizontal velocities tend to be constant along isopycnals throughout this deformation.

Passive organisms will follow the internal-wave-induced deformation of the background velocity field, experiencing the same background velocities as the wave passes. Depth-keeping organisms, on the other hand, will experience a range of background veloci-

ties advected past them during the passage of the wave (Garwood et al., chapter 2). These changes in the background velocities are proportional to the maximum wave-induced isopycnal vertical displacement (η_{max}), and the strength of the vertical shear in the background velocity ($\Delta u_B/\Delta z$). A large wave displacing a small vertical shear may induce a similar change in the background cross-shore velocities experienced by depth-keeping organisms as a small wave displacing a large vertical shear.

Background currents at our site were often surface-intensified and favored onshore transport of depth-keeping organisms in the upper water column. Thus, ocean conditions may be particularly advantageous for onshore transport in high-frequency internal waves if they are generated when there are surface-intensified cross-shore currents from, for example, the internal tide (Alford et al., 2010), or in areas with a preferentially onshore sea breeze. Our shallowest transport estimates are likely conservative, as the shear measured at 3-m depth was only extrapolated to 2.5 m, and not to the surface (Garwood et al., chapter 2). Further surface intensification of the background horizontal velocities would have led to even greater onshore transports. High-resolution, near-surface velocity measurements showed that winds regularly induce strong, surface-enhanced vertical shears in horizontal velocities that extend to depth (Lund et al., 2015; Laxague et al., 2018), with important implications for the transport of oil, plastics, and larvae. Moreover, the Stokes drift induced by surface waves will be important for larval transport closer to the surface, and should also be considered when estimating total larval transports in high-frequency internal waves.

Internal waves can affect community interactions by advecting organisms vertically, and by dispersing plankton both horizontally (Greer et al., 2014). In the observed internal wave fields, our analyses showed both more frequent and larger onshore transports of depth-keeping organisms in the upper water column than passive organisms. This would suggest that depth-keepers would be preferentially moved onshore, displacing them horizontally relative to passive organisms. This horizontal sorting could affect fundamental ecosystem

processes such as predation and infection.

In contrast to meroplanktonic larvae seeking adult habitats, it may be disadvantageous for holoplankonic organisms to be transported onshore in coastal waters. The decreased onshore transport predicted for passive organisms in weakly nonlinear internal waves with a background flow suggests behaviors that might reduce onshore transport and enhance offshore dispersal: remaining passive, i.e., following isopycnals (temperature surfaces), and residing deeper in the water column.

In this study, we have focused on two extreme swimming behaviors: passive and depth-keeping. However, other analyses have shown that these behaviors define two ends of a continuum of the effects of vertical swimming ability on transport (Franks et al., unpubl.; Garwood et al., chapter 2). Furthermore, even weakly swimming larvae can experience transport distances equivalent to those of a depth-keeper (Franks et al., unpubl.; Garwood et al. unpubl.). For the waves measured in this study, organisms with vertical swimming speeds much less than 1 cm s^{-1}, such as crab zoeae and other larvae (Chia et al., 1984), could still experience the maximum total transport distances reported. This is particularly true closer to the surface, where horizontal transport is high and vertical velocities are low. Thus, many organisms - even quite weak swimmers - with a tendency toward depth keeping could experience enhanced onshore transport through the interaction of swimming, weakly nonlinear waves, and a vertically sheared background current.

In regions with even moderate vertical shear in cross-shore velocities, vertical swimming in internal waves is likely to be more effective and less energetically costly in generating cross-shore transport than horizontal swimming. Larvae can relatively easily orient themselves vertically using the strong vertical gradients of properties such as pressure, light, or temperature (Cragg, 1980; Zeldis and Jillett, 1982; Daigle and Metaxas, 2011). Turbulence associated with shallow, coastal environments suitable for growth may also trigger active downward swimming in oyster larvae ready to recruit (Fuchs et al., 2013).

The cues for directed horizontal swimming, however, are not obvious. Indeed, horizontal swimming velocities of several cm s^{-1} would be necessary to produce horizontal transports similar to those estimated here for vertically swimming organisms (Drake et al., 2018).

The regular onshore nudging of larvae by the constant weakly nonlinear internal wave field could help maintain a pool of larvae near the coast. Indeed, most larvae tend to be found within 5 km of the coast (Morgan et al., 2009). Of the internal waves isolated at our mooring with $\eta > 1$ m, 90% were weakly nonlinear (those we included in our simulations), driving onshore total transport 57% of the time for depth-keeping organisms, and 50% of the time for passive organisms (Fig. 3.5). Our simulations showed wave-induced onshore transport $\Delta x_W \geq 50$ m for depth-keeping organisms near the surface roughly 20% of the time, but only 1% of the time for passive organisms. These results are consistent with a significantly enhanced probability of onshore transport for depth-keeping organisms compared to passive organisms in the upper water column. The sustained presence of these weakly nonlinear waves, therefore, presents a predictable mechanism for onshore meroplanktonic larval transport.

These weakly nonlinear waves, however, were sometimes punctuated by relatively rare, large, fully nonlinear waves with isopycnal displacements > 20 % of the water column depth. Shroyer et al. (2010) showed that much larger nonlinear internal waves on the New Jersey shelf induced surface cross-shore transport of passive tracers in excess of 1 km, though average values for the first three waves of a nonlinear internal wave train were $\sim$65 m per wave, comparable to the larger transports we have calculated for depth-keeping larvae. Large and infrequent nonlinear internal waves may account for significant, episodic larval transport to the nearshore (Shanks, 1983; Pineda, 1999). However, the effectiveness of these episodic events may depend on the retention of larvae near the coast by the sustained actions of the more frequent weakly nonlinear waves.

As they propagate upslope, internal waves will evolve and steepen prior to breaking

or dissipating. This implies that larval transport estimates will vary with cross-shore distance (Shroyer et al., 2010). Though we have focused on data acquired at the 20-m isobath, the average cross-shore velocities estimated at this location were similar to those of M-AUEs deployed between the 30-m and 25-m isobaths more than 1 km farther offshore. The 2-4-hour M-AUE deployments included time periods without internal waves, implying that the M-AUE average velocities we observed were less than those we would have predicted using the wave simulations - particularly in the upper water column where wave velocities were positive. Regardless of this difference in averaging, the M-AUE velocities fell well within the total predicted velocities from our wave-background simulations (Fig. 3.3), supporting our contention that our simulations provide sufficiently accurate predictions of the cross-shore movements of passive and depth-keeping organisms.

Generally, our data and analyses showed that both passive and depth-keeping larvae in the upper water column experienced onshore transport in high-frequency internal waves, while those at depth experienced offshore transport. Where internal wave trains appear regularly with respect to the internal tidal cycle, larvae could exploit the predictable vertical structure of cross-shore velocities at each phase of the tide to optimize offshore dispersal and onshore retention for various ontogenetic stages. For instance, after periods of high-frequency internal wave activity, Weidberg et al. (2019) showed that the vertical distribution in larval stages of various barnacle and decapod species shifted to greater depths, where bottom currents flowed onshore. Over longer time scales, even passive organisms may be able to modulate their depths via buoyancy adjustments (Richardson and Cullen, 1995; Gemmell et al., 2016); organisms that were defined as passive in our high-frequency internal waves should not, therefore, be assumed to follow the same water parcel over longer time scales (e.g., Cheriton et al., 2009).

Finally, although we focused on internal waves propagating onshore in a cross-shore current, internal waves propagating at all angles will deform the full background velocity

field. Therefore, when a vertical shear in alongshore velocities is present, weakly nonlinear internal waves propagating in the cross-shore direction will also modulate the alongshore transport of depth-keeping organisms, and vice versa. In this full 3-D system, the direction of transport will be set by the background currents brought to the organisms' depths, while estimates of residence time will be based on velocities along the wave's propagation axis (Lamb, 1997). Passive organisms will remain unaffected by these vertical shears.

3.6 Conclusions

The horizontal displacement of both passive and depth-keeping larvae was simulated in > 500 weakly nonlinear internal waves observed in the shallow, stratified coastal waters of Southern California. Average cross-shore velocities of depth-keeping larval mimics, the M-AUEs, were within the range of average velocities obtained in the simulations: -5 to 15 cm s^{-1}, over periods of 2-4 hours. After the passage of most internal waves, depth-keeping larvae in the surface layer were moved farther onshore than passive larvae, while depth-keeping larvae in the deeper layer experienced reduced offshore advection. In near surface waters, roughly 20% of shallow-water, weakly nonlinear internal waves displaced depth-keeping larvae ≥ 50 m towards shore. In comparison, only 1% of the observed internal waves induced similar displacements of passive organisms. The enhanced transport experienced by depth-keeping larvae was caused by the internal waves of depression displacing surface-intensified currents to the larvae's depths. Depth-keeping in weakly nonlinear internal waves with a background flow was shown to induce similar onshore transport as drifting passively in stronger, highly nonlinear internal waves. Due to stronger wave velocities and turbulence, vertical swimming in strongly nonlinear internal waves may not be as effective as in weakly nonlinear internal waves, while the vertical velocities associated with the simulated weakly nonlinear internal waves were well within the swimming ability of

many larvae (< 1 cm s^{-1}). Below mid-water, transport of both passive and depth-keeping larvae was predominantly offshore, but depth-keeping appeared to reduce offshore dispersal. Depth-keeping may therefore represent an adaptive behavior to promote retention of larvae in the nearshore environment, and their subsequent return to suitable, shallow-water adult habitats.

3.7 Acknowledgements

Chapter 3, in full, is currently being prepared for submission for publication of the material. Garwood, J.C., Lucas, A.J., Naughton, P., Roberts, P.L.D., Jaffe, J.S., deGelleke, L., and Franks, P.J.S. The dissertation author was the primary investigator and author of this material.

Chapter 4

Life in internal waves

4.1 Abstract

Internal waves are ubiquitous features of stratified, coastal oceans. Through their up-and-down motions, internal waves can concentrate and disperse plankton, move drifting organisms through light and pressure gradients, and modify the fluid properties surrounding organisms that can move with respect to water parcels. Although the effects of internal wave vertical motions on plankton have been considered extensively, the implications of plankton horizontal motions within the wave field have largely been ignored. Using numerical simulations of propagating internal waves, we show that the time series of environmental properties experienced by planktonic organisms are stretched and compressed, compared to those inferred from data collected at a mooring, and that this effect increases with wave nonlinearity. To demonstrate that this distortion of mooring time series also vary with planktonic vertical swimming ability, we also release both passive and depth-keeping virtual organisms in the simulated wave fields. Overall, results show that augmenting mooring measurements with numerical simulations and virtual organisms will produce more accurate estimates of the environmental conditions experienced by planktonic organisms.

Moreover, including horizontal motions throughout an internal wave flow field, and not only in bulk, may be particularly important to model interactions between plankton with varying vertical swimming ability.

4.2   Introduction

Internal waves can modulate the immediate environment experienced by coastal marine organisms in numerous ways. For example, internal waves can break and inject nutrients into the euphotic zone (Sandstrom and Elliott, 1984); displace phytoplankton vertically and affect the solar radiation they experience (Kamykowski, 1974; Holloway and Denman, 1989; Evans et al., 2008); transport and concentrate vertically swimming zooplankton (Zeldis and Jillett, 1982; Shanks, 1983; Franks, 1997; Lennert-Cody and Franks, 1999; Pineda, 1999); dampen thermal stress and provide nutrients to coral reefs (Leichter et al., 2003; Wall et al., 2015); and bring hypoxic deep water to shallow benthic environments (Booth et al., 2012; Walter et al., 2014). Here we show that the effects of internal-wave-induced vertical displacements will vary between marine organisms and communities. More specifically, we focus on the implications of internal-wave-deformation of a stratified fluid and its associated ambient properties, and the displacement of planktonic organisms both horizontally and vertically. We consider three categories of marine organisms: 1) organisms that are anchored to a substrate and are not moved by internal waves, such as coral reefs and mussel beds, 2) planktonic organisms that are moved by internal wave velocities in both the horizontal and vertical, such as non-swimming phytoplankton, and 3) planktonic organisms that are moved with internal wave velocities in the horizontal, but perfectly oppose wave vertical velocities in order to maintain a fixed depth, such as strong swimming larvae. Throughout this chapter, we refer to these organisms as "sessile", "passive", and "depth-keeping", respectively. Although planktonic organisms exhibit a range of swimming

abilities, including passive and depth-keeping behaviors captures both extremes of the continuum (Franks et al., unpubl.).

As high-frequency internal waves propagate in a stratified ocean, they deform ambient isopycnals, displacing organisms vertically. Here we consider high-frequency internal waves with wavelengths of $\mathcal{O}(100 \text{ m})$ and periods of $\mathcal{O}(10 \text{ min})$. Over these spatial and temporal scales, water properties such as temperature and nutrient concentrations are approximately constant along isopycnals, changing slowly in response to mixing, buoyant fluxes, and biological processes. Other environmental properties such as pressure and solar radiation, however, tend to be constant along depth surfaces. Here we will refer to these depth-constant properties as isobaric. Where vertical gradients in either isobaric or along isopycnal properties exist, the integrated environmental conditions experienced by an organism will be set by the time spent at a given depth and isopycnal. Over an internal wave period, sessile organisms or depth-keeping plankton will experience fixed depth-dependent properties. However, in maintaining depth, they will cross isopycnals and experience a range of along-isopycnal water properties. In contrast, passive organisms will follow isopycnals and experience constant along-isopycnal properties, but variable depth-dependent properties.

Vertical movements of isopycnals can be used to estimate the vertical positions of passive organisms during an internal wave, as well as to predict changes in the density fields experienced by sessile organisms or depth-keeping plankton. Measurements of vertical position and density can then be related to other environmental properties to estimate the average or integrated conditions experienced by these organisms. However, this must be done with caution as time series obtained at a fixed point (Eulerian) will reflect the environment experienced by sessile organisms, but not the environment experienced by organisms that move with the flow. Time series obtained moving with the wave (planktonic experience) will thus be Doppler shifted compared to Eulerian time series (sessile experience). Because

the Doppler shift depends on the velocity of the organisms, the distortion of mooring time series will vary with the horizontal wave velocities moving the organisms, and thus with depth.

Traditionally, Lagrangian measurements imply measurements collected while following a water parcel. These measurements apply to passive organisms, but not to depth-keeping plankton. To reflect the unique perspective of marine organisms and their ability to move with respect to water parcels, this chapter will refer to measurements along an organism's path, as opposed to Lagrangian measurements.

4.3   Linear and weakly nonlinear internal waves

As they propagate in a stratified ocean, internal waves will displace isopycnals vertically. When the maximum isopycnal displacement η_0 is small compared to the water height H, i.e., $\eta_0/(2H) \leq 0.1$, and background velocities are small compared to the wave propagation speed, waves will tend to be linear. In this case, isopycnals will be displaced up and down by the same vertical distance, corresponding to the wave's amplitude ($\eta_0/2$). The structure of a mode-1, linear progessive wave is described by a sinusoid in the horizontal (e.g., Woodson, 2018) (Fig. 4.1, **Linear**):

$$\eta\left(x, z, t\right) = \frac{\eta_0}{2} + \phi\left(z\right)\cos\left(kx - \omega t\right) \tag{4.1}$$

where ϕ is the wave's vertical structure function, k is the horizontal wavenumber [rad m^{-1}], ω is the wave frequency [rad s^{-1}], and t is time [s]. In this case, x [m] is positive in the direction of wave propagation, and z [m] is positive up. The horizontal wavenumber and wave frequency can be calculated from the wavelength, λ [m], and the wave period, T [s], with $k = 2\pi/\lambda$ and $\omega = 2\pi/T$. The wave propagation speed, c_p [m s^{-1}], is related to the wavelength by $c_p = \lambda/T$.
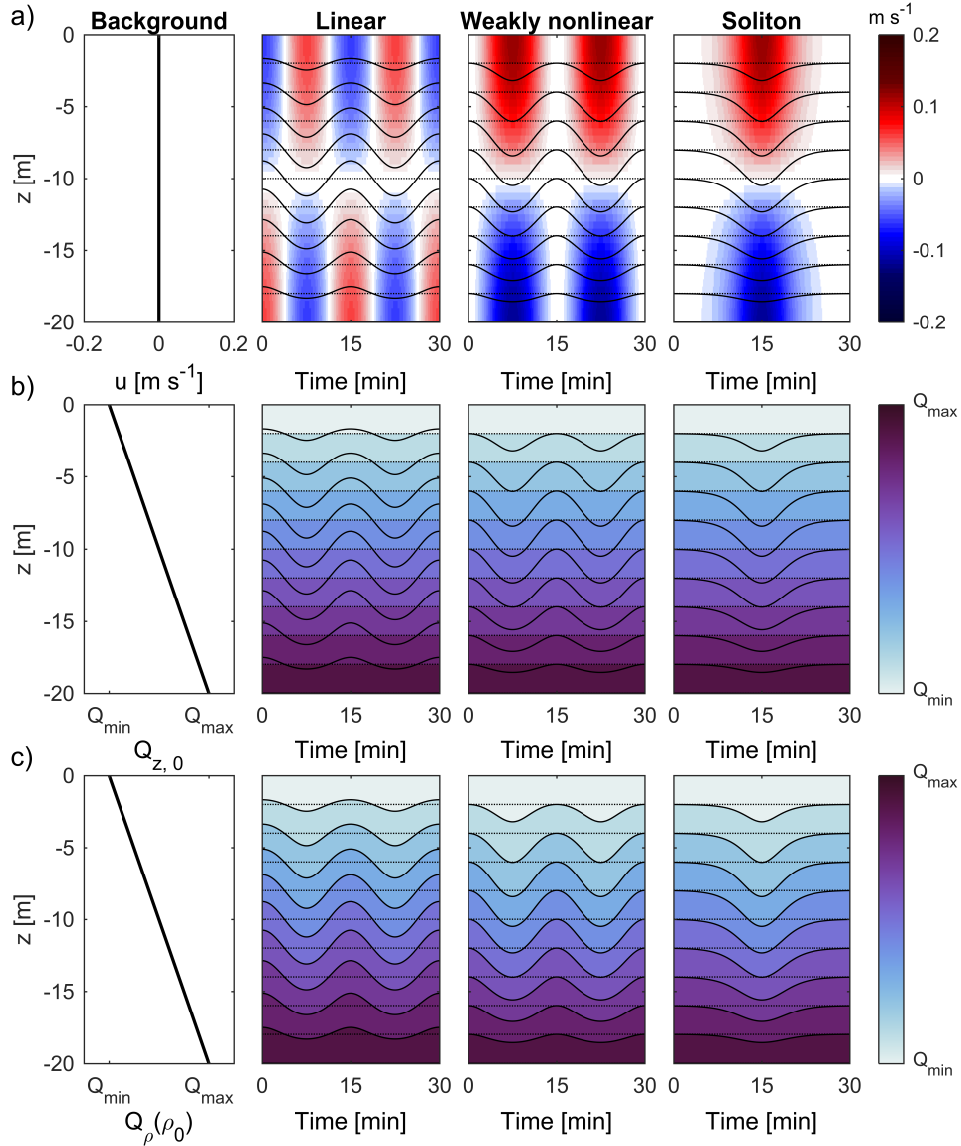
Figure 4.1: (a) Horizontal velocities [m s^{-1}], (b) isobaric property Q_z, and (c) along-isopycnal property Q_ρ in an unperturbed ocean (background), and during the passage of a linear (cos), weakly nonlinear (cos^2), and solitary (sech^2 shape) wave. Two wave periods are shown. Solid lines show isopycnal displacement, while dotted lines show the isopycnals at rest, which is also the depth of organisms in an unperturbed ocean, z_0. In all cases, $H = 20$ m, $\omega = 15$ min, $\eta_0 = 2.5$ m, $c_p = 0.3$ m s^{-1}, and $\phi = -\sin(\pi z/H)$.

As internal waves propagate into shallower coastal waters, they steepen and become increasingly nonlinear before they break or dissipate. Generally, waves of depression, i.e., those with downward isopycnal displacements, will form where the pycnocline is above mid-water, while waves of elevation will occur elsewhere (Lee, 1961). Over the continental shelf, internal waves that begin as waves of depression offshore may thus flip into waves of elevation as they reach shallower onshore waters (Bourgault et al., 2007). Here, we will focus on waves of depression, although the equations below could describe either type of waves. Various mathematical functions, including cnoidal functions, can be used to capture the wide range of weakly nonlinear wave shapes (see review by Apel 2002). The linear limit of the cnoidal function is associated with a cosine-squared wave (4.2) (Fig. 4.1, **Weakly nonlinear**), while the most nonlinear limit is associated with a hyperbolic secant wave (4.3) (Fig. 4.1, **Soliton**), also known as a solitary wave or soliton:

$$\eta\left(x, z, t\right) = \eta_c + \eta_0 \phi\left(z\right) \cos^2\left(\frac{kx - \omega t}{2}\right) \tag{4.2}$$

$$\eta\left(x, z, t\right) = \eta_0 \phi\left(z\right) \operatorname{sech}^2\left(\frac{kx - \omega t}{2}\right) \tag{4.3}$$

where η_c is a displacement adjustment at the wave crest [m]. In solitary waves, isopycnals return to their equilibrium depths at infinity, thus η_c is equal to zero and not included in (4.3). Equations (4.2) and (4.3) are solutions to the Korteweg-de Vries (KdV) equation, which can be used to relate environmental properties, such as background density and velocity profiles, to wave characteristics (Apel, 2002; Grimshaw et al., 2004). Background velocities, for instance, can influence wave shape and propagation speed. To compare the isopycnal displacement and velocity field associated with each wave shape, we set all wave parameters to be equal in our examples, ignoring the fact that ocean conditions would determine wave shape (Fig. 4.1); we set η_c to 0 m, η_0 to 2.5 m, H to 20 m, c_p to 0.3 m s^{-1},

and T to 900 s (15 min). Although these wave properties are realistic (e.g., Garwood et al.,

chapter 2), examples are provided for illustrative purposes only. In all cases, horizontal

and vertical velocities, u and w [m s^{-1}] respectively, were calculated from propagating the

wave shape (Chang et al., 2011), with:

$$u\left(x, z, t\right) = c_p \frac{\partial \eta\left(x, z, t\right)}{\partial z}, \tag{4.4}$$

$$w\left(x, z, t\right) = -c_p \frac{\partial \eta\left(x, z, t\right)}{\partial x}. \tag{4.5}$$

To contrast the effects of linear and nonlinear internal waves on the environmental

properties experienced by sessile/benthic organisms, as well as passive and depth-keeping

plankton, we used equation (4.1) to simulate a linear internal wave, and equation (4.2)

to simulate a weakly nonlinear internal wave (Fig. 4.1). Passive organisms were then

numerically advected through the wave field using equations (4.4) and (4.5), evaluated at

the organisms' positions (x_{org}, z_{org}) at time t. We used a time step of 1 s. Depth-keeping

organisms were advected in the horizontal only, using (4.4), while sessile/benthic organisms

were not moved by the flow, but the flow they experienced was recorded. On all figures,

the environmental conditions experienced by passive, depth-keeping, and sessile organisms

are compared to a mooring record, as if collected by fixed-depth sensors on a taut line or

column. For comparison with passive organisms, mooring measurements are also shown for

given isopycnals.

Overall, we consider environmental properties that are depth-dependent (e.g. light)

and dependent on ocean density (e.g. nutrient concentrations), which we represent using

Q_z and Q_ρ, respectively. Of course, depth and density are not independent; this notation

was simply used to distinguish properties that would remain constant at a given depth

throughout the internal waves from properties that would follow the internal-wave-induced

deformation of the fluid. For simplicity, the unperturbed vertical profiles of both properties were set to increase linearly with depth and density, respectively (Fig. 4.1B and C). For each organism, the environmental conditions they experienced were calculated from their horizontal and vertical position (x_{org}, z_{org}) at time t, with:

$$Q_z(z_{org}) = Q_{z,0}(z_{org}), \tag{4.6}$$

$$\rho(x_{org}, z_{org}, t) = Q_\rho(\rho_0[z_{org} - \eta(x_{org}, z_{org}, t)]). \tag{4.7}$$

where $Q_{z,0}$ is the unperturbed vertical profile of a depth-dependent property, and ρ_0 is the density profile in an unperturbed ocean.

4.4 Horizontal motions and transport

Internal waves induce areas of convergence and divergence above their troughs and crests, respectively (Ewing, 1950a; Ewing, 1950b). In low wind, these areas interact with surface films and capillary waves to produce a banding pattern at the ocean surface: convergence zones smooth ripples and produce surface slicks, while divergence zones remain rough (Ewing, 1950a; Ewing, 1950b). Planktonic organisms that at least partially resist vertical velocities, such as positively buoyant eggs or swimming plankton, can often be concentrated in areas of surface convergence associated with internal wave downwelling (Ewing, 1950b; Franks, 1997; Lennert-Cody and Franks, 1999; Lennert-Cody and Franks, 2002; Omand et al., 2011). For instance, a shallow-water internal wave was found to concentrate a subsurface red tide layer; the wave subsequently broke and mixed this red tide layer to the surface (Omand et al., 2011). Enhanced concentrations of plankton, fish larvae, and pelagic crabs have also been documented in surface slicks and/or internal

waves (Zeldis and Jillett, 1982; Shanks, 1983; Jillett and Zeldis, 1985; Shanks and Wright, 1987; Shanks, 1988). Even organisms that are not vulnerable to ocean currents such as fish and pilot whales have been found to associate with internal wave troughs (Kingsford and Choat, 1986; Moore and Lien, 2007). These relationships may be indicative of a reactive process, where higher trophic levels seek higher concentrations of preys and/or drift algae due to internal wave activity (Kingsford and Choat, 1986; Moore and Lien, 2007; Lévy et al., 2018). At a small offshore bank, a three-way interaction between euphausiid swimming behavior, internal waves, and topography was hypothesized to induce shoals of euphausiids near the surface, which were then exploited by herring, seabirds, and whales (Stevick et al., 2008). Internal waves of depression have also been found to concentrate zooplankton prey above the pycnocline and to increase the vertical space available for Peruvian anchoveta to school and feed (Bertrand et al., 2008). While they concentrate prey, internal waves may also concentrate plastic and contaminants (Shanks, 1987). We are, however, unaware of any documented impacts of this concentration to higher trophic levels. Variability in depth-regulating abilities between planktonic prey and predators can also lead to differential vertical advection by internal waves and/or concentration patterns, and influence trophic interactions (Macías et al., 2010; Greer et al., 2014). In the Benguela Current, the thickening of a turbid surface layer above internal wave crests decreased light penetration and induced vertical migration of foraging fish (Kaartvedt et al., 2012). By affecting light penetration in the ocean, internal waves can thus also increase feeding opportunities for predators that must avoid their own visual predators (Kaartvedt et al., 2012).

As internal waves propagate, they may concentrate planktonic organisms locally, and these high-concentration regions may propagate with the wave. However, this does not imply that any individual organism will sustain significant net transport by the waves (Franks, 1997). In parts of Massachusetts Bay, however, patches of low chlorophyll *a*

concentrations are thought to be caused by nonlinear waves transporting phytoplankton away from these areas (Lai et al., 2010). Shallow-water internal waves usually enhance onshore transport of larvae, which is perceived to promote recruitment (Shanks, 1983; Shanks, 1988; Pineda, 1999), however highly energetic nonlinear internal waves may also expose larvae to mechanical stress and transport them away from productive areas (Ruvalcaba-Aroche et al., 2019).

Traditionally, only highly nonlinear internal waves were assumed to transport plankton over large distances (Pineda, 1994; Shanks, 1995; Lamb, 1997; Pineda, 1999). This is because nonlinear internal waves transport mass. For instance, mode-1 internal waves of depression induce wave velocities that are constantly in the direction of wave propagation above the pycnocline, and opposite at depth (Apel et al., 1985) (e.g., Fig. 4.1, **Weakly nonlinear** and **Soliton**). Linear internal waves, however, induce alternating positive and negative wave velocities at all depths (e.g., Fig. 4.1, **Linear**). Though Eulerian currents are circular, vertical gradients in horizontal displacement induce a net drift in the direction of wave propagation, known as the "Stokes Drift" (e.g., Thorpe, 1968; Dewar, 1980, ; Franks et al., unpubl.), which tends to be small compared to the horizontal transport associated with nonlinear internal waves (e.g., compare transport of passive and depth-keeping organisms in Figs. 4.2 and 4.3). Horizontal transport will occur along the same axis as internal wave propagation, and while this may be in the cross-shore direction for many coastal internal waves (e.g., Lee, 1961; Shroyer et al., 2011; Richards et al., 2013; Colosi et al., 2018; Sinnett et al., 2018), some coastlines may favor along-shore displacements (e.g., Liévana MacTavish et al., 2016).

Figure 4.2: Horizontal displacement [m] from 0-20 m depth, (a) as predicted from the Eulerian velocities associated with the linear internal wave in Fig. 4.1, and for (b) sessile, (c) passive, and (d) depth-keeping organisms in the same flow field as in (a). The horizontal line shows no net horizontal transport, while the vertical dash-dot line shows the wave period. Colors show depth.

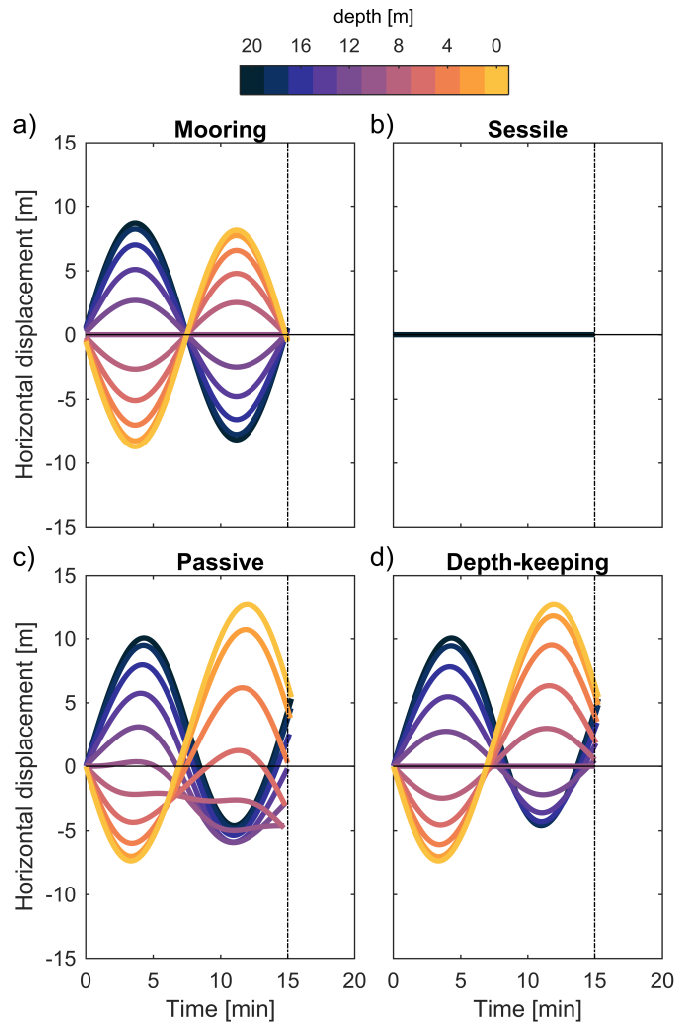**Figure 4.3**: Horizontal displacement [m] from 0-20 m depth, (a) as predicted from the Eulerian velocities associated with the weakly nonlinear internal wave in Fig. 4.1, and for (b) sessile, (c) passive, and (d) depth-keeping organisms in the same flow field as in (a). The horizontal line shows no net horizontal transport, while the vertical dash-dot line shows the wave period. Colors show depth.
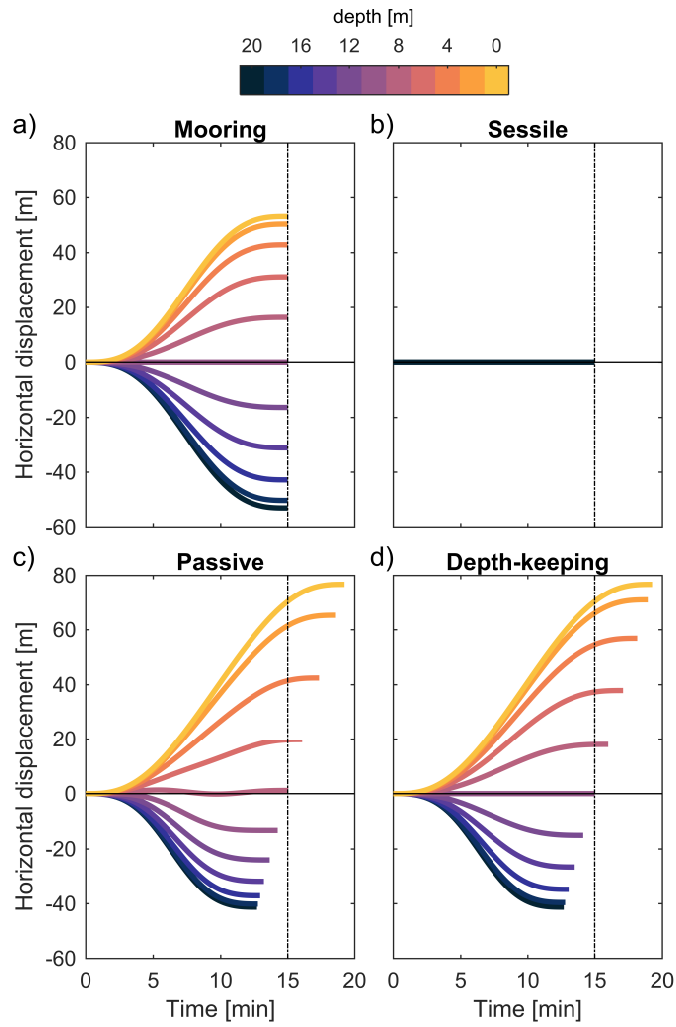
4.5   Stokes drift

Stokes drift is defined as the difference between the horizontal displacement calculated by integrating velocities at a point (Eulerian) and the actual horizontal displacement experienced by an organism moving with the flow. For example, no net horizontal displacement was predicted from our linear wave velocities as sampled by a mooring, yet organisms moving with the flow experienced a small net displacement (Fig. 4.2). This difference is due to the fact that organisms spent more time in parts of the waves where velocities aligned with the wave propagation speed, i.e., above wave troughs and below wave crests (Fig. 4.1), and less time where velocities opposed each other. Our weakly nonlinear wave example makes this concept particularly obvious. Notice how the time organisms spent in the wave differs with depth: organisms in the top half of the water column spent more time in the wave, while organisms in the bottom half spent less time in the wave (Fig. 4.3). Moreover, these residence times differed significantly from the wave's period (Fig. 4.3). The same phenomenon also occurred in the linear wave although differences in residence times were small and thus less noticeable (Fig. 4.2). Note that total transport is the sum of transport due to the Eulerian mean flow (as measured at a mooring) and the Stokes drift. This means that, although Stokes drift represented the total transport in the linear wave, it was an additional contribution to transport in the nonlinear wave (compare the total displacements in Figs. 4.2 and 4.3, with Fig. 4.4).

For internal waves in the absence of a mean flow, Stokes drift will be in the direction of wave propagation for both passive and depth-keeping organisms found near the top and bottom of the water column (Franks et al., unpubl.) (e.g., Fig. 4.4). Mid-water, passive organisms will be transported in the opposite direction, while depth-keeping organisms will experience no net transport (Franks et al., unpubl.) (e.g., Fig. 4.4). Throughout the water column, Stokes drift of weak swimmers will fall between these two extremes (Franks et al., unpubl.).
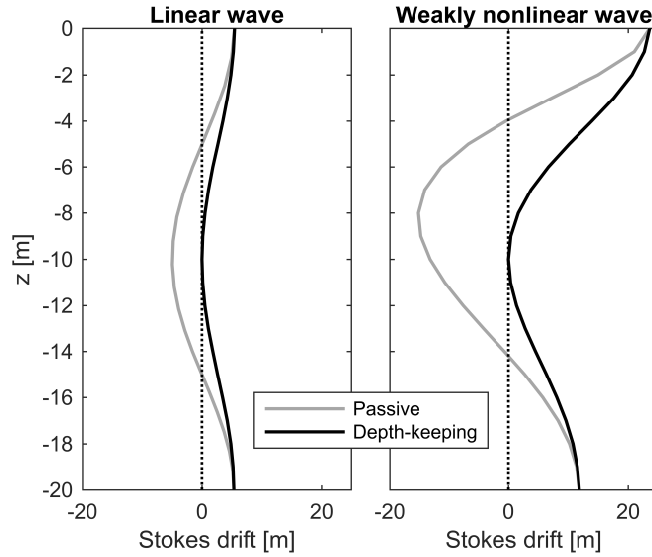
Figure 4.4: Stokes drift [m] experienced by passive (grey) and depth-keeping (black) organisms in the linear and weakly nonlinear waves shown in Fig. 4.1. The vertical dotted line shows no net transport.

Overall, the time an organism spends traveling with a wave, and thus the distance over which it is transported, both increase as the organism's maximum velocity approaches that of the wave propagation speed ($u_{max}/c_p \to 1$) (Lamb, 1997; Pineda, 1999). Highly nonlinear internal waves have u_{max}/c_p approaching 1, or even reaching 1 when fluid travels at the same speed as the wave, i.e., when a trapped core is formed, while linear internal waves have $u_{max}/c_p \ll 1$ (e.g., Fig. 4.1). Stokes drift is thus stronger in nonlinear internal waves than in linear waves (Fig. 4.4). We will see that the sampling of a wave from a plankton's perspective stretches and compresses Eulerian time series: compared to estimates derived from measurements at a mooring (Eulerian), plankton will spend more time in the environment associated with internal wave throughs and less time in the environment associated with internal wave crests. Sessile organisms, on their part, are fixed and experience no such distortion.

79
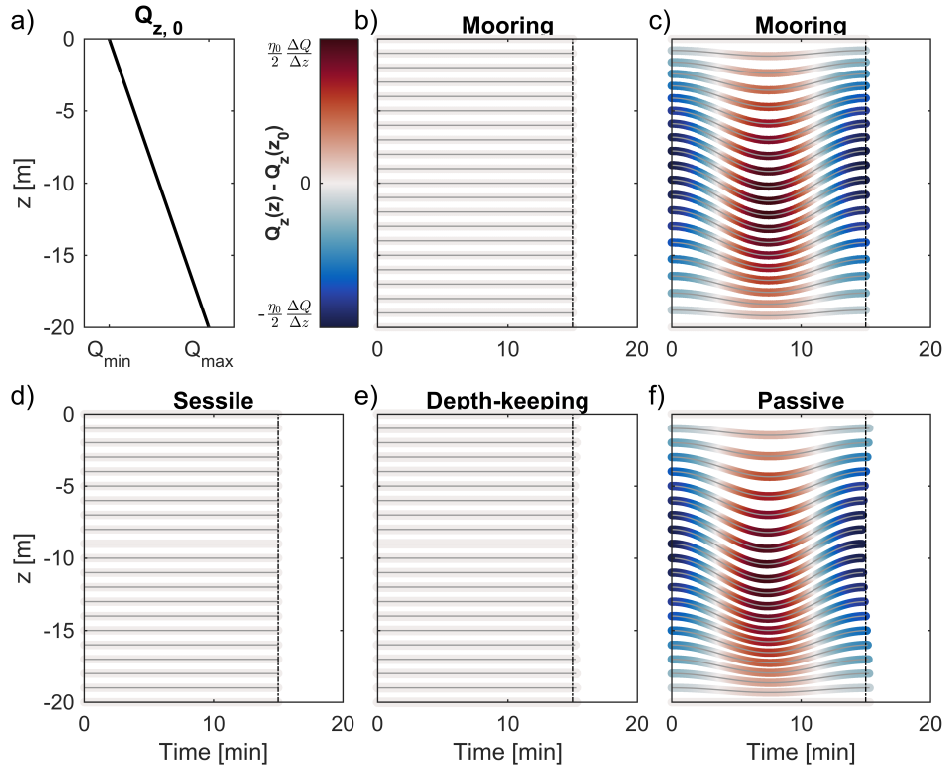
Figure 4.5: Anomaly in isobaric property $Q_z(z) - Q_z(z_0)$ for the linear internal wave in Fig. 4.1. The units of Q_z depend on the measurements of interest; z_0 is the depth of the organisms in an unperturbed ocean. (a) Vertical profile of Q_z in an unperturbed ocean. Anomaly as calculated from a mooring (b) at fixed depths vs. (c) along isopycnals, and for (d) sessile, (e) passive, and (f) depth-keeping organisms in the same flow field. The vertical dash-dot line shows the wave period.
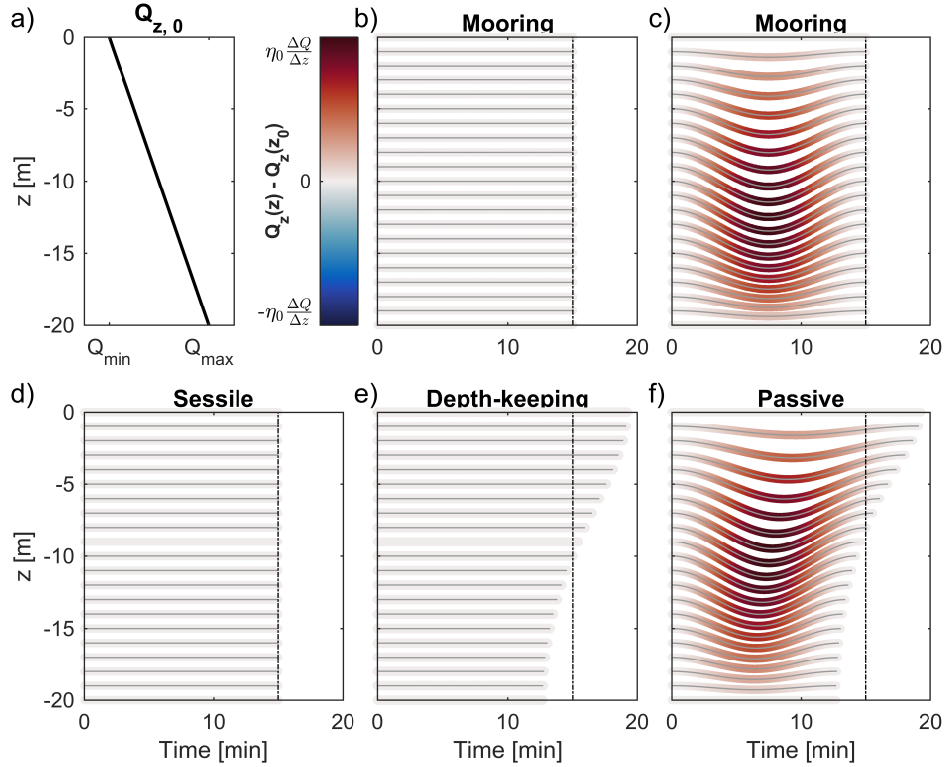
Figure 4.6: Anomaly in isobaric property $Q_z(z) - Q_z(z_0)$ for the weakly nonlinear internal wave in Fig. 4.1. The units of Q_z depend on the measurements of interest; z_0 is the depth of the organisms in an unperturbed ocean. (a) Vertical profile of Q_z in an unperturbed ocean. Anomaly as calculated from a mooring (b) at fixed depths vs. (c) along isopycnals, and for (d) sessile, (e) passive, and (f) depth-keeping organisms in the same flow field. The vertical dash-dot line shows the wave period.

4.6 Depth-dependent properties

One of the main impacts of internal waves on passive phytoplankton is to displace them vertically, thus affecting the total solar radiation they experience and potentially their growth rate (e.g., Kamykowski, 1974; Kahru, 1983; Holloway and Denman, 1989; Evans et al., 2008). Bands of enhanced chlorophyll a have been observed via remote sensing, consistent with a deep chlorophyll maximum being lifted by internal waves (da Silva, 2002; Muacho et al., 2013). This process was also shown to have the potential to increase primary productivity with respect to an unperturbed ocean (da Silva, 2002; Muacho et al., 2013). In the South China Sea, regions in which internal waves were present but not breaking were associated with higher chlorophyll a than nearby regions without much internal wave activity (Pan et al., 2012). However, regions in which internal waves were breaking displayed the highest chlorophyll a values (and lower sea surface temperature), consistent with internal waves breaking, and injecting nutrients upward into the euphotic zone (Pan et al., 2012). To properly assess how vertical motions may affect primary production, however, the phasing of internal waves with respect to variable surface insolation must also be taken into account. For instance, the phasing of M2 internal tides with respect to daylight hours, or the phasing of higher-frequency waves with respect to patchy cloud coverage have both been shown to have the potential to modulate primary production (Kamykowski, 1974; Evans et al., 2008; Muacho et al., 2013). Bottle experiments in Toolik Lake also demonstrated that internal waves with small amplitudes ($\sim$1 m) and periods of 2-6 h could modify photosynthesis by -15% to 200%, compared to an unperturbed water column (Evans et al., 2008). These values were higher than those predicted from models, potentially because the theory did not account for photoacclimation, i.e., the ability of phytoplankton's photosynthetic processes to adapt to the light available (Evans et al., 2008).

Many of the studies mentioned above investigated how the vertical position of

phytoplankton and thus the light levels they experienced were modulated by the M2 internal tide, yet the principles outlined should equally apply to high-frequency internal waves (Haury et al., 1983). Strongly nonlinear internal wave packets in Massachusetts Bay, for instance, can be associated with downward isopycnal displacements of tens of meters; their passage can therefore significantly deepen any isopycnal-following subsurface chlorophyll maximum and reduce the total solar radiation that reaches photosynthetic organisms (Haury et al., 1983). However, internal motions need not be that large to influence plankton (Cheriton et al., 2009). High-frequency internal waves may also have a stronger effect on primary production than the internal tide, as phytoplankton were found to display higher daily photosynthesis when subjected to rapidly changing light than phytoplankton subjected to slowly fluctuating light, despite an overall equal average light level (Flameling and Kromkamp, 1997).

In the ocean, light decreases exponentially with depth, with many studies presenting equations to capture this relationship and other processes it may influence, as with photosynthesis-irradiance (P-I) curves (e.g., Kamykowski, 1974; Kahru, 1983; Holloway and Denman, 1989). However, other environmental properties such as pressure will increase with depth. Organisms that regulate their buoyancy through gas vacuoles, such as cyanobacteria (Oliver, 1994), will become less buoyant if internal waves displace them to greater depth, and vice versa. As any diver would know, such perturbations will grow due to the positive feedback between depth and gas compression. Could internal waves increase the metabolic costs of depth-regulators that rely on gas vacuoles or swim bladders? In laboratory experiments, grey mullet fish larvae were found to experience higher survival when water motions kept them below the water surface, thus preventing excessive bladder inflation (Nash et al., 1977). Moreover, early sunlight exposure can be fatal to these larvae (Nash et al., 1974), and seabirds have been observed to feed above internal wave crests (Haney, 1987); it is possible that fluctuations in the internal wave regime thus modulate the survival

of mullet fish larvae and other zooplankton.

4.7   Along-isopycnal properties

In the absence of mixing and over short timescales, many ocean properties such as temperature, and nutrient, oxygen, or phytoplankton concentrations can be assumed to be constant along isopycnals. This means that the isopycnal-following phytoplankton communities moved up and down by internal waves will experience a fluctuating light regime, but a constant temperature, for example. However, organisms that move with respect to water parcels, including those that maintain a fixed depth, will experience a range of along-isopycnal properties over a wave period. Grazers that can resist internal wave motion may therefore see layers of high phytoplankton density advected to them from above or below. At a rocky subtidal site for instance, Witman et al. (1993) documented pulses of phytoplankton associated with the internal-wave-induced downward displacement of the subsurface chlorophyll maxima. Many studies have also documented internal waves displacing deep waters to shallower depths in kelp forests (e.g., Zimmerman and Kremer, 1984; McPhee-Shaw et al., 2007), macroalgal communities (e.g., Ladah et al., 2012), and coral reefs (e.g., Leichter et al., 1996; Leichter et al., 2006). Because these deeper waters can be associated with enhanced zooplankton concentrations, they may bring "plankton storms" that supply reefs with both larvae and food (Leichter et al., 1998). The cooler, nutrient-rich waters moved by the internal waves may also deliver nutrients (Zimmerman and Kremer, 1984; Leichter et al., 1996; Leichter et al., 2003), and decrease thermal stress (Wall et al., 2015), likely influencing zonation in many coastal environments. Although the water motions eventually reverse, internal waves can have a lasting impact on coastal communities if mixing occurs or if biological processes such as prey capture and nutrient absorption occur more rapidly than the timescale of each wave.

In Monterey Bay, CA, high-frequency internal waves are responsible for intrusions of low oxygen, low pH waters in coastal ecosystems (Booth et al., 2012; Walter et al., 2014). In these shallow water environments, market squid are known to lay their egg capsules directly on the seafloor (Zeidberg et al., 2012); by modulating the oxygen, pH, and temperature, internal waves may thus affect squid embryonic development (Navarro et al., 2016). Not only will low oxygen/low pH intrusions modify the environmental conditions experienced by sessile organisms or egg capsules, they may also determine the vertical distribution of zooplankton (e.g., Wishner et al., 2013). The effects of internal waves on water properties, however, need not be instantaneous. At Dongsha Atoll, a lasting depletion in dissolved oxygen was observed, potentially caused by internal waves delivering enhanced particulate organic matter, which was subsequently degraded by microbes (Wang et al., 2007).

Similarly to benthic ecosystems, depth-regulating plankton will experience a range of along-isopycnal properties over a wave period. However, unlike sessile, benthic organisms, depth-regulating plankton are moved by internal waves and experience net horizontal displacement (e.g., Shanks, 1983; Shanks and Wright, 1987; Pineda, 1999, ; Franks et al., unpubl.); thus the environmental conditions experienced by sessile/benthic organisms and depth-regulating plankton, even if at the same depth, will be different.

4.8   Virtual organisms in internal waves

In linear waves, passive organisms are moved up and down an equal vertical distance from their equilibrium depths in an unperturbed ocean, z_0 [m] (Fig. 4.1, **Linear**); passive organisms thus experience both decreased and enhanced isobaric properties over a wave period, compared to what they would experience if they remained at their unperturbed depth (Fig. 4.5F). In the weakly nonlinear waves we simulated, isopycnals were only displaced downward (Fig. 4.1, **Weakly nonlinear**), so passive organisms only experienced

Figure 4.7: Anomaly in along-isopycnal property $Q_\rho(\rho) - Q_\rho(\rho_0)$ for the linear internal wave in Fig. 4.1. The units of Q_ρ depend on the measurements of interest; ρ_0 is the density experienced by the organisms in an unperturbed ocean. (a) Vertical profile of Q_ρ in an unperturbed ocean. Anomaly as calculated from a mooring (b) at fixed depths vs. (c) along isopycnals, and for (d) sessile, (e) passive, and (f) depth-keeping organisms in the same flow field. The vertical dash-dot line shows the wave period.

enhancement of isobaric properties that increased with depth (Figs. 4.1B and 4.6F). For environmental properties that decrease with depth, such as light levels, passive organisms would experience decreased isobaric properties in a weakly nonlinear internal wave of depression. Unsurprisingly, passive organisms did not experience any fluctuation in along-isopycnal properties (Figs. 4.7F and 4.8F).

As expected, isobaric properties experienced by sessile/benthic organisms and depth-keeping plankton in our simulations did not vary (Figs. 4.5 and 4.6, D and E). However, in the linear internal wave simulated, these organisms experienced both enhanced and decreased along-isopycnal properties over a wave period (Fig. 4.7, D and E), while they
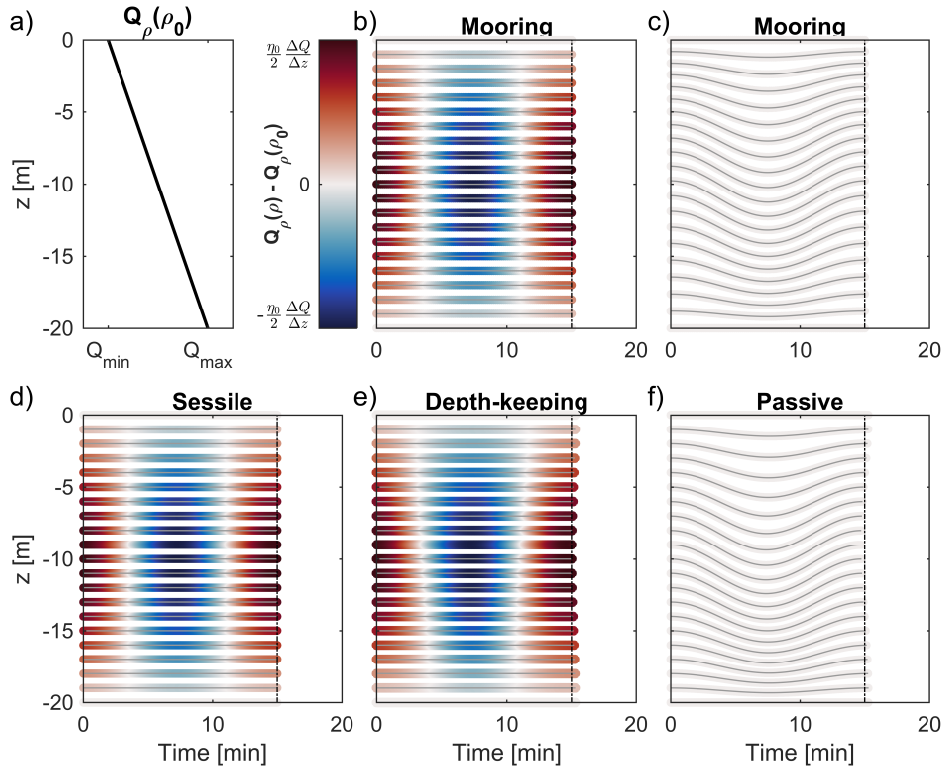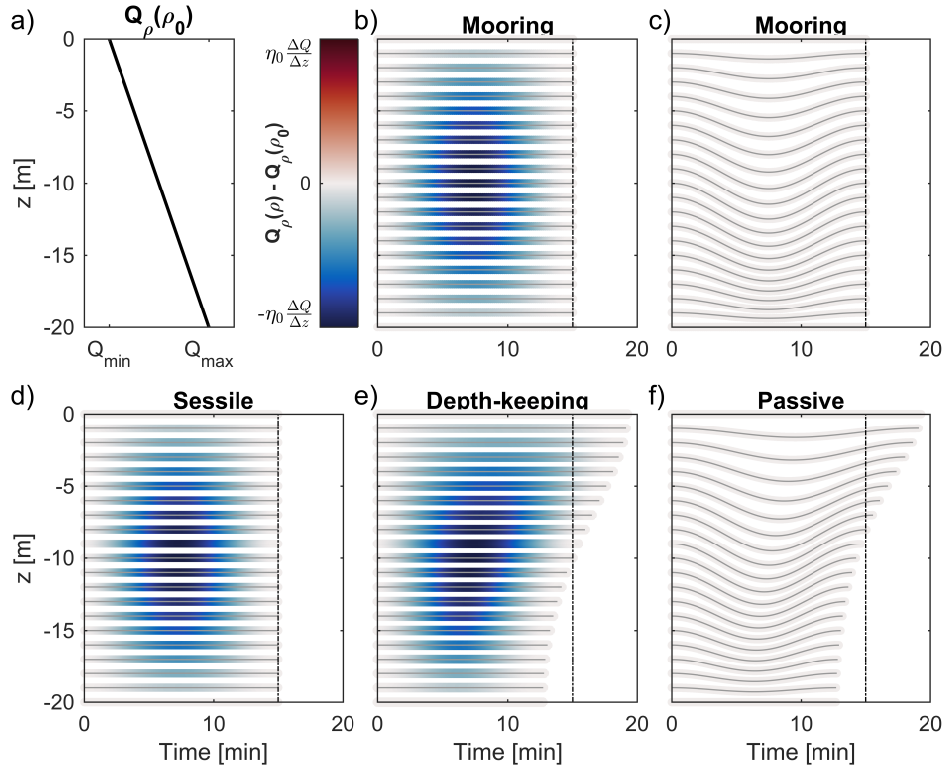
Figure 4.8: Anomaly in along-isopycnal property $Q_\rho(\rho) - Q_\rho(\rho_0)$ for the weakly nonlinear internal wave in Fig. 4.1. The units of Q_ρ depend on the measurements of interest; ρ_0 is the density experienced by the organisms in an unperturbed ocean. (a) Vertical profile of Q_ρ in an unperturbed ocean. Anomaly as calculated from a mooring (b) at fixed depths vs. (c) along isopycnals, and for (d) sessile, (e) passive, and (f) depth-keeping organisms in the same flow field. The vertical dash-dot line shows the wave period.

experienced decreased along-isopycnal properties in the weakly nonlinear wave of depression (Fig. 4.8, D and E). Again, this depletion was due to our decision to focus on a property that increases with depth, such as nutrient levels. Other environmental properties such as temperature and oxygen concentration tend to decrease with depth. In these cases, internal waves of depression would be associated with enhancements for depth-keeping organisms.

Note that although both $Q_{z,0}$ and $Q_\rho(\rho_0)$ effectively increased with depth, passive organisms experienced an enhancement of Q_z in the weakly nonlinear internal wave, while organisms at a fixed depth experienced a reduction in Q_ρ in the same wave (Figs. 4.6 vs. 4.8, Fig. 4.9A vs. D). Time periods of enhancement and decline in environmental properties were also reversed between passive and fixed-depth organisms in the linear wave (Figs. 4.5 and 4.7). These differences can be explained by the fact that whenever an internal wave moved passive organisms to greater depths, it also brought waters from shallower depths (and thus less dense) to organisms that maintained their depths. By resisting vertical velocities, fixed-depth organisms effectively moved in the opposite direction as passive organisms, with respect to the wave field. Overall, the range of environmental properties experienced by either group will be set by the wave amplitude they experience, as well as the local gradient in these environmental properties over the vertical excursion of the wave. This means that a large wave displacing passive organisms in a region where light attenuates slowly may induce as much change as a small wave displacing passive organisms through a region where light attenuates quickly. Because density often does not vary linearly with depth, and because environmental properties may also not vary linearly with depth or density, the simple dynamics used are for illustration purposes only; in the real ocean, many of these effects are nonlinear.
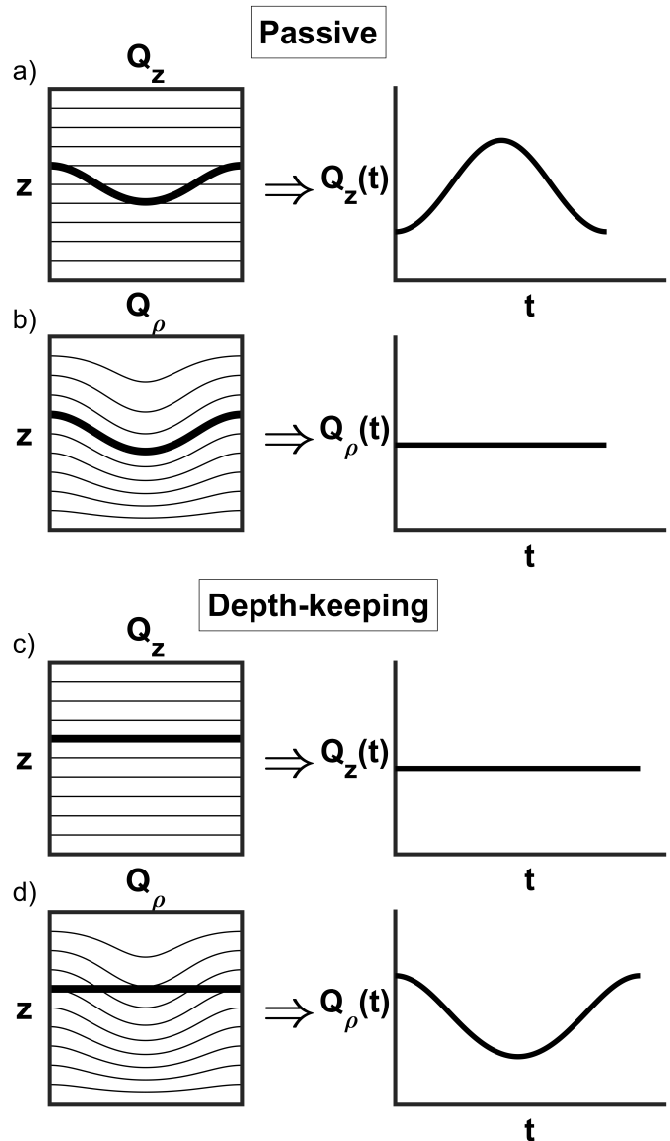
Figure 4.9: Schematic showing passive and depth-keeping plankton being moved through isobaric (Q_z) and along-isopycnal (Q_ρ) property fields by an internal wave. Note that the length of the time series for Q vary between swimming strategies, and that the direction of the perturbation for passive organisms is opposite that of depth-keeping organisms.

4.9 Estimating environmental conditions

In general, the isobaric environmental condition Q_z experienced by passive organism at time t will depend on its vertical position z_{org}, while the along-isopycnal environmental conditions Q_ρ experienced by organisms that maintain their depth at time t will depend on the water density at their position, with $\rho_{org} = \rho(x_{org}, z_{org}, t)$. The horizontal and vertical positions of benthic/sessile organisms are fixed; thus the environmental conditions they experience are well captured by mooring measurements (Figs. 4.5-4.8, B and D). Planktonic organisms, however, are moved by the wave itself; their relative position with respect to the wave thus fluctuates unevenly every time step. This means that the average environmental conditions experienced by planktonic organisms are not equivalent to the average environmental conditions measured at a mooring, even if measurements along isopycnals are considered for passive organisms (Figs. 4.5-4.8, C and F), and along depth for depth-keepers (Figs. 4.5-4.8, B and E). Although this is true for both linear and nonlinear waves, the time series associated with the weakly nonlinear internal wave highlight the difference between fixed measurements and measurements along an organism's path more clearly (Figs. 4.6 and 4.8). For instance, we can see that passive organisms experienced the trough of the wave – and the enhanced Q_z associated with it – for a longer time period near the ocean surface than near the bottom (Fig. 4.6F). Similarly, depth-keeping organisms experienced the trough of the wave – and the reduced Q_ρ associated with it – for a longer time period near the surface than near the bottom (Fig. 4.8E). In both cases, these time periods also differed from those measured at a mooring (Figs. 4.6C and F, and 4.8B and E).

For passive plankton, the average isobaric environmental conditions $\bar{Q}_{z,P}$ (Fig. 4.9A) and along-isopycnal conditions $\bar{Q}_{\rho,P}$ (Fig. 4.9B) can be calculated from:

$$\bar{Q}_{z,P} = \frac{1}{\tau} \int_0^\tau Q_z(z_{org}, t) \, dt, \tag{4.8}$$

and

$$\begin{aligned}
\bar{Q}_{\rho,P} &= \frac{1}{\tau} \int_0^\tau Q_\rho(\rho_0) \, dt, \\
&= Q_\rho(\rho_0),
\end{aligned} \tag{4.9}$$

respectively. While the average conditions for depth-keeping organisms (Fig. 4.9B, C) can be calculated from:

$$\begin{aligned}
\bar{Q}_{z,DK} &= \frac{1}{\tau} \int_0^\tau Q_z(z_0) \, dt, \\
&= Q_z(z_0),
\end{aligned} \tag{4.10}$$

and

$$\bar{Q}_{\rho,DK} = \frac{1}{\tau} \int_0^\tau Q_\rho \left(\rho(x_{org}, z_{org}, t) \right) \, dt. \tag{4.11}$$

Note that because passive organisms remain in the same isopycnal, internal waves will have no impact on the average along-isopycnal conditions they experience (Fig. 4.9B, eq. 4.9). Similarly, internal waves will not affect the average isobaric conditions experienced by depth-keeping organisms (Fig. 4.9C, eq. 4.10). In the cases where conditions are changing for each of these organisms (Fig. 4.9A and D, equations 4.8 and 4.11), it is important to remember that the x and z positions refer to those of the organisms in the moving wave flow field, and that the periods of integration are over the respective residence times of the organisms, not the wave period. As long as an estimate of wave propagation

speeds can be obtained, propagating organisms numerically through internal waves will yield more accurate time series, integrals, and averages of the environmental properties experienced by planktonic organisms than Eulerian measurements. The velocity structure of the wave can then be obtained by using *in situ* measurements (Garwood et al., chapter 2), by parameterizing the theoretical equations presented here (e.g., Garwood et al., chapter 3), by solving the dynamically consistent KdV equation (e.g., Garwood et al., chapter 2), and/or by using more complex nonlinear wave models.

4.10   Conclusions

Internal waves can modulate the environment experienced by marine organisms either by displacing them vertically or by advecting waters with different properties to their depths. Overall, mooring observations of wave-perturbed oceans provide a good characterization of the environment experienced by sessile/benthic organisms. However, to fully capture how planktonic organisms experience internal waves, the horizontal displacement of plankton within the wave should be considered, either by using theoretical flow fields or *in situ* velocities. Although previous studies have addressed the Lagrangian experience of passive particles in the vertical (Kahru, 1983) or measured environmental properties relevant to plankton using drifting arrays (Stevens et al., 2012), to our knowledge, none has investigated the implications of horizontal advection by internal waves on the average environmental conditions experienced by both passive and depth-regulating plankton. The effect of horizontal advection should be more important in highly nonlinear internal waves as their maximum velocities approach wave propagation speeds. However, weakly nonlinear internal waves propagating in ambient velocities on the same order as wave propagation speeds could produce similar effects. Moreover, when internal waves deform vertically sheared ambient horizontal velocities, the background velocities experienced by depth-keeping organisms

will fluctuate over a wave period, which will modulate their residence time in various parts of the wave and thus total transport (Garwood et al., chapter 2). Using measurements collected by a swarm of subsurface plankton mimics and wave simulations, Garwood et al. (chapters 3 and 4) demonstrated that this mechanism enhanced larval cross-shore transport at their site; their methodology could easily be adapted to better estimate the average environmental conditions experienced by drifting organisms.

4.11   Acknowledgements

Chapter 4, in full, is currently being prepared for submission for publication of the material. Garwood, J.C., Musgrave, R.C., Lucas, A.J., and Franks, P.J.S. The dissertation author was the primary investigator and author of this material.

Chapter 5

Conclusions

5.1 Summary of results

Overall, the work presented in this dissertation highlighted the importance of considering horizontal displacement induced by the interaction of larval swimming, internal waves, and ambient velocities when assessing the environmental conditions and cross-shore transport experienced by planktonic organisms. In fact, as organisms are moved by internal waves, they will either experience a range of depths (passive organisms) or a range of fluid densities (depth-keeping organisms); the experience of weak swimmers will fall between these extremes. Internal waves will therefore modulate passive organisms' experience of isobaric environmental conditions, such as light availability and pressure, while they will modulate depth-keepers' experience of along-isopycnal ocean properties, such as temperature and nutrient/oxygen concentrations. Because planktonic organisms are moved with respect to the wave field, the average environmental conditions experienced will also differ from the averages calculated at a mooring and for sessile organisms.

As part of this dissertation, field experiments using subsurface larval mimics were carried out to assess how high-frequency internal waves can modulate larval cross-shore

transport in the coastal environment. In these experiments, the mimics were programmed to maintain depth, but they did this imperfectly. This imperfect depth-holding was ideal as the mimics' overall vertical swimming speeds (< 2 mm s^{-1}) were representative of many planktonic organisms. Results showed that as an internal wave propagated through the larval mimics, the deformation of along-isopycnal ambient velocities brought faster waters past the mimics, accelerating them towards shore. However, passive organisms did not experience enhanced ambient velocities because they followed isopycnals. These unique observations highlighted the importance of considering how the vertical structure of internal wave and ambient horizontal velocities, as well as swimming behavior interact to determine both the total larval cross-shore transport and residence time throughout the waves.

Finally, theoretical wave models were validated against the transport measured by the larval mimics. These wave models were then used to estimate and contrast the cross-shore transport experienced by both passive and depth-keeping organisms in shallow-water, weakly nonlinear internal waves observed during a 14-day sampling period. On average, in the waves observed, depth-keeping was found to promote onshore transport throughout the water column, compared to passive organisms. This was particularly true closer to the surface, where $\sim 20\%$ of the waves observed induced cross-shore transport distances > 50 m for depth-keepers, compared to 1% for passive organisms. These transport distances are comparable to average transport distances for passive organisms in highly nonlinear internal waves (Shroyer et al., 2010), yet weakly nonlinear internal waves are much more common. Depth-keeping could, therefore, represent a significant advantage for organisms that must return to shallower, adult habitats.

5.2 Recommendations for future work

Although the work presented in this dissertation highlighted the impact depth-keeping in internal waves might have on cross-shore transport, how various plankton respond (if at all) to a wave's vertical displacement remains unknown. While our larval mimics responded to pressure perturbations, plankton may instead respond to the vertical velocities themselves, light cues, or optimal average temperature/salinity to name a few. As horizontal transport in internal waves was shown to depend on vertical swimming abilities, internal waves could induce horizontal sorting of planktonic organisms and/or larval stages, based on swimming ability. In regions where internal waves occur as predictable wave packets, this hypothesis could be tested by sampling plankton in the cross-shore direction during calm conditions, as any horizontal sorting should last beyond the passage of the waves. Finally, the average environmental conditions experienced by both passive and depth-keeping organisms were found to differ from averages calculated at a mooring. These differences, however, would only have an impact on plankton populations if they led to differences in the rate of important biological processes such as photosynthesis, growth, or nutrient absorption. Are these biological processes sensitive enough to the differences between estimates calculated along an organism's path vs. at a mooring? To investigate this question, nonlinear internal waves could be included into biological-physical models of plankton photosynthesis, growth, etc. Only simulating the vertical motions of plankton in internal waves would not be sufficient to address these questions *in situ*. Instead, drogues with bottle experiments at a single depth could be considered to study depth-keeping organisms, although no simple suggestion exists for passive organisms (not that the depth-keeping aspect is truly simple). Moreover, surface waves in the coastal environment imply that fixed distances between surface floats and subsurface drogues are only an approximation of depth-keeping. As a first step, sensors could be placed in this arrangement and environmental conditions reproduced in laboratory experiments.

References

Alford, M. H., Lien, R.-C., Simmons, H., Klymak, J. M., Ramp, S., Yang, Y.-J., Tang, D., and Chang, M.-H. (2010). Speed and evolution of nonlinear internal waves transiting the South China Sea. *Journal of Physical Oceanography*, 40:1338–1355.

Apel, J. R. (2002). Oceanic internal waves and solitons. In Jackson, C. R. and Apel, J. R., editors, *An Atlas of Internal Solitary-like Waves and their Properties*, pages 1–40.

Apel, J. R., Holbrook, J. R., Liu, A. K., and Tsai, J. J. (1985). The Sulu Sea internal soliton experiment. *Journal of Physical Oceanography*, 15:1625–1651.

Armstrong, F. A. J. and LaFond, E. C. (1966). Chemical nutrient concentrations and their relationship to internal waves and turbidity off Southern California. *Limnology and Oceanography*, pages 538–547.

Bertrand, A., Gerlotto, F., Bertrand, S., Gutiérrez, M., Alza, L., Chipollini, A., Díaz, E., Espinoza, P., Ledesma, J., Quesquén, R., Peraltilla, S., and Chavez, F. (2008). Schooling behaviour and environmental forcing in relation to anchoveta distribution: An analysis across multiple spatial scales. *Progress in Oceanography*, 79(2-4):264–277.

Booth, J. A. T., McPhee-Shaw, E. E., Chua, P., Kingsley, E., Denny, M., Phillips, R., Bograd, S. J., Zeidberg, L. D., and Gilly, W. F. (2012). Natural intrusions of hypoxic, low pH water into nearshore marine environments on the California coast. *Continental Shelf Research*, 45:108–115.

Bourgault, D., Blokhina, M. D., Mirshak, R., and Kelley, D. E. (2007). Evolution of a shoaling internal solitary wavetrain. *Geophysical Research Letters*, 34(3):1–5.

Chang, M.-H., Lien, R.-C., Yang, Y. J., and Tang, T. Y. (2011). Nonlinear internal wave properties estimated with moored ADCP measurements. *Journal of Atmospheric and Oceanic Technology*, 28(6):802–815.

Cheriton, O. M., McManus, M. a., Stacey, M. T., and Steinbuck, J. V. (2009). Physical and biological controls on the maintenance and dissipation of a thin phytoplankton layer. *Marine Ecology Progress Series*, 378(2003):55–69.

Chia, F.-S., Buckland-Nicks, J., and Young, C. M. (1984). Locomotion of marine invertebrate larvae: A review. *Canadian Journal of Zoology*, 62:1205–1222.

Cleveland, W. S. and Grosse, E. (1991). Computational methods for local regression. *Statistics and Computing*, 1:47–62.

Colosi, J. a., Kumar, N., Suanda, S. H., Freismuth, T. M., and MacMahan, J. (2018). Statistics of internal tide bores and internal solitary waves observed on the inner continental shelf off Point Sal, California. *Journal of Physical Oceanography*, 48:123–143.

Cragg, S. M. (1980). Swimming behaviour of the larvae of *Pecten maximus* (L.) (Bivalvia). *Journal of the Marine Biological Association of the United Kingdom*, 60(3):551–564.

da Silva, J. C. B. (2002). On the observability of internal tidal waves in remotely-sensed ocean colour data. *Geophysical Research Letters*, 29(12):1569.

Daigle, R. M. and Metaxas, A. (2011). Vertical distribution of marine invertebrate larvae in response to thermal stratification in the laboratory. *Journal of Experimental Marine Biology and Ecology*, 409(1-2):89–98.

Dewar, W. K. (1980). *The effect of internal waves on neutrally buoyant floats and other near-Lagrangian tracers.* Master's thesis, Massachusetts Institute of Technology.

DiBacco, C., Fuchs, H. L., Pineda, J., and Helfrich, K. (2011). Swimming behavior and velocities of barnacle cyprids in a downwelling flume. *Marine Ecology Progress Series*, 433:131–148.

Dorman, C. E. (1982). Winds between San Diego and San Clemente Island. *Journal of Geophysical Research*, 87:9636–9646.

Drake, P. T., Edwards, C. A., Morgan, S. G., and Satterthwaite, E. V. (2018). Shoreward swimming boosts modeled nearshore larval supply and pelagic connectivity in a coastal upwelling region. *Journal of Marine Systems*, 187(December 2017):96–110.

Evans, M. A., MacIntyre, S., and Kling, G. W. (2008). Internal wave effects on photosynthesis: Experiments, theory, and modeling. *Limnology and Oceanography*, 53(1):339–353.

Ewing, G. C. (1950a). Relation between band slicks at the surface and internal waves in the sea. *Science*, 111(2874):91–94.

Ewing, G. C. (1950b). Slicks, surface films and internal waves. *Journal of Marine Research*, 9(3):161–187.

Flameling, I. A. and Kromkamp, J. (1997). Photoacclimation of *Scenedesmus protuberans* (Chlorophyceae) to fluctuating irradiances simulating vertical mixing. *Journal of Plankton Research*, 19(8):1011–1024.

Franks, P. J. S. (1997). Spatial patterns in dense algal blooms. *Limnology and Oceanography*, 42(5_part_2):1297–1305.

Fuchs, H. L., Hunter, E. J., Schmitt, E. L., and Guazzo, R. A. (2013). Active downward propulsion by oyster larvae in turbulence. *Journal of Experimental Biology*, 216(8):1458–1469.

Fuchs, H. L., Mullineaux, L. S., and Solow, A. R. (2004). Sinking behavior of gastropod larvae (*Ilyanassa obsoleta*) in turbulence. *Limnology and Oceanography*, 49(6):1937–1948.

Fujimura, A. G., Reniers, A. J. H. M., Paris, C. B., Shanks, A. L., Macmahan, J. H., and Morgan, S. G. (2014). Numerical simulations of larval transport into a rip-channeled surf zone. *Limnology and Oceanography*, 59(4):1434–1447.

Gemmell, B. J., Oh, G., Buskey, E. J., and Villareal, T. A. (2016). Dynamic sinking behaviour in marine phytoplankton: Rapid changes in buoyancy may aid in nutrient uptake. *Proceedings of the Royal Society B: Biological Sciences*, 283(1840).

Genin, A. (2005). Swimming Against the Flow: A Mechanism of Zooplankton Aggregation. *Science*, 308(5723):860–862.

Greer, A. T., Cowen, R. K., Guigand, C. M., Hare, J. A., and Tang, D. (2014). The role of internal waves in larval fish interactions with potential predators and prey. *Progress in Oceanography*.

Grimshaw, R., Pelinovsky, E., Talipova, T., and Kurkin, A. (2004). Simulation of the transformation of internal solitary waves on oceanic shelves. *Journal of Physical Oceanography*, 34:2774–2791.

Hagerty, M. L., Reyns, N., and Pineda, J. (2018). Constrained nearshore larval distributions and thermal stratification. *Marine Ecology Progress Series*, 595:105–122.

Haney, C. J. (1987). Ocean internal waves as sources of small-scale patchiness in seabird distribution on the Blake Plateau. *The Auk*, 104(1):129–133.

Haury, L. R., Wiebe, P. H., Orr, M. H., and Briscoe, M. G. (1983). Tidally generated high-frequency internal wave packets and their effects on plankton in Massachusetts Bay. *Journal of Marine Research*, 41(1):65–112.

Helfrich, K. R. and Pineda, J. (2003). Accumulation of particles in propagating fronts. *Limnology and Oceanography*, 48(4):1509–1520.

Hendrickson, J. and MacMahan, J. (2009). Diurnal sea breeze effects on inner-shelf cross-shore exchange. *Continental Shelf Research*, 29(18):2195–2206.

Hill, A. E. (1998). Diel vertical migration in stratified tidal flows: Implications for plankton dispersal. *Journal of Marine Research*, 56(5):1069–1096.

Holloway, G. and Denman, K. (1989). Influence of internal waves on primary production. *Journal of Plankton Research*, 11(2):409–414.

Inall, M. E., Shapiro, G. I., and Sherwin, T. J. (2001). Mass transport by non-linear internal waves on the Malin Shelf. *Continental Shelf Research*, 21(13-14):1449–1472.

Jaffe, J. S., Franks, P. J., Roberts, P. L., Mirza, D., Schurgers, C., Kastner, R., and Boch, A. (2017). A swarm of autonomous miniature underwater robot drifters for exploring submesoscale ocean dynamics. *Nature Communications*, 8:1–8.

Jillett, J. B. and Zeldis, J. R. (1985). Aerial observations of surface patchiness of a planktonic crustacean. *Bulletin of Marine Science*, 37(2):609–619.

Kaartvedt, S., Klevjer, T. a., and Aksnes, D. L. (2012). Internal wave-mediated shading causes frequent vertical migrations in fishes. *Marine Ecology Progress Series*, 452:1–10.

Kahru, M. (1983). Phytoplankton patchiness generated by long internal waves: A model. *Marine Ecology Progress Series*, 10:111–117.

Kamykowski, D. (1974). Possible interactions between phytoplankton and semidiurnal internal tides. *Journal of Marine Research*, 32(1):67–89.

Kingsford, M. and Choat, J. (1986). Influence of surface slicks on the distribution and onshore movement of small fish. *Marine Biology*, 91:161–171.

Klymak, J. M., Pinkel, R., Liu, C.-t., Liu, A. K., and David, L. (2006). Prototypical solitons in the South China Sea. *Geophysical Research Letters*, 33:L11607.

Kunze, H. B., Morgan, S. G., and Lwiza, K. M. (2013). Field test of the behavioral regulation of larval transport. *Marine Ecology Progress Series*, 487:71–87.

Ladah, L. B., Filonov, A., Lavín, M. F., Leichter, J. J., Zertuche-González, J. A., and Pérez-Mayorga, D. M. (2012). Cross-shelf transport of sub-thermocline nitrate by the internal tide and rapid (3-6h) incorporation by an inshore macroalga. *Continental Shelf Research*, 42:10–19.

Lai, Z., Chen, C., Beardsley, R. C., Rothschild, B., and Tian, R. (2010). Impact of high-frequency nonlinear internal waves on plankton dynamics in Massachusetts Bay. *Journal of Marine Research*, 68(2):259–281.

Lamb, K. G. (1997). Particle transport by nonbreaking, solitary internal waves. *Journal of Geophysical Research*, 102(C8):18641.

Largier, J. L. (2003). Considerations in estimating larval dispersal distances from oceanographic data. *Ecological Applications*, 13(1 SUPPL.):71–89.

Laxague, N. J., Özgökmen, T. M., Haus, B. K., Novelli, G., Shcherbina, A., Sutherland, P., Guigand, C. M., Lund, B., Mehta, S., Alday, M., and Molemaker, J. (2018). Observations of near-surface current shear help describe oceanic oil and plastic transport. *Geophysical Research Letters*, 45(1):245–249.

Lee, O. S. (1961). Observations on internal waves in shallow water. *Limnology & Oceanography*, 6(3):312–321.

Leichter, J. J., Helmuth, B., and Fischer, A. M. (2006). Variation beneath the surface: Quantifying complex thermal environments on coral reefs in the Caribbean, Bahamas and Florida. *Journal of Marine Research*, 64(4):563–588.

Leichter, J. J., Shellenbarger, G., Genovese, S. J., and Wing, S. R. (1998). Breaking internal waves on a Florida (USA) coral reef: A plankton pump at work? *Marine Ecology Progress Series*, 166:83–97.

Leichter, J. J., Stewart, H. L., and Miller, S. L. (2003). Episodic nutrient transport to Florida coral reefs. *Limnology and Oceanography*, 48(4):1394–1407.

Leichter, J. J., Wing, S. R., Miller, S. L., and Denny, M. W. (1996). Pulsed delivery of subthermocline water to Conch Reef (Florida Keys) by internal tidal bores. *Limnology and Oceanography*, 41(7):1490–1501.

Lennert-Cody, C. E. and Franks, P. J. S. (1999). Plankton patchiness in high-frequency internal waves. *Marine Ecology Progress Series*, 186:59–66.

Lennert-Cody, C. E. and Franks, P. J. S. (2002). Fluorescence patches in high-frequency internal waves. *Marine Ecology Progress Series*, 235:29–42.

Lerczak, J. A. (2000). *Internal waves on the Southern California shelf*. PhD dissertation, University of California, San Diego.

Lerczak, J. A., Winant, C. D., and Hendershott, M. C. (2003). Observations of the semidiurnal internal tide on the southern California slope and shelf. *Journal of Geophysical Research: Oceans*, 108(C3):3068.

Lévy, M., Franks, P. J., and Smith, K. S. (2018). The role of submesoscale currents in structuring marine ecosystems. *Nature Communications*, 9(1):4758.

Lien, R.-C., D'Asaro, E. A., Henyey, F., Chang, M.-H., Tang, T.-Y., and Yang, Y.-J. (2012). Trapped core formation within a shoaling nonlinear internal wave. *Journal of Physical Oceanography*, 42(4):511–525.

Liévana MacTavish, A., Ladah, L. B., Lavín, M. F., Filonov, A., Tapia, F. J., and Leichter, J. (2016). High frequency (hourly) variation in vertical distribution and abundance of meroplanktonic larvae in nearshore waters during strong internal tidal forcing. *Continental Shelf Research*, 117:92–99.

Lucas, A. J., Dupont, C. L., Tai, V., Largier, J. L., Palenik, B., and Franks, P. J. S. (2011a). The green ribbon: Multiscale physical control of phytoplankton productivity and community structure over a narrow continental shelf. *Limnology and Oceanography*, 56(2):611–626.

Lucas, A. J., Franks, P. J. S., and Dupont, C. L. (2011b). Horizontal internal-tide fluxes support elevated phytoplankton productivity over the inner continental shelf. *Limnology and Oceanography: Fluids and Environments*, 1(1):56–74.

Lund, B., Graber, H. C., Tamura, H., Collins, C. O., and Varlamov, S. M. (2015). A new technique for the retrieval of nearsurface vertical current shear from marine X–band radar images. *Journal of Geophysical Research: Oceans*, 120(12):8466–8486.

Macías, D., Somavilla, R., González-Gordillo, J. I., and Echevarría, F. (2010). Physical control of zooplankton distribution at the Strait of Gibraltar during an episode of internal wave generation. *Marine Ecology Progress Series*, 408:79–85.

McPhee-Shaw, E. E., Siegel, D. A., Washburn, L., Brzezinski, M. A., Jones, J. L., Leydecker, A., and Melack, J. (2007). Mechanisms for nutrient delivery to the inner shelf: Observations from the Santa Barbara Channel. *Limnology and Oceanography*, 52(5):1748–1766.

Metaxas, A. and Saunders, M. (2009). Quantifying the "Bio-" components in biophysical models of larval transport in marine benthic invertebrates: Advances and pitfalls. *Biological Bulletin*, 216(3):257–272.

Mileikovsky, S. A. (1973). Speed of active movement of pelagic larvae of marine bottom invertebrates and their ability to regulate their vertical position. *Marine Biology*, 23:11–17.

Moore, S. E. and Lien, R. C. (2007). Pilot whales follow internal solitary waves in the South China Sea. *Marine Mammal Science*, 23(1):193–196.

Morgan, S. G., Fisher, J. L., Miller, S. H., Mcafee, S. T., and Largier, J. L. (2009). Nearshore larval retention in a region of strong upwelling and recruitment limitation. *Ecology*, 90(12):3489–3502.

Morgan, S. G., Shanks, A. L., Macmahan, J., Reniers, A. J. H. M., Griesemer, C. D., Jarvis, M., and Fujimura, A. G. (2017). Surf zones regulate larval supply and zooplankton subsidies to nearshore communities. *Limnology & Oceanography*, 62:2811–2828.

Muacho, S., Da Silva, J. C. B., Brotas, V., and Oliveira, P. B. (2013). Effect of internal waves on near-surface chlorophyll concentration and primary production in the Nazaré Canyon (west of the Iberian Peninsula). *Deep-Sea Research Part I: Oceanographic Research Papers*, 81:89–96.

Murphy, D. W., Webster, D. R., and Yen, J. (2013). The hydrodynamics of hovering in Antarctic krill. *Limnology & Oceanography: Fluids & Environments*, 3:240–255.

Nash, C. E., Kuo, C. M., Madden, W. D., and Paulsen, C. L. (1977). Swim bladder inflation and survival of *Mugil cephalus* to 50 days. *Aquaculture*, 12:89–94.

Nash, C. E., Kuo, C. M., and McConnel, S. C. (1974). Operational procedures for rearing larvae of the grey mullet (*Mugil cephalus* L.). *Aquaculture*, 3:15–24.

Nash, J., Shroyer, E., Kelly, S., and Inall, M. (2012). Are any coastal internal tides predictable? *Oceanography*, 25(2):80–95.

Nash, J. D. and Moum, J. N. (2005). River plumes as a source of large-amplitude internal waves in the coastal ocean. *Nature*, 437(7057):400–403.

Navarro, M. O., Kwan, G. T., Batalov, O., Choi, C. Y., Pierce, N. T., and Levin, L. A. (2016). Development of embryonic market squid, *Doryteuthis opalescens*, under chronic exposure to low environmental pH and [O2]. *PLoS ONE*, 11(12):1–17.

Oliver, R. L. (1994). Floating and sinking in gas-vacuolate cyanobacteria. *Journal of Phycology*, 30(2):161–173.

Omand, M. M., Leichter, J. J., Franks, P. J. S., Guza, R. T., Lucas, A. J., and Feddersen, F. (2011). Physical and biological processes underlying the sudden surface appearance of a red tide in the nearshore. *Limnology and Oceanography*, 56(3):787–801.

Pan, X., Wong, G. T., Shiah, F. K., and Ho, T. Y. (2012). Enhancement of biological productivity by internal waves: Observations in the summertime in the northern South China Sea. *Journal of Oceanography*, 68(3):427–437.

Peterson, W. T., Miller, C. B., and Hutchinson, A. (1979). Zonation and maintenance of copepod populations in the Oregon upwelling zone. *Deep Sea Research Part A, Oceanographic Research Papers*, 26(5):467–494.

Pineda, J. (1994). Internal tidal bores in the nearshore: Warm-water fronts, seaward gravity currents and the onshore transport of neustonic larvae. *Journal of Marine Research*, 52(3):427–458.

Pineda, J. (1999). Circulation and larval distribution in internal tidal bore warm fronts. *Limnology and Oceanography*, 44(6):1400–1414.

Pinkel, R., Goldin, M. A., Smith, J. A., Sun, O. M., Aja, A. A., Bui, M. N., and Hughen, T. (2011). The Wirewalker : A vertically profiling instrument carrier powered by ocean waves. *Journal of Atmospheric and Oceanic Technology*, 28:426–435.

Rainville, L. and Pinkel, R. (2001). Wirewalker: An autonomous wave-powered vertical profiler. *Journal of Atmospheric and Oceanic Technology*, 18(6):1048–1051.

Richards, C., Bourgault, D., Galbraith, P. S., Hay, A., and Kelley, D. E. (2013). Measurements of shoaling internal waves and turbulence in an estuary. *Journal of Geophysical Research: Oceans*, 118(1):273–286.

Richardson, T. L. and Cullen, J. J. (1995). Changes in buoyancy and chemical composition during growth of a coastal marine diatom: Ecological and biogeochemical consequences. *Marine Ecology Progress Series*, 128(1-3):77–90.

Ruvalcaba-Aroche, E. D., Filonov, A., Sánchez-Velasco, L., Ladah, L. B., and Cruz-Hernández, J. (2019). Internal tidal waves in Tiburon Basin (Gulf of California, Mexico) modulate fish larvae aggregations. *Continental Shelf Research*, 178(1):41–50.

Sandstrom, H., Elliot, J. A., and Cochrane, N. A. (1989). Observing groups of solitary internal waves and turbulence with BATFISH and echo-sounder.

Sandstrom, H. and Elliott, J. A. (1984). Internal tide and solitons on the Scotian Shelf: A nutrient pump at work. *Atlantic*, 89(4):6415–6426.

Scotti, A. and Pineda, J. (2007). Plankton accumulation and transport in propagating nonlinear internal fronts. *Journal of Marine Research*, 65(1):117–145.

Shanks, A. (1985). Behavioral basis of internal-wave-induced shoreward transport of megalopae of the crab *Pachygrapsus crassipes*. *Marine Ecology Progress Series*, 24:289–295.

Shanks, A. L. (1983). Surface slicks associated with tidally forced internal waves may transport pelagic larvae of benthic invertebrates and fishes shoreward. *Marine Ecology Progress Series*, 13:311–315.

Shanks, A. L. (1987). The onshore transport of an oil spill by internal waves. *Science*, 235(4793):1198–1200.

Shanks, A. L. (1988). Further support for the hypothesis that internal waves can cause shoreward transport of larval invertebrates and fish. *Fishery Bulletin*, 86(4):703–714.

Shanks, A. L. (1995). Orientated swimming by megalopae of several eastern North Pacific crab species and its potential role in their onshore migration. *Journal of Experimental Marine Biology and Ecology*, 186(1):1–16.

Shanks, A. L. (2009). Pelagic larval duration and dispersal distance revisited. *Biological Bulletin*, 216(3):373–385.

Shanks, A. L. and Brink, L. (2005). Upwelling, downwelling, and cross-shelf transport of bivalve larvae: Test of a hypothesis. *Marine Ecology Progress Series*, 302(Rumrill 1990):1–12.

Shanks, A. L. and Wright, W. G. (1987). Internal-wave-mediated shoreward transport of cyprids, megalopae, and gammarids and correlated longshore differences in the settling rate of intertidal barnacles. *Journal of Experimental Marine Biology and Ecology*, 114(1):1–13.

Shroyer, E. L., Moum, J. N., and Nash, J. D. (2009). Observations of polarity reversal in shoaling nonlinear internal waves. *American Meteorological Society*, 39:691–701.

Shroyer, E. L., Moum, J. N., and Nash, J. D. (2010). Vertical heat flux and lateral mass transport in nonlinear internal waves. *Geophysical Research Letters*, 37(8):1–5.

Shroyer, E. L., Moum, J. N., and Nash, J. D. (2011). Nonlinear internal waves over New Jersey's continental shelf. *Journal of Geophysical Research: Oceans*, 116(C3):C03022.

Sinnett, G., Feddersen, F., Lucas, A. J., Pawlak, G., and Terrill, E. (2018). Observations of nonlinear internal wave run-up to the surfzone. *Journal of Physical Oceanography*, 48:531–554.

Smyth, W. D., Moum, J. N., and Nash, J. D. (2010). Narrowband oscillations in the upper equatorial ocean. Part II: Properties of shear instabilities. *Journal of Physical Oceanography*, 41:412–428.

Stastna, M. and Lamb, K. G. (2002). Large fully nonlinear internal solitary waves: The effect of background current. *Physics of Fluids*, 14(9):2987–2999.

Stevens, C. L., Sutton, P. J., and Law, C. S. (2012). Internal waves downstream of Norfolk Ridge, western Pacific, and their biophysical implications. *Limnology and Oceanography*, 57(4):897–911.

Stevick, P. T., Incze, L. S., Kraus, S. D., Rosen, S., Wolff, N., and Baukus, A. (2008). Trophic relationships and oceanography on and around a small offshore bank. *Marine Ecology Progress Series*, 363:15–28.

Sulkin, S. D. (1984). Behavioral basis of depth regulation in the larvae of brachyuran crabs. *Marine Ecology Progress Series*, 15:181–205.

Tapia, F. J. and Pineda, J. (2007). Stage-specific distribution of barnacle larvae in nearshore waters: Potential for limited dispersal and high mortality rates. *Marine Ecology Progress Series*, 342:177–190.

Thorpe, S. A. (1968). On the shape of progressive internal waves. *Philosophical Transactions of the Royal Society A: Mathematical, Physical and Engineering Sciences*, 263(1145):563–614.

van den Bremer, T. S., Yassin, H., and Sutherland, B. R. (2019). Lagrangian transport by vertically confined internal gravity wavepackets. *Journal of Fluid Mechanics*, 864:348–380.

Wall, M., Putchim, L., Schmidt, G. M., Jantzen, C., Khokiattiwong, S., and Richter, C. (2015). Large-amplitude internal waves benefit corals during thermal stress. *Proceedings of the Royal Society B: Biological Sciences*, 282(1799).

Walter, R. K., Woodson, C. B., Leary, P. R., and Monismith, S. G. (2014). Connecting wind-driven upwelling and offshore stratification to nearshore internal bores and oxygen variability. *Journal of Geophysical Research: Oceans*, 119:3517–3534.

Wang, Y. H., Dai, C. F., and Chen, Y. Y. (2007). Physical and ecological processes of internal waves on an isolated reef ecosystem in the South China Sea. *Geophysical Research Letters*, 34(18):1–7.

Weidberg, N., Goschen, W., Jackson, J. M., Pattrick, P., McQuaid, C. D., and Porri, F. (2019). Fine scale depth regulation of invertebrate larvae around coastal fronts. *Limnology and Oceanography*, 64(2):785–802.

Weidberg, N., Lobón, C., López, E., García Flórez, L., Fernández Rueda, M., Largier, J., and Acuña, J. (2014). Effect of nearshore surface slicks on meroplankton distribution: Role of larval behaviour. *Marine Ecology Progress Series*, 506:15–30.

Wishner, K. F., Outram, D. M., Seibel, B. A., Daly, K. L., and Williams, R. L. (2013). Zooplankton in the eastern tropical north Pacific: Boundary effects of oxygen minimum zone expansion. *Deep-Sea Research Part I: Oceanographic Research Papers*, 79:122–140.

Witman, J. D., Leichter, J. J., Genovese, S. J., and Brooks, D. A. (1993). Pulsed phytoplankton supply to the rocky subtidal zone: Influence of internal waves. *Ecology*, 90:1686–1690.

Woodson, C. (2018). The fate and impact of internal waves in nearshore ecosystems. *Annual Review of Marine Science*, 10(1):421–441.

Wunsch, C. (1971). Note on some Reynolds stress effects of internal waves on slopes. *Deep Sea Research*, 18:583–591.

Zeidberg, L. D., Butler, J. L., Ramon, D., Cossio, A., Stierhoff, K. L., and Henry, A. (2012). Estimation of spawning habitats of market squid (*Doryteuthis opalescens*) from field surveys of eggs off Central and Southern California. *Marine Ecology*, 33(3):326–336.

Zeldis, J. R. and Jillett, J. B. (1982). Aggregation of pelagic *Munida gregaria* (Fabricius) (Decapoda, Anomura). *Journal of Plankton Research*, 4(4):839–857.

Zhang, S., Alford, M. H., and Mickett, J. (2015). Characteristics, generation and mass transport of nonlinear internal waves on the Washington continental shelf. *Journal of Geophysical Research C: Oceans*, 120:741–758.

Zimmerman, R. C. and Kremer, J. N. (1984). Episodic nutrient supply to a kelp forest ecosystem in Southern California. *Journal of Marine Research*, 42(3):591–604.